NTNU

Norwegian University of
Science and Technology

Impact on Wind Turbine Systems from Transient Fluctuations in Offshore Utility Grids

Torger Einervoll

Master of Science in Energy and Environment
Submission date: July 2009
Supervisor: Lars Einar Norum, ELKRAFT
Co-supervisor: Bjarne Idsøe Næss, Unitech Power Systems AS

Norwegian University of Science and Technology
Department of Electric Power Engineering

Problem Description

Electrical utility grids at offshore installations in the North Sea are mostly powered by the use of local generators driven by gas turbines. These gas turbines contribute to a significant amount of the total CO2 emissions in Norway. A method for reducing these emissions is to supply electrical power to the oil installations from offshore wind turbines which is located near the installations. This is an interesting solution for existing oil installations where the accessible gas turbines can be operated together with the wind turbines and also function as back-up system due to the variable wind.

The transient fluctuations in the electrical grid on a typical offshore installation differ from the onshore utility grid. One of the main characteristic of an electrical grid at an offshore installation is the start of large squirrel cage motors on a relatively small generator capacity. In addition transients due to short circuits and operation of the circuit breakers will occur. It is thus of interest to study the impact of such fluctuations on different types of wind turbine technologies by the use of a transient simulation tool like EMTDC/PSCAD.

Assignment given: 04. February 2009
Supervisor: Lars Einar Norum, ELKRAFT

Preface

This master thesis is the final work for completion of my studies at NTNU. The issues studied here were proposed by Bjarne Idsøe Næss at Unitech Power Systems A/S back in December 2008. It has been a challenging task, but it has developed my understanding of electrical systems as well as my analytical skills.

The main supervisor for the thesis work has been Professor Lars Norum at NTNU.

I would like to thank Lars Norum and Bjarne Idsøe Næss for their help, input and valuable discussions throughout the thesis work. Also, I would like to thank Trond Toftevaag of SINTEF Energiforsking A/S for helpful input on the modelling of the offshore oil platform utility grid.

I would also like to thank all of my co-eds here at NTNU for the great times we have had throughout the years.

Lastly, thanks to my family and my beloved Maren for being caring and supportive. My life would not be the same without you.

Trondheim, July 2009

Torger Einervoll

Summary

Gas turbines in offshore power systems contribute to about 23% of Norway's total emissions of CO_2. One method for reducing these emissions could be the addition of wind turbines to the offshore utility grids. Power from shore is another alternative, but has been proven costly due to long cables and expensive HVDC converter stations.

In this thesis work, the behaviours of different wind turbine technologies during transient fluctuations in an offshore utility grid have been studied. For this purpose, a dynamic model for an offshore oil platform was developed. Models of squirrel cage and doubly fed induction generator based turbines were developed as well.

None of the modelled generators experienced problems with the disturbances caused by the electromechanical transient fluctuations. Based on the behaviour of the DFIG's grid side converter, it is believed that the result would be the same for a wind turbine with full frequency conversion. Variable speed wind turbines are expected to remain controllable throughout electromechanical transient fluctuations such as for the simulated case. However, the controllers, converters and equipment have to be designed while bearing these fluctuations in mind.

The controllability of the variable speed wind turbines could be used to contribute to voltage control by production and consumption of reactive power. A controller scheme with the purpose of stabilising the voltage at the gas turbine generators' terminal was developed, but had low impacts on the power system behaviour.

A stator flux feed forward term for the speed controller was developed. The term stabilised the power output of the doubly fed induction generator. However, the impact on the power system's frequency response was minimal, and there is probably no material value of such an addition to the control loop.

Table of Contents

Nomenclature and definitions

AC – Alternating Current
AVR – Automatic Voltage Regulator
DC – Direct Current
DFIG – Doubly Fed Induction Generator
DOL – Direct On Line
DYn11 – A frequently used transformer type with delta coupled windings on primary side and star windings on secondary side, making the secondary side voltage vector lag 30 degrees compared to the primary.
FFT – Fast Fourier Transform
HVDC – High Voltage Direct Current
IEC – International Electrotechnical Commission
IGBT – Insulated Gate Bipolar Transistor
MATLAB – The numerical computing tool used as part of the thesis work
PLL – Phase Locked Loop
PSCAD – The simulation tool used in the thesis work
RMS – Root Mean Square
SISO – Single Input Single Output
SIMULINK – Simulation Add-On for MATLAB
SCIG – Squirrel Cage Induction Generator
STATCOM - Static Synchronous Compensator
WRIG – Wound Rotor Induction Generator

Symbols:
C – Capacitance
f – Frequency
i/I – Current
L – Inductance
P – Real Power
Q – Reactive Power
R – Resistance
s – Slip
S – Apparent Power
Te/Tel – Electrical Torque
Tm – Mechanical Torque
v/V – Voltage
X – Reactance
Z - Impedance
ω – Angular velocity
ω_s – Synchronous angular velocity
θ – Angle
ψ – Flux

Capitalised letters for currents and voltages denotes RMS values, whereas small letters refers to instantaneous values.

Indexing for synchronously referred quantities are the same as used by Kundur in [1]. The first subscript index denotes the direction while the second refers to the position. E.g. the symbol i_{dr} refers to the rotor d-axis current. Other positional indexes should be apparent from the context.

1 Introduction

1.1 CO_2 Emissions from Offshore Installations on the Norwegian Continental Shelf

Electrical utility grids at offshore installations on the Norwegian continental shelf are mostly powered by use of local generators driven by gas turbines. Exceptions are either powered by diesel engines or by power from shore. In the 2009 version of the annual report "FACTS – The Norwegian Petroleum Sector" [1], data for the emissions of CO_2 from the Norwegian petroleum sector in 2007 are published. Figure 1.1 and Figure 1.2 below visualise these data.

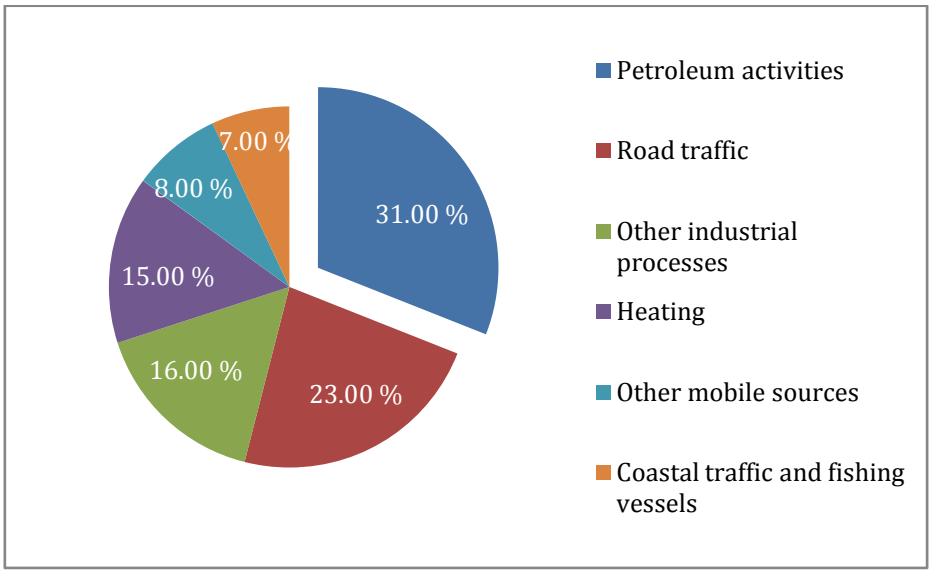

Figure 1.1 - Sources of Norwegian CO2 Emissions, 2007

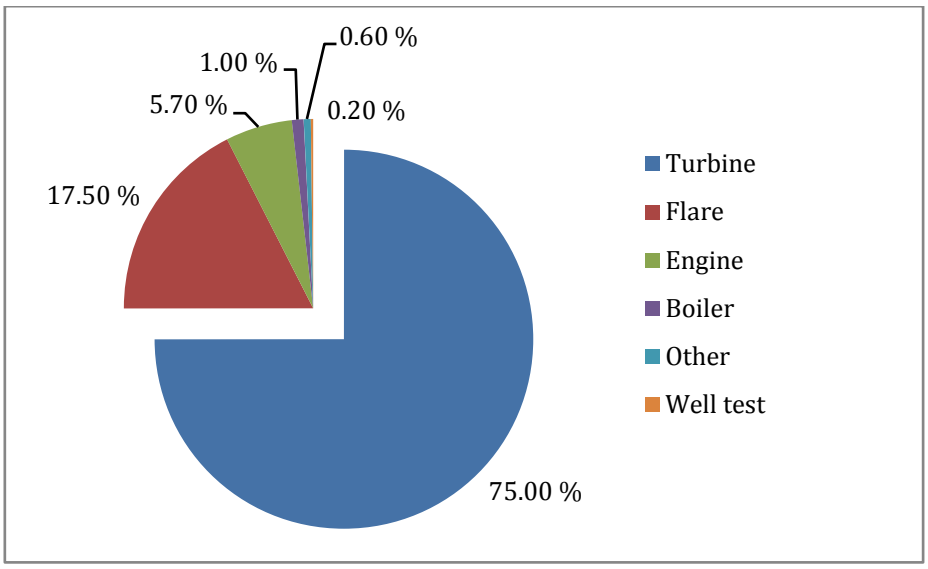

Figure 1.2 - CO2 Emissions from the Norwegian Petroleum Sector, 2007

As seen from the figures on the previous page, it is evident that significant parts of the Norwegian CO_2 emissions can be traced back to gas turbines on offshore oil and gas installations. By combining data from the two figures on the previous page it can be seen that gas turbines contribute with about 23% of the nation's total emissions. The referred report [1] also states that emissions per produced volume of petroleum are rising as a result of tail end production from older oil fields that produce increasing quantities of water, which then has to be separated and re-injected into the reservoir. In addition, new field developments tend to be more marginal economically than older ones, requiring increased amounts of power per barrel of oil produced. Production of natural gas is on the rise and requires more energy than production of oil and gas liquids.

As a result of growing concern for the environment and the climate changes, numerous actions have been taken by Norway to reduce emissions from the petroleum sector. Since 1st January 1991, companies extracting oil from the Norwegian continental shelf have been subject to a CO_2 tax based on produced volume of oil and gas. As of January 1st 2008, this fee was equivalent to 184 NOK per metric tonne of CO_2 [1]. Since 2008 the Norwegian petroleum sector has also been subject to the Norwegian CO_2 quota system. This means that emissions have to be covered by carbon contracts based on the EUA or the CER quota systems. In 2008, most of the quotas from the petroleum sector were based on the EUA system [2]. As of June 12th 2009, EUA quotas were traded for around 13 € per metric tonne of CO_2 [3], which is approximately 115 NOK.

Several studies have been conducted in order to investigate the possibilities to power existing offshore installations from shore. The latest official study [4] concludes that the resulting cost of emission reductions will be in the range from 1600 NOK to 4750 NOK per metric tonne of CO_2, depending on the offshore location and market situations. The high costs are caused by expensive infrastructure, most notably by long subsea cables and by inverter/rectifier stations required for enabling of DC transmission.

The official study [4] also mentions the possibilities for using offshore wind turbines to power oil installations. It concludes that using offshore wind turbines in a system that includes power from shore is not economically feasible, as this solution does not reduce the need for transmission capacity. However, there is a possibility to power offshore installations by wind turbines in a locally isolated utility system. The study says that gas turbines are highly controllable, which makes them suitable for such applications. However, there are technical issues affecting the reliability of supply that have to be taken into account. No official studies have been conducted on these issues, nor has the cost of such a system been investigated. Offshore wind power was found immature and was not included as part of the proposed technical solutions in the report.

1.2 The Offshore Utility Grid

Offshore power systems set high demands to the electrical equipment. Due to the relatively small size of the systems and the heavy industrial loads, their behaviours are highly dynamic. The IEC 61892-series of standards [5] ensures that electrical installations on mobile and fixed offshore units are reliable and operates within given requirements. These requirements are often tougher on electrical equipment than what is required for equipment used for the vast mainland utility grids.

Below are requirements found from IEC 61892-1:2001 paragraph 4.9.2.1, IEC 61892-3:2001 paragraphs 4.3.3.2, 4.10.3 and 4.3.5.1.

Table 1.1 - Requirements Found in the IEC 61892-Series of Standards.

	Permanent voltage variation:	Transient voltage variation:	Voltage transient recovery time:	Frequency tolerance (continuous)	Frequency transient tolerance:	Frequency recovery time:
Variations at any point of the system:	+6% -10%	±20%	1.5 s	±5%	±5% transient ±10% total	5 s
Terminals of AC generators with speed governors:	±3%	+20% -15%	1.5 s			

IEC 61892-3:2001 paragraph 4.3.5.1 states that the total harmonic distortion should be taken as 5% when evaluating equipment.

These numbers deviate significantly from the electrical specifications found on most wind turbines available today. As an example, the 60 Hz version of the state of the art Vestas V90 3 MW turbine requires voltage variations to be kept within ±5% and frequency deviations to be kept within +1 Hz/-3 Hz [6].

1.3 Wind Turbine Technology

Wind energy is currently the world's fastest growing source of renewable energy [7]. However, there are drawbacks related to the use of wind turbines. Among these are the visual and audible impacts on the local environment. As a result of these drawbacks there has been made large investments in order to develop solutions for placing wind turbines offshore. As of 2009 there are several installations around the world with wind turbines on fixed pillars and other technological solutions suited for shallow waters. The first full scale prototype of a floating wind turbine, Hywind, is expected to start production of power in autumn 2009.

Both of the leading Norwegian developers of technology for floating wind turbines are looking at powering offshore installations as the next logical step after successful testing of prototypes [8], [9]. This means that it might be that this kind of projects is developed for the Norwegian continental shelf as early as from 2012 and onwards.

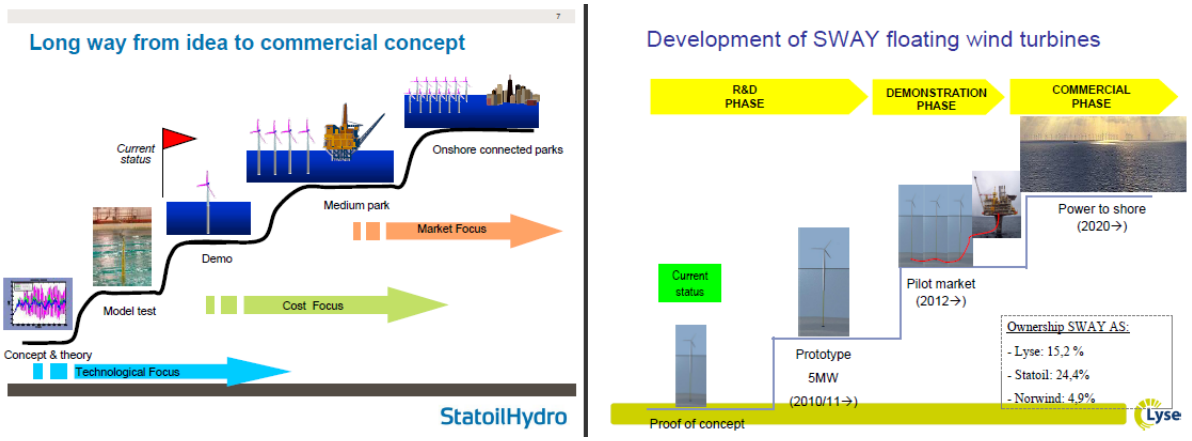

Figure 1.3 – Hywind's and Sway's Plans for Future Development Includes Powering Offshore Installations in Isolated Systems, sources: [8], [9].

For the conversion of mechanical to electrical power there is an ongoing development of novel technologies. Reduction of nacelle weight is seen as a necessary step in the process of making offshore wind turbines economical. Therefore, several technological firms are looking at opportunities for developing technology in order to move the generator, transformer and other heavy weight equipment down to the surface level. Among these are the Norwegian ChapDrive and Anglewind enterprises.

In general, three different technologies for conversion of power have been most prevalent in the industry to this date. These are the squirrel cage induction generator, the doubly fed induction generator and a range of generators with full frequency conversion. The following subsections will give a brief explanation of the different power conversion technologies.

1.3.1 Squirrel Cage Induction Generator

Since the earliest models of wind turbines, the squirrel cage induction generators (SCIGs) have been used as a mean to generate electric power. The technology is well proven as the designs of these electric machines have been refined trough decades of mass production. Squirrel cage induction motors are often referred to as the workhorses of the industry.

This technology has a major drawback since the angular velocity of the rotor is relatively fixed. This makes them unable to keep optimal blade speed at all times. Therefore, the turbines will not have the opportunity to produce as much power as they theoretically could with variable speed. The speed is entirely based on system frequency and torque-slip characteristics, and cannot be controlled. The fact that wind turbines of this design are not controllable makes them vulnerable to variations in the operating conditions given by the grid. Any change in terminal voltage or frequency would affect these machines.

Another drawback is that both the generator itself and the transformer consume reactive power. For this reason it is normal to locally install devices that could produce reactive power, either for each unit individually or for an entire wind park.

Lastly, the generator requires a higher rotational speed than the blades' angular velocity, which makes a gearbox inevitable. This item is known as one of the most maintenance intensive components of a wind turbine.

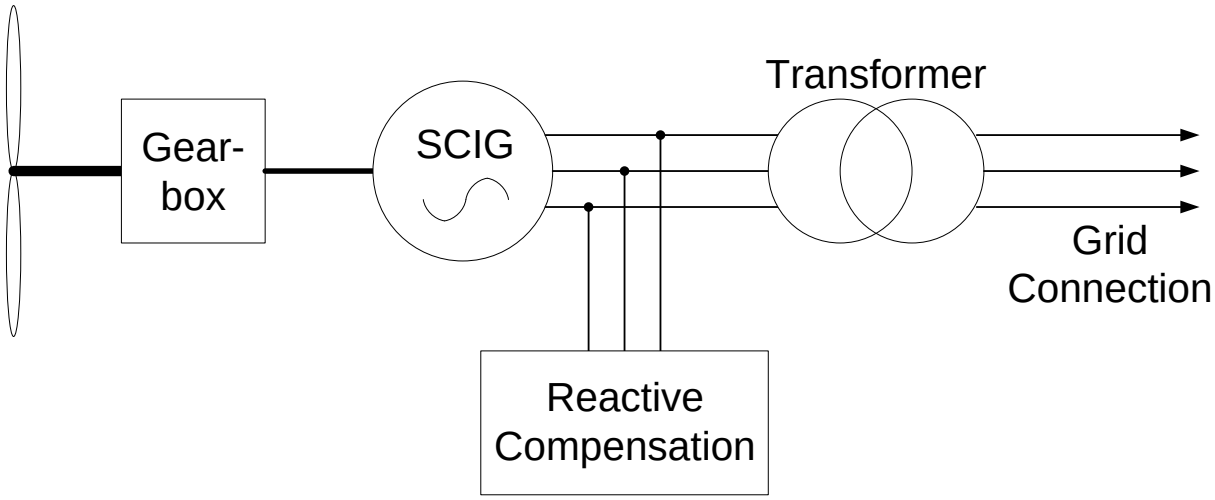

Figure 1.4 - The General Configuration of a Squirrel Cage Induction Generator

Wind turbines with SCIG type configuration are currently produced for power ratings up to 2.3 MW. The technology has a predominant market share for wind turbines in the lower end of power ratings.

1.3.2 Doubly Fed Induction Generator

Doubly induction generators (DFIGs) are able to vary the speed by as much as ±30% from the rated value [7], [10], [11]. This enables them to fully utilize the potential of the wind to produce energy at most wind speeds. Figure 1.5 illustrates the general configuration of a doubly fed induction generator. Auxiliary components and eventual line filters are not shown.

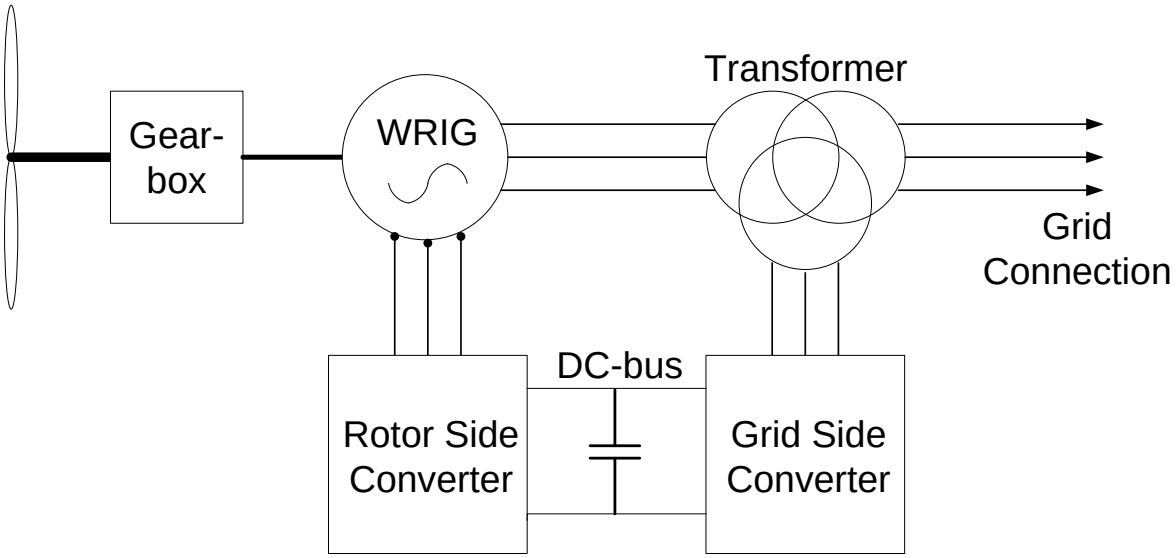

Figure 1.5 – The General Configuration of a Doubly Fed Induction Generator

To be able to vary the speed, the wound rotor induction generator (WRIG) needs to have a frequency converter of approximately $\frac{1}{3}$ of the generators MVA rating attached to the rotor circuit [10], [11]. This converter controls both the frequency and the voltage on the rotor terminals. The grid side converter either supplies or draws power from the DC-bus, depending on the slip and generator production needed to maintain a stable DC voltage.

The converters can produce or consume reactive power trough both the rotor and the grid. However, reactive currents trough the machine will generate heat and thus the machine's MVA rating will limit the ability to compensate with reactive power.

DFIG based wind turbines require a gearbox to achieve the necessary angular velocity of the rotor.

A problem associated with the doubly fed induction generators are their problematic fault ride-trough capabilities. Rapid voltage distortions, be it balanced or asymmetrical, can lead to high voltages in the rotor circuit and hereby produce large inrush currents that are harmful for the machine as well as the converters [11]. Methods of limiting this problem include converter disconnection or an actively controlled resistor connected to the stator terminals, the rotor terminals (active crowbar) or the DC bus (DC chopper).

1.3.3 Generators with Full Frequency Conversion

Generators with full frequency conversion are gaining popularity due to the vast possibilities for configurations. Virtually any type of generator could be used as a part of this design. Synchronous generators, permanent magnet generators, axial flux synchronous generators, induction generators are some of the models that have been investigated over the years. Models where the gearbox is avoided by having large numbers of poles have been well developed. According to Blaabjerg & Chen in [7], the technology had a 16% market share as of 2001. It can be assumed that the market share is even higher today as a result of technological development and cost reduction for power electronic converters. The same source states that power semiconductors are expected to decrease in cost by 2-5% per year.

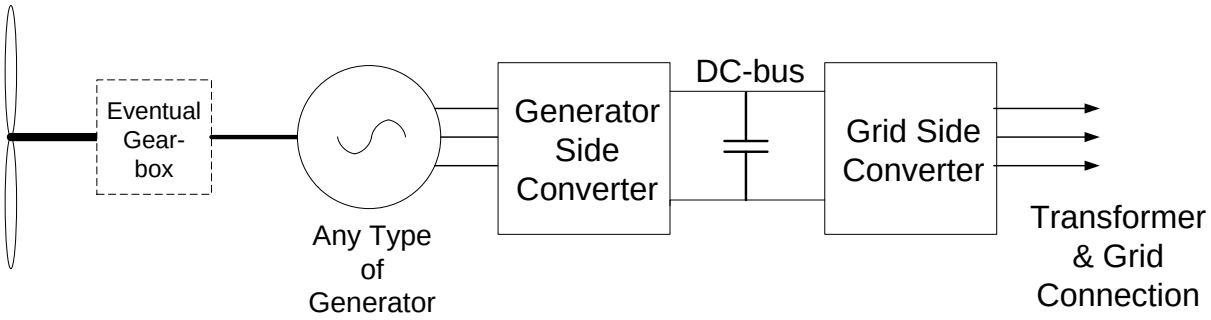

Figure 1.6 - General Overview of a Wind Turbine with Full Frequency Conversion

Wind turbines with full frequency conversion are able to keep optimal blade velocity at any wind speed, making them ideal for gathering energy from wind. They are able to produce reactive power trough the grid side converter. The amount of reactive power is only limited to the ratings of the converter equipment and the heating of the transformer windings.

The use of full frequency conversion means that the behaviour of the AC grid on either side could be relatively decoupled from the other. For any type of generator configuration the converter control will be essential for determining how the system will react to a disturbance in the utility grid.

Frequency converters are currently in use offshore for variable speed drives and HVDC-Light applications. As of June 2009, the BP operated Valhall oil field in the southern part of the North Sea is now being converted to use of electrical power via HVDC-Light connection to shore. This pioneering project is the first of its kind in Norway. Previous undertakings regarding power from shore have been limited to brand new offshore installations, mostly subsea, and the Troll A gas pre-compression units.

1.4 Aim and Outline of the Thesis

In this thesis work, the behaviours of different wind turbine generator technologies during electromechanical transients have been explored. The simulated event was a direct on line (DOL) start up sequence of a large motor on a relatively small generating capacity. This incident caused fluctuations in both the voltage and the frequency of the isolated utility system.

The first parts of this report give an introduction to the challenges studied, and theoretical background information. Later, the developed models and their behaviour are studied in detail. For increased readability, the detailing of the offshore oil platform utility system was added as an appendix.

Sections 4 and 5, as well as appendices 2 to 6, cover the development of models for wind turbines based on squirrel cage and doubly fed induction generators. For the DFIG model, a stator current controlling strategy was chosen, which could affect the outcome of the simulations. However, it would be equally easy to model and simulate a rotor current controlling strategy.

A stator flux feed forward term was developed for the speed control loop of the doubly fed induction generator. The purpose of this term was to stabilise the power output throughout the transient events. Also, an AC voltage reactive compensator control scheme for stabilising the voltage at the gas turbine generators' terminals was investigated.

1.4.1 Simplifications

Magnetic saturation, temperature variations, asymmetric load situations and other control loop detuning effects have been neglected for all the wind turbine systems throughout the final simulations. However, the control loops were tested for detuning effects and found stable during initial testing.

2 Theoretical Background

2.1 The Rotating Reference Frame and the Phase Locked Loop

When modelling electrical machines, it is often useful to transform three phase variables into quantities rotating in synchronism with the rotor, as for synchronous machines, or another rotating reference. This practice dates all the way back to the works of André Blondel [12] and is commonly used for vector control of power converters as well as for describing dynamic data for synchronous machines. The transformational technique used most frequently today is known as the Park transformation or the dq0 transformation [12], [13], [14].

By transforming the three phase variables we end up with quantities referred to as an orthogonal coordinate system. The three dimensions are described by the direct (d), quadrature (q) and zero-sequence (0) axes. The d-axis follows the reference and the q-axis is perpendicular to this axis in the rotating plane. However, there is a slight variation in practice with respect to the direction of the quadrature axis. In this thesis the direction is chosen to be 90 electrical degrees ahead of the d-axis. The same practice is used in IEEE Std. 1110-2002 [12] and by P. Kundur in [13]. This is the opposite direction of the one used in [14] and in the PSCAD Master Library abc-to-dq0 transformation block [15].

Figure 3.1 illustrates how the chosen direct and quadrature axes can be rotated with respect to the fixed axes of the three phase system.

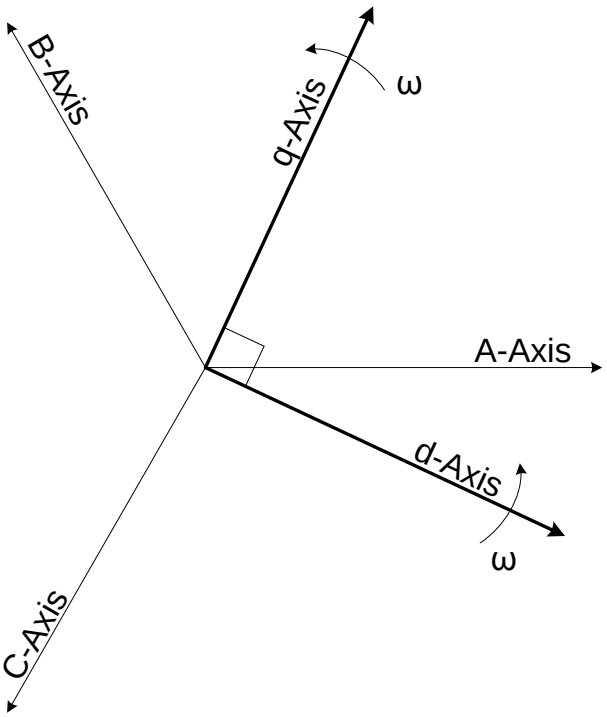

Figure 2.1 - D-q-axis Coordinate System Rotating Around the Neutral Point of a Stationary Three Phase System.

The version of the Park transformation matrix used for this thesis work is written:

$$\begin{bmatrix} i_d \\ i_q \\ i_0 \end{bmatrix} = \frac{2}{3} \begin{bmatrix} \cos(\theta) & \cos\left(\theta - \frac{2\pi}{3}\right) & \cos\left(\theta + \frac{2\pi}{3}\right) \\ -\sin(\theta) & -\sin\left(\theta - \frac{2\pi}{3}\right) & -\sin\left(\theta + \frac{2\pi}{3}\right) \\ \frac{1}{2} & \frac{1}{2} & \frac{1}{2} \end{bmatrix} \begin{bmatrix} i_a \\ i_b \\ i_c \end{bmatrix} \quad (2.1)$$

The inverse transformation matrix is:

$$\begin{bmatrix} i_a \\ i_b \\ i_c \end{bmatrix} = \frac{2}{3} \begin{bmatrix} \cos(\theta) & -\sin(\theta) & 1 \\ \cos\left(\theta - \frac{2\pi}{3}\right) & -\sin\left(\theta - \frac{2\pi}{3}\right) & 1 \\ \cos\left(\theta + \frac{2\pi}{3}\right) & -\sin\left(\theta + \frac{2\pi}{3}\right) & 1 \end{bmatrix} \begin{bmatrix} i_d \\ i_q \\ i_0 \end{bmatrix} \quad (2.2)$$

The symbol θ notes the angular difference between the d-axis and the a-axis. A rotating reference makes this angle time-variant. For power electronic applications this reference is found using a phase locked loop (PLL).

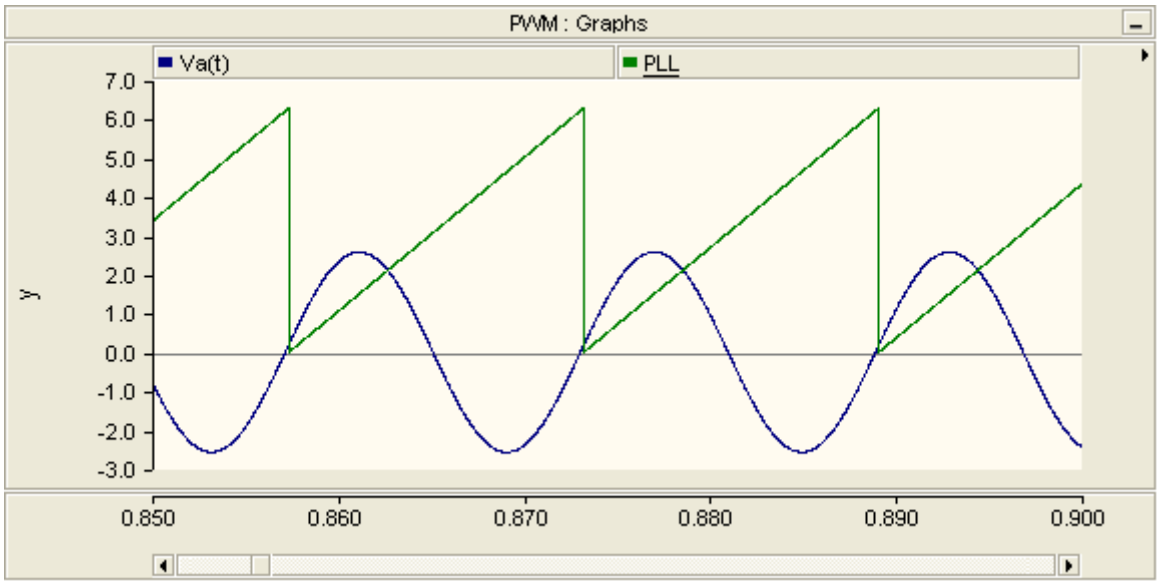

Figure 2.2 – PLL Tracking the Zero Crossing of the A-axis Voltage.

An example of the phase locked loop's output in PSCAD is illustrated in the figure above. The PLL gives an angular output in radians which is reset at each a-phase voltage zero crossing. This information could be used to find the angular position of the rotating instantaneous voltage vector referred to the a-phase by subtracting $\frac{\pi}{2}$ radians. The PLL signal would then be shifted to reset at each A-phase positive voltage maximum.

The phase locked loop can also be used to estimate the rotational frequency of the reference by deriving the angular position. The relation is given below.

$$\frac{d\theta}{dt} = \omega = 2\pi f \tag{2.3}$$

This calculation is done by the PLL module which is featured in the PSCAD Master Library. When the phase locked loop is used in a system subjected to disturbances and harmonic content it will have a frequently oscillating output which needs to be filtered using a low-pass filter. The filter will cause a certain delay in the time-response of the frequency estimation. Simulations done as part of the thesis work confirms that frequency changes at the simulated offshore utility grid happens at a relatively slow rate compared to the frequency of the disturbances. Thus it should be an easy task to choose a filter that fulfils the requirements by giving a steady and accurate output signal.

By experimental trial and error it was found that it was sufficient for this system to have a small low pass filter which gives the following transfer function from tracked frequency (f1) to a smoothed frequency estimate (f2).

$$f2 = f1\frac{1}{1+0.001S} \tag{2.4}$$

Figure 2.3 - Tracked frequency PLL output vs. Smoothed frequency estimate clearly shows how this filter compensates for major parts of the oscillating error caused by the phase locked loop's tracking of the rotating reference. The tracked frequency output of the PLL is fluctuating due to disturbances and imperfect sine-waves of the input signals, but the frequency estimate is relatively smooth and accurate. Y-axis gives the values (in Hz) of the two frequency estimates. Time is given by the horizontal X-axis.

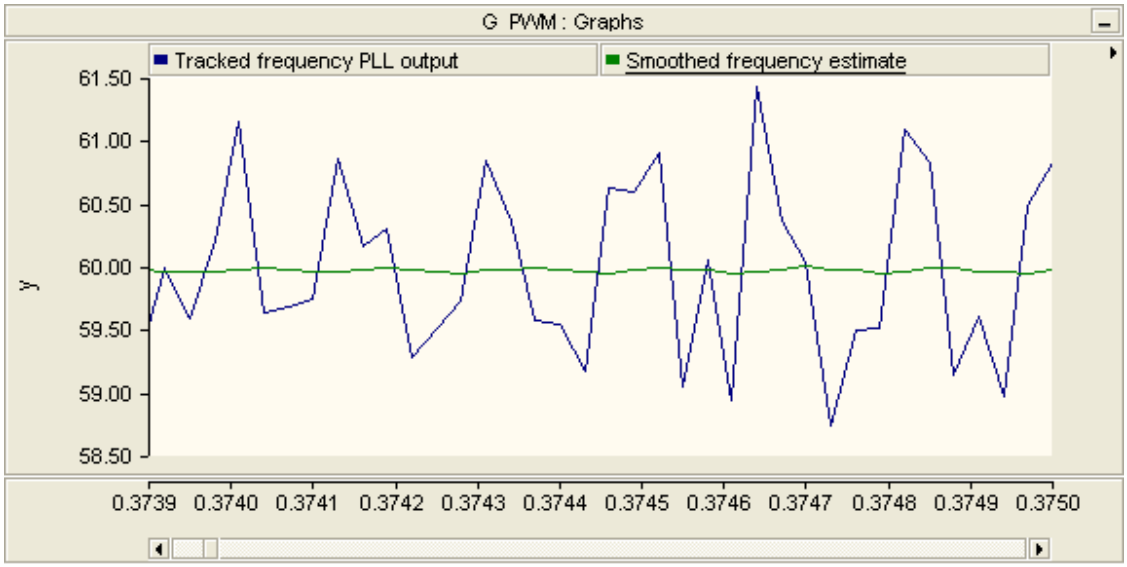

Figure 2.3 - Tracked Frequency PLL Output vs. Smoothed Frequency Estimate

2.2 The Peak Value Based Per Unit System

Throughout this report there will be made calculations in the synchronous rotating reference frame with instantaneous values. All these calculations will be referred to the peak value based per unit system. This also counts for control loops made for the doubly fed induction generator. The purpose of this section is to explain the peak value based per unit system and why it is used when dealing with instantaneous values referred to the synchronous rotating reference frame.

As for the well known RMS value based per unit system, the purpose is to simplify calculations. The difference is that we use peak values for voltages and currents as bases. We have the following relations:

Phase voltages:

$$u_{base,peak} = U_{base,RMS} \cdot \sqrt{2} \tag{2.5}$$

Phase currents:

$$i_{base,peak} = I_{base,RMS} \cdot \sqrt{2} \tag{2.6}$$

Powers:

$$S_{base,peak} = S_{base,RMS} = \frac{3}{2} u_{base,peak}\, i_{base,peak}^{*} \tag{2.7}$$

Impedances:

$$Z_{base,peak} = Z_{base,RMS} = \frac{u_{base,peak}}{i_{base,peak}} \tag{2.8}$$

Angular velocity:

$$\omega_{base} = 2 \cdot \pi \cdot f_{base} \tag{2.9}$$

It is assumed that the reader should be able to utilize the given values in order to find other bases e.g. for inductance and capacitance bases.

There are several benefits of using the peak value based per unit system e.g.:

- Instantaneously measured quantities with a value of 1 correspond to the rated values. As an example this could be used when limiting the size of current references for the converters.
- There is no need to include an ideal voltage step-up transformer in the doubly fed induction machine model as this is dealt with by the base values.
- It is not necessary to include the factor $\frac{3}{2}$ in power and electrical torque relations as it is already included by using the peak based per unit system.

2.3 The Fifth Order Induction Machine Model in the Rotating Reference Frame

Figure 2.4 depicts the fifth order induction machine model, which will be used as basis for control loops and general analysis in this thesis. Motor convention was used as both stator and rotor currents have positive direction into the machine. The model is also known as the electromagnetic transient model. No presence of an ideal transformer indicates that the model is made suitable for per unit equations. It is assumed that the reader is familiar with induction machine parameters and that no detailed explanation is necessary.

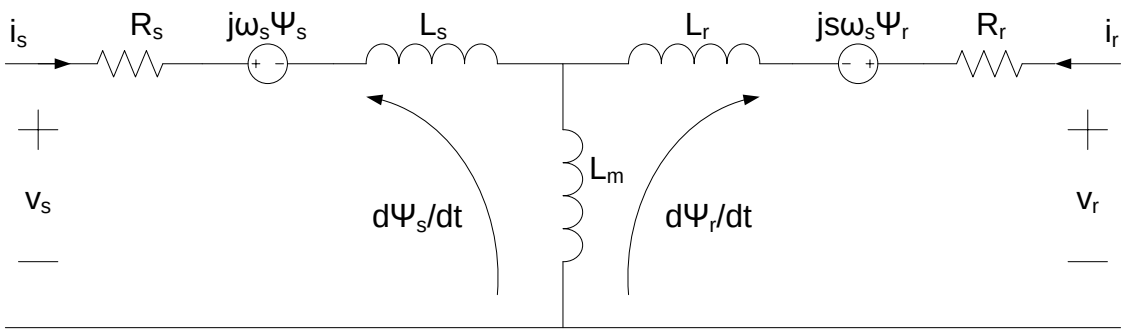

Figure 2.4 - The Fifth Order induction Machine Model

A squirrel cage induction generator has a short circuited cage in the rotor. To model this type of induction machine the rotor voltage is set to zero.

The model in figure 2.4 has a rotating reference which is not specified. In this thesis the stator flux was chosen as a direct axis reference. By doing this, we get the following relations:

$$\psi_{qs} = 0 \tag{2.10}$$

$$\frac{d\psi_{qs}}{dt} = 0 \tag{2.11}$$

Figures 2.5 and 2.6 on the next page explains how we end up with two circuit equivalents for the induction machine in the synchronous rotating reference frame; one for the d-axis and one for the q-axis.

Please note that another rotating reference could have been chosen, but this would have given different circuit equivalents.

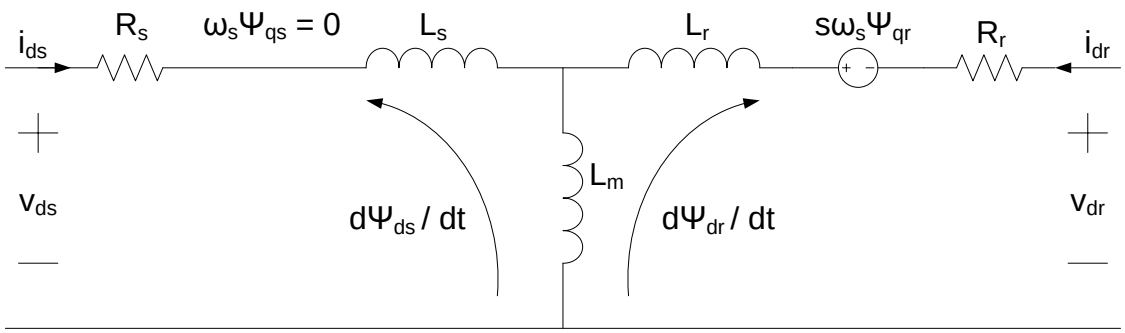

Figure 2.5 - Direct Axis Circuit Equivalent for the Fifth Order Induction Machine Model

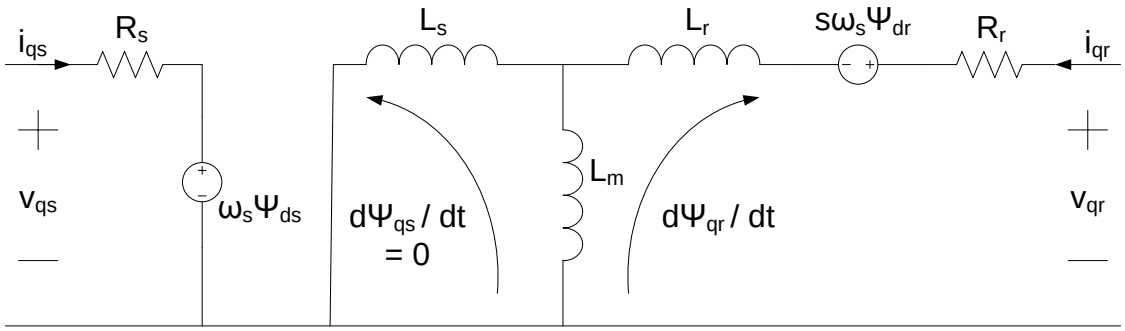

Figure 2.6 - Quadrature Axis Circuit Equivalent for the Fifth Order Induction Machine Model

Quadrature axis voltage and direct axis flux are strictly perpendicular in the d-q coordinate system, but with a small difference in magnitude determined by the quantities of i_{qs}, R_s and ω_s. Also, based on equations found in [13], [16], it could be shown that for a stator flux oriented model the electrical torque could be expressed as:

$$T_{el} = \psi_{qr} i_{dr} - \psi_{dr} i_{qr} \tag{2.12}$$

Please note that the sources do not refer the equations to a peak value based per unit system.

Using the expressions found for rotor currents and fluxes in section 5.3 we get:

$$T_{el} = A i_{qs} \left(\frac{\psi_{ds}}{L_m} - \mathrm{Bi_{ds}} \right) + \mathrm{Bi_{qs}} (C\psi_{ds} + A i_{ds}) \tag{2.13}$$

$$T_{el} = A i_{qs} \left(\frac{\psi_{ds}}{L_m} \right) + \mathrm{Bi_{qs}} (C\psi_{ds}) \tag{2.14}$$

$$T_{el} = A i_{qs} \left(\frac{\psi_{ds}}{L_m} \right) + \mathrm{Bi_{qs}} (C\psi_{ds}) \tag{2.15}$$

$$T_{el} = (1 - \mathrm{BC}) i_{qs} \psi_{ds} + \mathrm{BCi_{qs}} \psi_{ds} \tag{2.16}$$

$$T_{el} = i_{qs} \psi_{ds} \tag{2.17}$$

This equals to:

$$T_{el} = i_{qs} \left(\frac{v_{qs} - R_s i_{qs}}{\omega_s} \right) \tag{2.18}$$

It would be natural to control the speed by controlling the q-axis current. The d-axis current could be used to control reactive power. The philosophy is that a positive current in the q-axis will consume active power from the grid. Negative q-axis current will deliver active power to the grid. A positive current in the d-axis delivers reactive power to the grid, etc.

The figures will be helpful for readers investigating section 5.3.

2.4 Expected Squirrel Cage Induction Machine Behaviour Based on First Order Model

A lot of information can be derived from the general response of a squirrel cage induction machine by just looking at the steady state characteristics. The figure below illustrates a single cage model of an induction machine. Calculations are given for RMS value based per unit system.

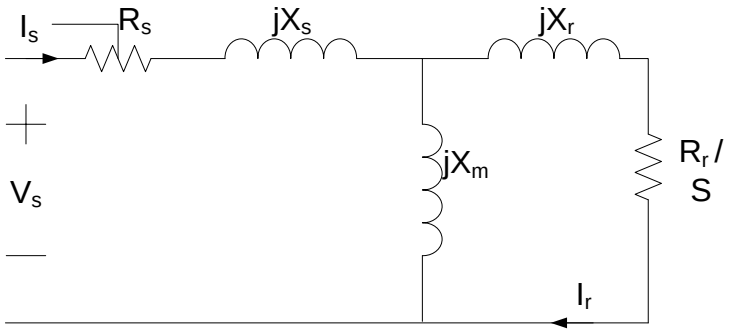

Figure 2.7 - First Order Model of a Squirrel Cage Induction Machine

Xm is usually relatively high and can be transferred to the stator terminals without unacceptable error in the further calculations. We get the relation:

$$I_s \approx \frac{V_s}{\left(R_S+\frac{R_r}{s}\right)+j(X_s+X_r)} + \frac{V_s}{X_m} \tag{2.19}$$

Further: (slip is relatively low -> simplifications)

$$S_s = P_s + jQ_s = V_s I_s^* = \frac{|V_s|^2}{\left(R_S+\frac{R_r}{s}\right)-j(X_s+X_r)} + \frac{j|V_s|^2}{X_m} \tag{2.20}$$

$$P_s = Re(S_s) = \frac{\left(R_S+\frac{R_r}{s}\right)|V_s|^2}{\left(R_S+\frac{R_r}{s}\right)^2+(X_s+X_r)^2} \approx \frac{s|V_s|^2}{R_r} \tag{2.21}$$

$$Q_s = Im(S_s) = \frac{(X_s+X_r)|V_s|^2}{\left(R_S+\frac{R_r}{s}\right)^2+(X_s+X_r)^2} + \frac{|V_s|^2}{X_m} \approx \frac{s^2(X_s+X_r)|V_s|^2}{{R_r}^2} + \frac{|V_s|^2}{X_m} \tag{2.22}$$

Torque expressions:

$$T_{el} = \frac{|I_r|^2 R_r}{s\omega_s} = \frac{|V_s|^2 R_r}{s\omega_s\left(\left(R_S+\frac{R_r}{s}\right)^2+(X_s+X_r)^2\right)} \approx \frac{s|V_s|^2}{\omega_s R_r} \tag{2.23}$$

$$T_{el} - T_{mech} = J\frac{d\omega_{mech}}{dt} \tag{2.24}$$

The expression for slip gives:

$$s = \frac{\omega_s - \omega_{mech}}{\omega_s} = 1 - \frac{\omega_{mech}}{\omega_s} \tag{2.25}$$

$$\frac{s}{\omega_s} = \frac{\omega_s - \omega_{mech}}{{\omega_s}^2} \tag{2.26}$$

2.4.1 Voltage Variation

Based on equations (2.21) to (2.23) a voltage drop should give even higher relative drops in real power, reactive power and electrical torque.

2.4.2 Frequency Variation

When frequency changes, the induction machine's moment of inertia (J) will determine how well the machine can follow the synchronous speed. The heavier the rotor is, the higher the probability is for large changes in slip. A sudden decrease in frequency causes a decrease in slip, which again causes induction machines to decelerate. This means that motoring units will draw less power, and generating units will produce more until they reach their torque equilibrium.

Reactive power will be even more dramatically affected by a change in slip. The disturbance is approximately related to the slip squared at the operating point. Motors will consume less power, generators more.

As seen from (2.21), (2.23) and (2.25), a small but rapid change in synchronous speed (frequency) could heavily affect the power drawn by the motor and its electrical torque. In the event of a sudden frequency drop as a consequence of a DOL motor start, the motors running prior to the start up sequence are expected to draw less power. Also, SCIG based wind turbines are expected to deliver extra power since they operate with negative slip and have a high moment of inertia. The opposite will happen in the case of a sudden rise in frequency.

The conclusion can be drawn that the heaviest induction machines will dampen the frequency variation.

2.4.3 General Remarks

Results from dynamic simulations will vary from calculations based on the steady state induction machine model.

Reference is made to the first part of section four where the behaviour of a squirrel cage induction generator in the specific case is discussed.

3 Offshore Oil Platform Model

It is of interest to simulate wind turbines that are subjected to fluctuations in frequency and terminal voltage, such as fluctuations caused by a load change in the utility grid of an offshore oil platform. For this purpose, a case model in PSCAD was built. A visual overview of the platform is given by the figure below:

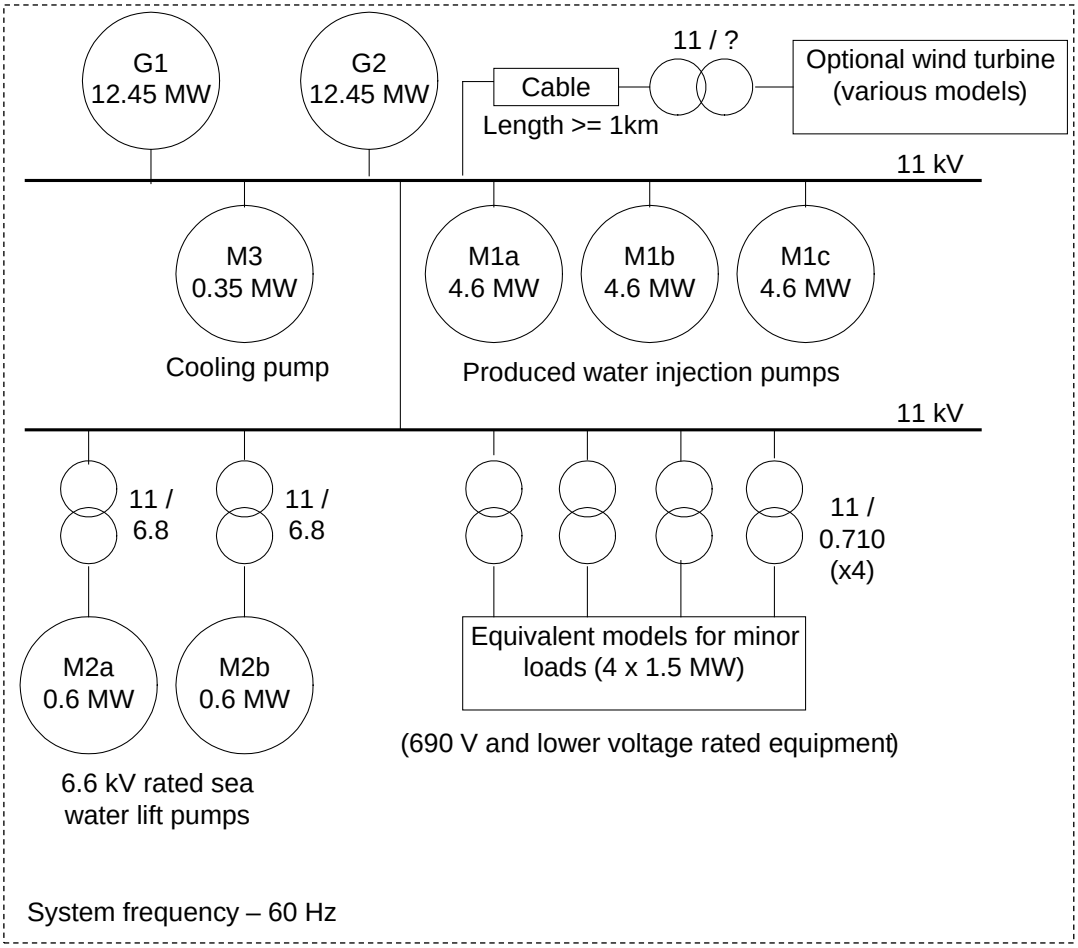

Figure 3.1 - Overview of the Offshore Oil Platform Utility Grid

The simulated utility grid contains dynamic models of:

- Two 12.45 MW gas turbine generators
- Transient load models, e.g. start up model of produced water injection pump
- Two water injection pumps
- Two sea water lift pumps
- A cooling pump
- Equivalents for minor loads, e.g. heating, lighting, control systems and auxiliary
- Optional wind turbine generator attached by subsea cable

Full details about the configuration of the power system case model and the implementation in PSCAD are included in appendix 1.

A series of tests were conducted while modelling the offshore utility grid. Figure A1.8 in appendix 1 illustrates how the start up sequence model of a produced water injection pump was tuned into matching specifications.

Other tests were performed such as:

- Tests of generator models with quick set ups of reactance and resistance loads. Voltage and frequency were observed as they recovered to acceptable levels.
- Test of each motor connected to a perfect voltage source in order to verify that it draws the correct amount of active and reactive power. This also includes a test of the M1, M2 models of coherent machines compared to two models of the same machines.
- General tests with different parameter alterations on governors and automatic voltage regulators.

None of these tests have been found important enough to include figures in this report.

Two major findings resulted from the preliminary tests. The first one was that the generator models internal output for power measurement was rapidly varying and somewhat oscillatory. Therefore it was decided to use an external power meter to give input for the governors. Generator speed or a PLL frequency output has to be used in order to find a frequency estimate. In theory, a FFT function can do the trick as well, but the standard models from PSCAD treat each phase individually.

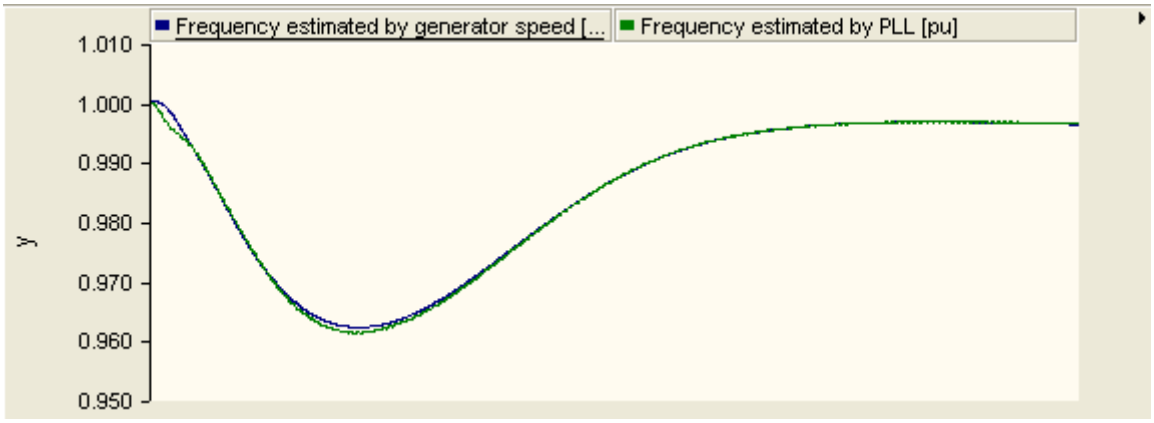

Figure 3.2 - Comparison of Frequency Estimates by Generator Speed (blue) and by PLL Output (green).

Figure 3.2 illustrates how PLL frequency estimate and generator speed varies trough the initialization of the modelled system. The time frame is approximately two seconds. Any deviation between the two estimates will be very low, and therefore frequency measurements will be based on generator speed in the parts of this thesis covering system analysis.

Since PSCAD lacks the opportunity to set initial values by data found from load flow calculations, the system gives a highly dynamic behaviour throughout the initializing

sequence. It takes approximately 15 simulated seconds before any dynamic simulation could be conducted with reliable results. This could mean several hours waiting time when simulating large systems at small time steps for models that include power electronic switching.

3.1 Simulation: Power from Gas Turbines, DOL Motor Start Up Sequence

The first simulation of the power system is a direct on line start up of the produced water injection pump model. Measured parameters from the generator module are illustrated in the figure below.

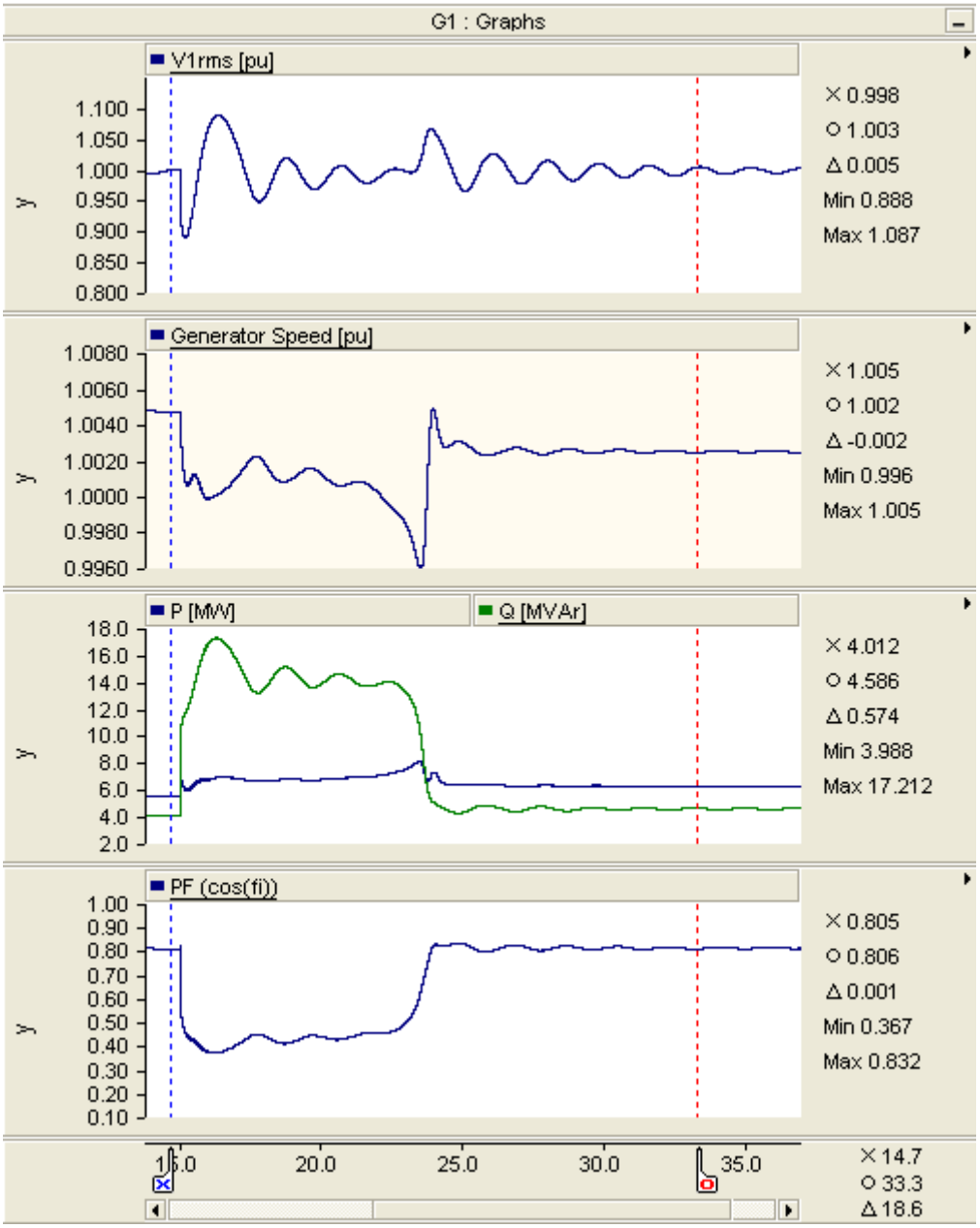

Figure 3.3 - Generator Terminal Voltage, Generator Speed, Active and Reactive Power Delivered to Grid and the Generators' Power Factor during the DOL Start Up Sequence

It can be clearly seen that the motor draws a lot of active and reactive power throughout the start up sequence. This causes a voltage disturbance which has to be compensated by the AVR. It also causes a drop in frequency. A certain part of the frequency variation is caused by the droop function in the gas turbine governors' control loop.

The following observations were made from the initial case model:

Table 3.1 - Gas Turbine Generator Terminal Voltage, Initial Test Case

Incident:	**Voltage [pu]:**	**Time [seconds]:**
Initial value:	0.998	15.00
Low peak:	0.888	15.18
Low peak:	0.946	17.82
Low peak:	0.966	19.66
High peak:	1.064	23.89
High peak:	1.024	26.07
High peak:	1.013	28.00

The reason for using three high values from the beginning and three low values from the end is that this will make it easy to find the recovery time by curve fitting, if needed for a comparison.

Table 3.2 - Gas Turbine Generator Speed, Initial Test Case

Incident:	**Speed [pu]:**	**Time [seconds]:**
Initial value:	0.997	15.00
Low peak at beginning of start up:	0.986	15.92
Low peak at motor torque peak:	0.981	23.14
Stable value after start up sequence:	0.994	40.00

The maximum value for real power was measured to 12.735 MW drawn from each generator. This is slightly higher than the generators are rated for. Observed behaviour may indicate that the simulated load situation could be a somewhat extreme compared to what can be expected in a real system. Also, the motor draws a very high start up current that could lead to overheating of the generator windings.

Frequency transient response is quite far from the IEC limits, but the change rate is high. The voltage deviation will also put the equipment to a test. Based on the information above, it seems like some of the running motors have to be stopped in order to simulate more severe transients.

Figure 3.4 below depicts the dynamic behaviour of the motor at start up. The source of the torque scatter on the torque-speed characteristic is unknown to the author.

Motor start up time is approximately unchanged, but other values vary. The figure was added to illustrate that most of the fluctuations in both active and reactive power are caused by the started motor.

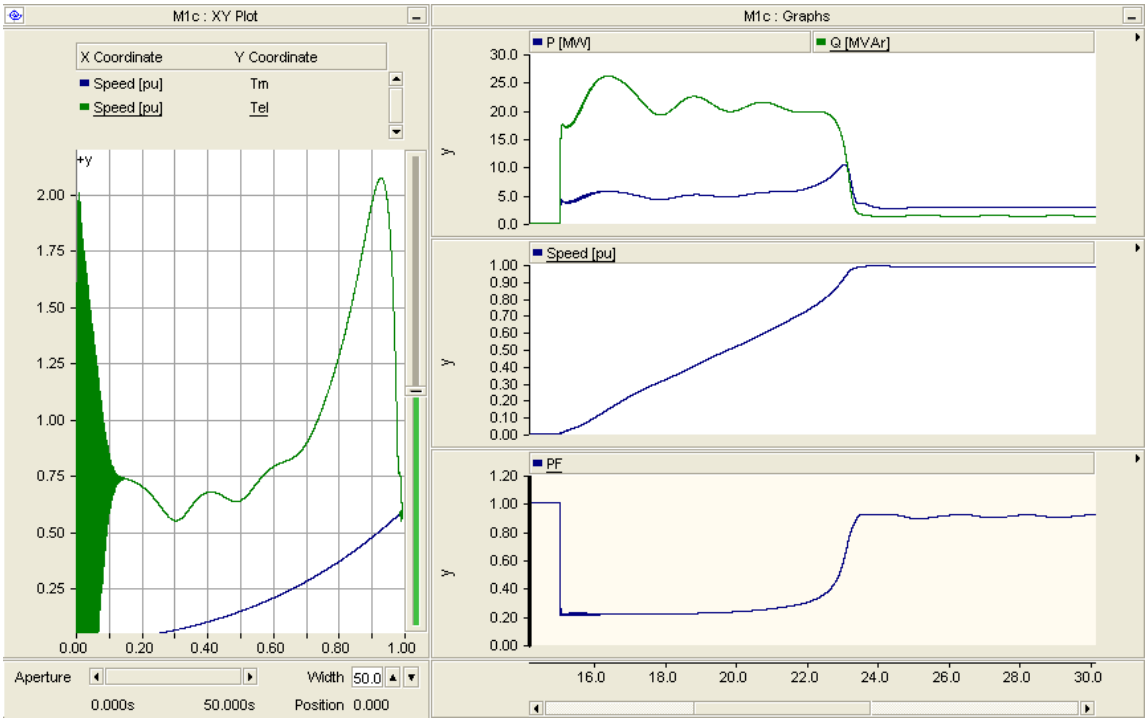

Figure 3.4 - Torque-Speed Characteristics, Active & Reactive Power, Speed and Power Factor for the Simulated Motor Start Up Sequence

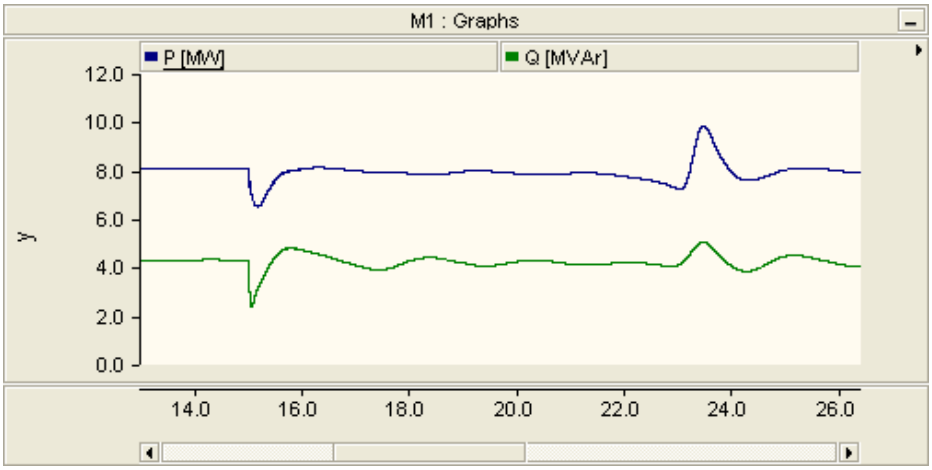

Figure 3.5 - Active and Reactive Power of the Two Pre Running M1 Type Motors

Figure 3.5 illustrates the active and reactive power drawn by the two pre-running water injection pumps. The power peaks coincide as expected with the most rapid changes in frequency and the voltage peaks. The reader is referred to section 2.4 where the first order model of an induction machine is discussed.

3.1.1 Modification of Simulated Case in Order to Achieve Faster Fluctuations

In order to get a faster frequency variation, the two running produced water injection pumps will be stopped throughout the remainder of the simulations. Hereby, it is the first of the tree water injection pumps that are started. The rest of the system remains unchanged.

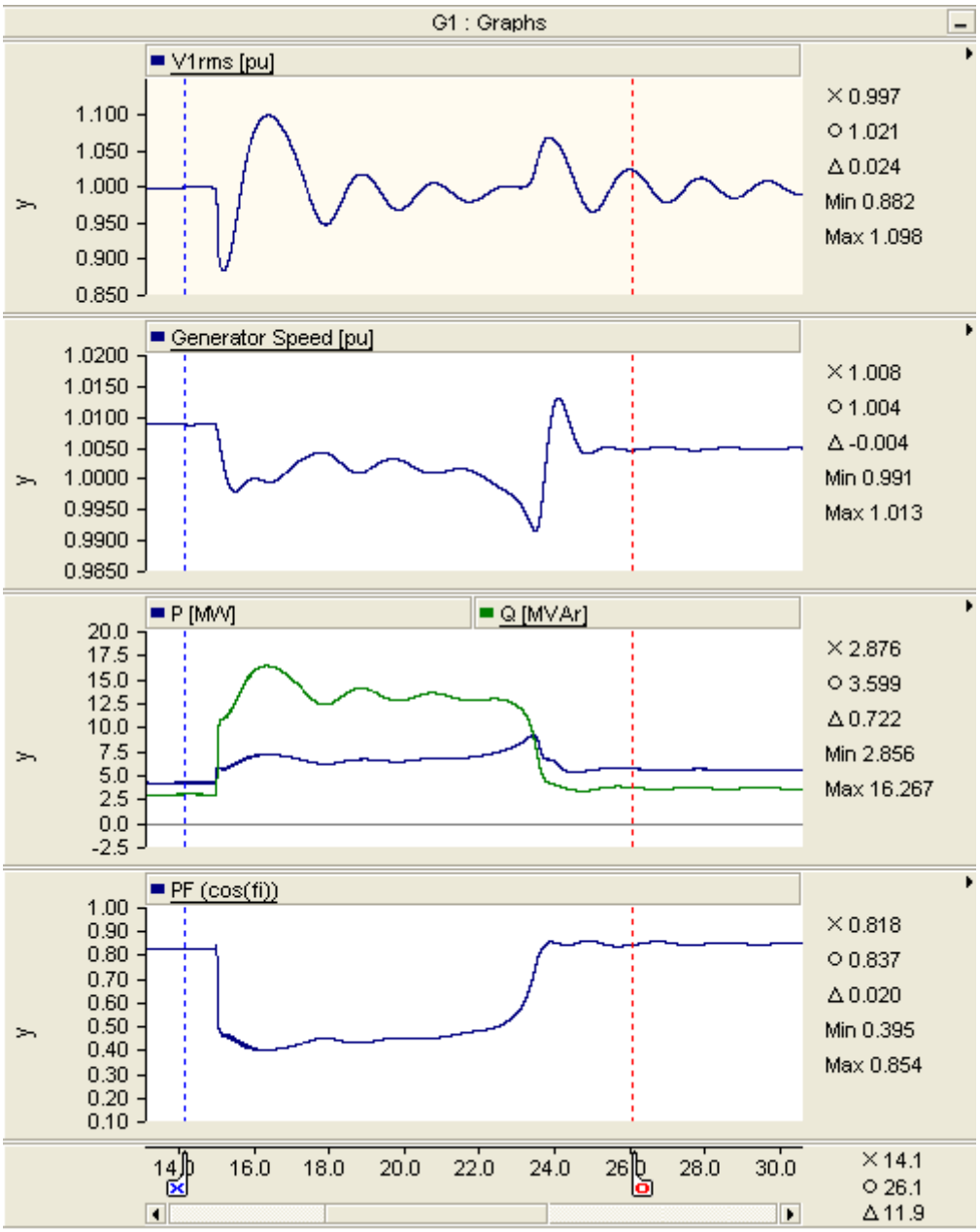

Figure 3.6 - Generator Terminal Voltage, Generator Speed, Active and Reactive Power Delivered to Grid and the Generators' Power Factor during the modified DOL Start Up Sequence

As seen from the figure, the frequency change rate is higher for this load situation. From measurements given on the next page it can be seen that the magnitudes of voltage and frequency deviation are quite similar to the first simulation.

The following observations were made for the modified case model:

Table 3.3 - Gas Turbine Generator Terminal Voltage, Modified Test Case

Incident:	**Voltage [pu]:**	**Time [seconds]:**
Initial value:	0.997	15.00
Low peak:	0.882	15.20
Low peak:	0.946	17.90
Low peak:	0.966	19.88
High peak:	1.067	23.86
High peak:	1.022	25.99
High peak:	1.010	27.97

Table 3.4 – Gas Turbine Generator Speed, Modified Test Case

Incident:	**Speed [pu]:**	**Time [seconds]:**
Initial value:	1.008	15.00
Low peak at beginning of start up:	0.998	15.47
Low peak at motor torque peak:	0.991	23.49
Stable value after start up sequence:	1.004	40.00

The development of a new model with even lower frequency peak will only be conducted if the need arises in later simulations. General statements based on observations and circuit equivalent calculations could be done without further simulations.

The simulated DOL start up sequence will be a good test for wind turbines, and is likely to uncover some of the challenges wind turbines will be subjected to in offshore power applications.

4 Squirrel Cage Induction Generator

A model of a SCIG based wind turbine was developed. It is based on typical data found in [10]. This book states that a multi-mass and shaft model has to be included in fixed speed wind turbine simulations. The reason is that the slow rotating shaft of the rotor is relatively soft and, even more importantly, that the rotor blades are somewhat flexible. However, the shaft spring constant from the book gave oscillations with a frequency of 0.05 Hz when implemented into PSCAD. This is a rather low value compared to what could be expected. Also, a damping constant is not given. For this reason the values for shaft spring constant and damping found in [17] were used. All parameter values are supplied in appendix 2.

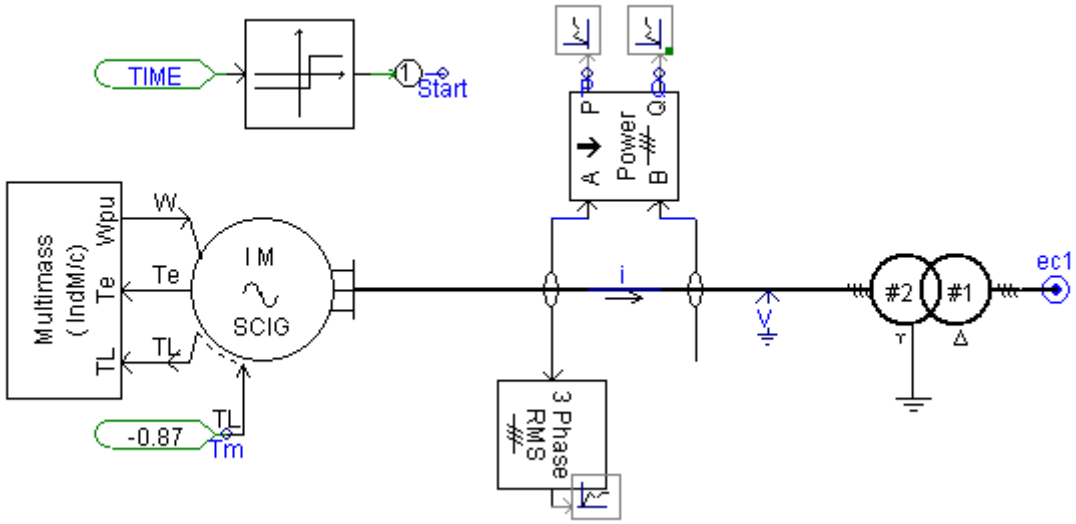

Figure 4.1 - Overview of the SCIG Based Wind Turbine Module

The module contains models for:

- A squirrel cage induction generator
- A two-mass and shaft model
- A transformer

It is assumed that no reactive compensation is desirable due to the relatively short distance between the wind turbine and the gas turbines. A capacitor bank in the wind turbine is not likely to be cost effective if gas turbine generators are capable of producing the reactive power needed.

The values used in this case are general, but it will give a rough estimate on how an SCIG based offshore wind turbine will behave in the event of electromechanical transient fluctuations. From initial tests the mutual damping seems quite high. Therefore, a simulation without any mutual damping was included as well.

To exclude any disturbances from wind variations from the test, a constant torque model was used for all simulations. If slip and losses are neglected, the rated torque on shaft could quickly be estimated to a value of about the rated power factor (0.87). Based on equations in section 2.4, some of the characteristics of the squirrel cage machine were plotted using MATLAB.

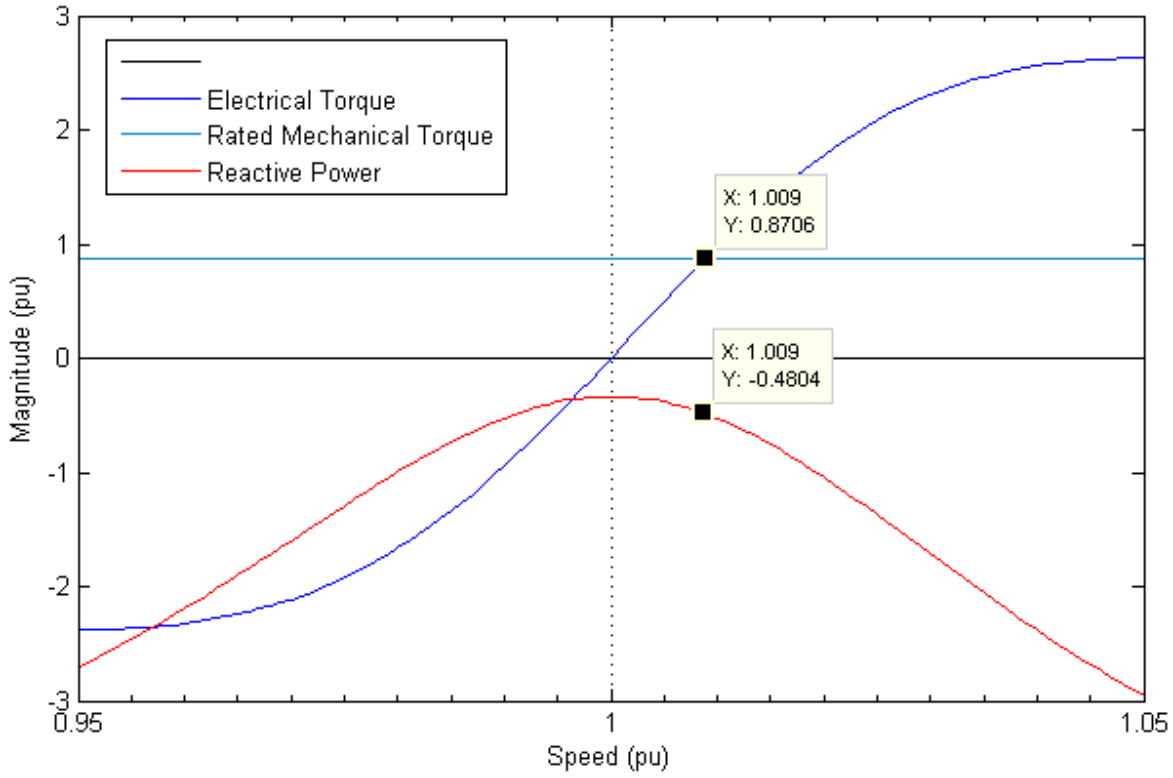

Figure 4.2 – Electrical Torque (blue) and Reactive Power (red) for Versus Speed of the SCIG at Rated Conditions. Rated Operating Point is Marked.

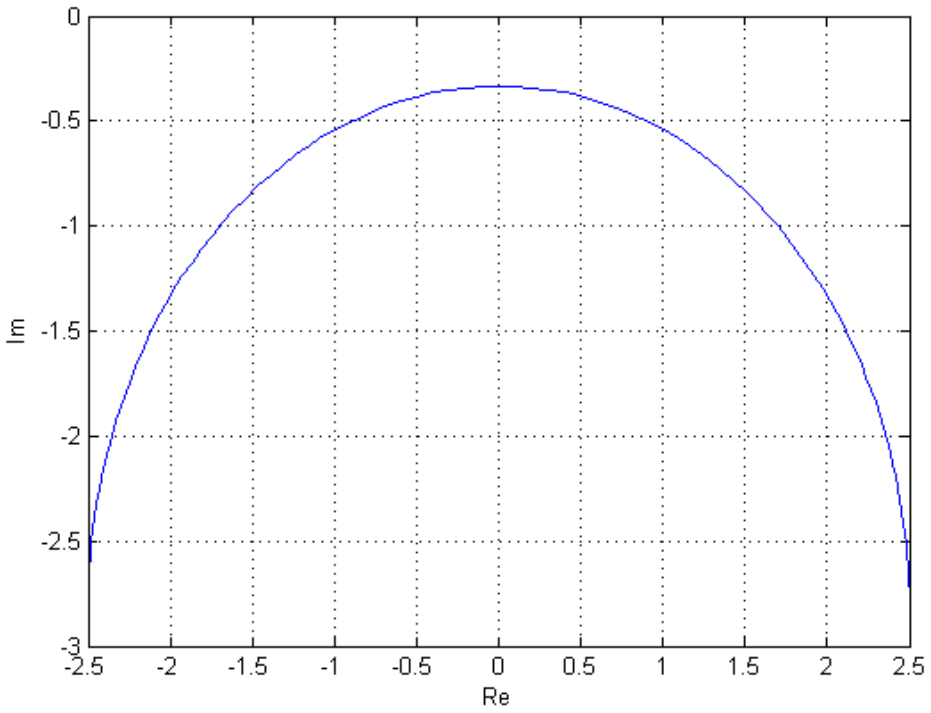

Figure 4.3 - Current Locus Characteristic of the SCIG

Figure 4.2 and Figure 4.3 on the previous page illustrate some of the properties that will affect the behaviour of the machine. If the rotor suddenly runs ahead of the torque equilibrium as a result of frequency change, additional torque and power will be generated. However, if the voltage drops at the same time, this will reduce torque magnitude. It will be interesting to see how these two conflicting properties will affect the response to the simulated case.

From Figure 4.2 it is apparent that the machine will draw more reactive power if the slip is decreased. Equation 2.22 shows that we also have two conflicting properties for reactive power when slip and voltage is decreased at the same time. As seen from Figure 4.3 and equation 2.22, a major part of the reactive power is drawn trough the mutual inductance. This part is also affected by a voltage drop. The resulting behaviour will be entirely dependent on the voltage and frequency trajectory throughout the transient event.

It is hard to predict the behaviour of the SCIG based wind turbine during the DOL motor start up sequence. Characteristics for torque, real and reactive power all have conflicting properties when the machine is subjected to a drop in frequency and voltage at the same time. The influences of a frequency drop and a voltage drop will to some extent counteract each other.

4.1 Simulations: SCIG Based Wind Turbine

4.1.1 SCIG Model Including Mutual Damping Coefficient

A simulation of the squirrel cage induction generator, based on wind turbine connected to the offshore oil platform during the direct on line motor start up, was conducted.

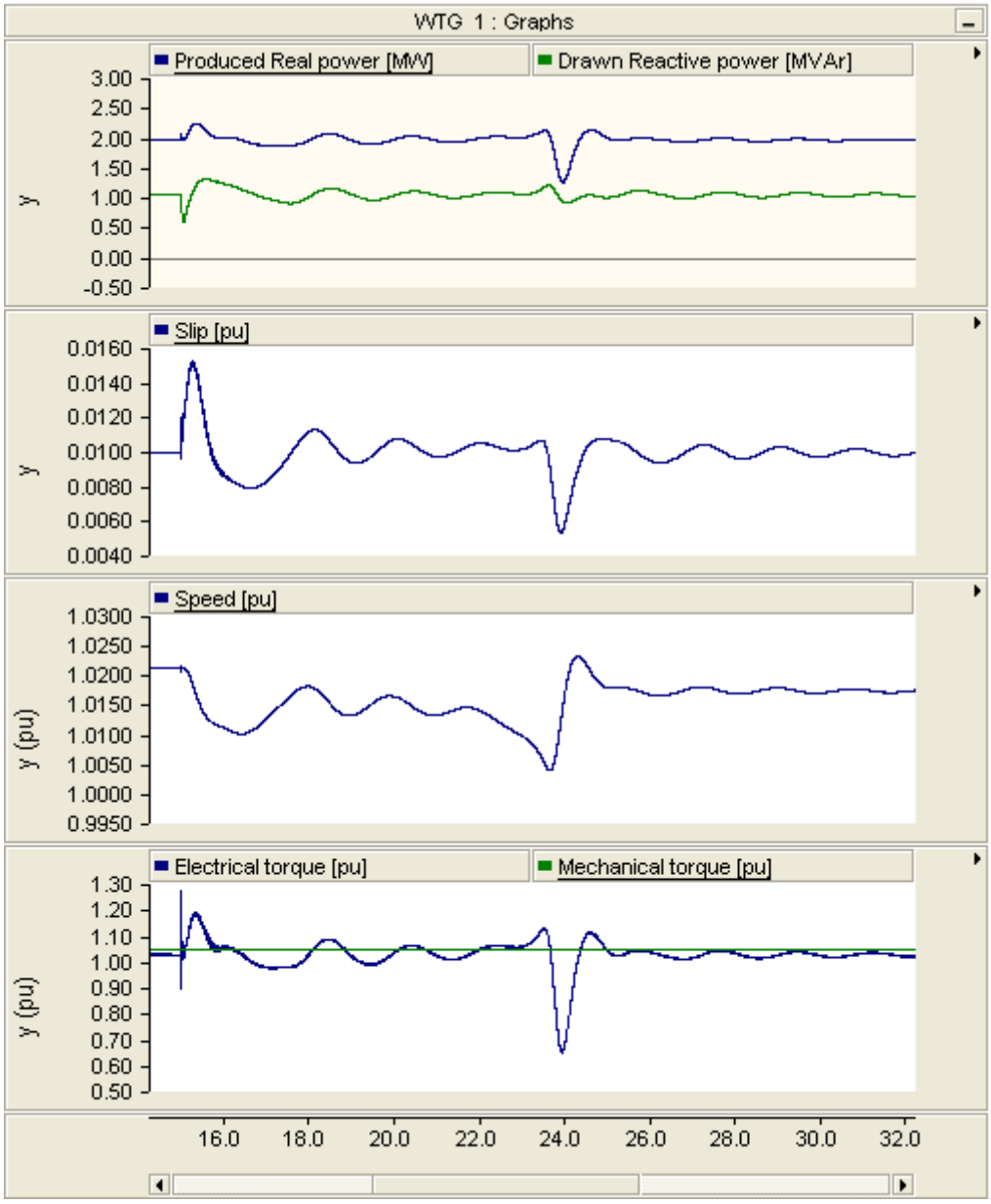

Figure 4.4 – Wind Turbine Produced Power, Consumed Reactive Power, Slip, Speed, Electrical and Mechanical Torque during the DOL Start Up Sequence

Comparing the figure above to figure 3.5, the disturbances for a generating induction machine are relatively low. However, the high moment of inertia makes a certain impact on the generated power and electrical torque when the started motor reaches full speed.

The behaviour of the gas turbine generators have also been observed during the simulations:

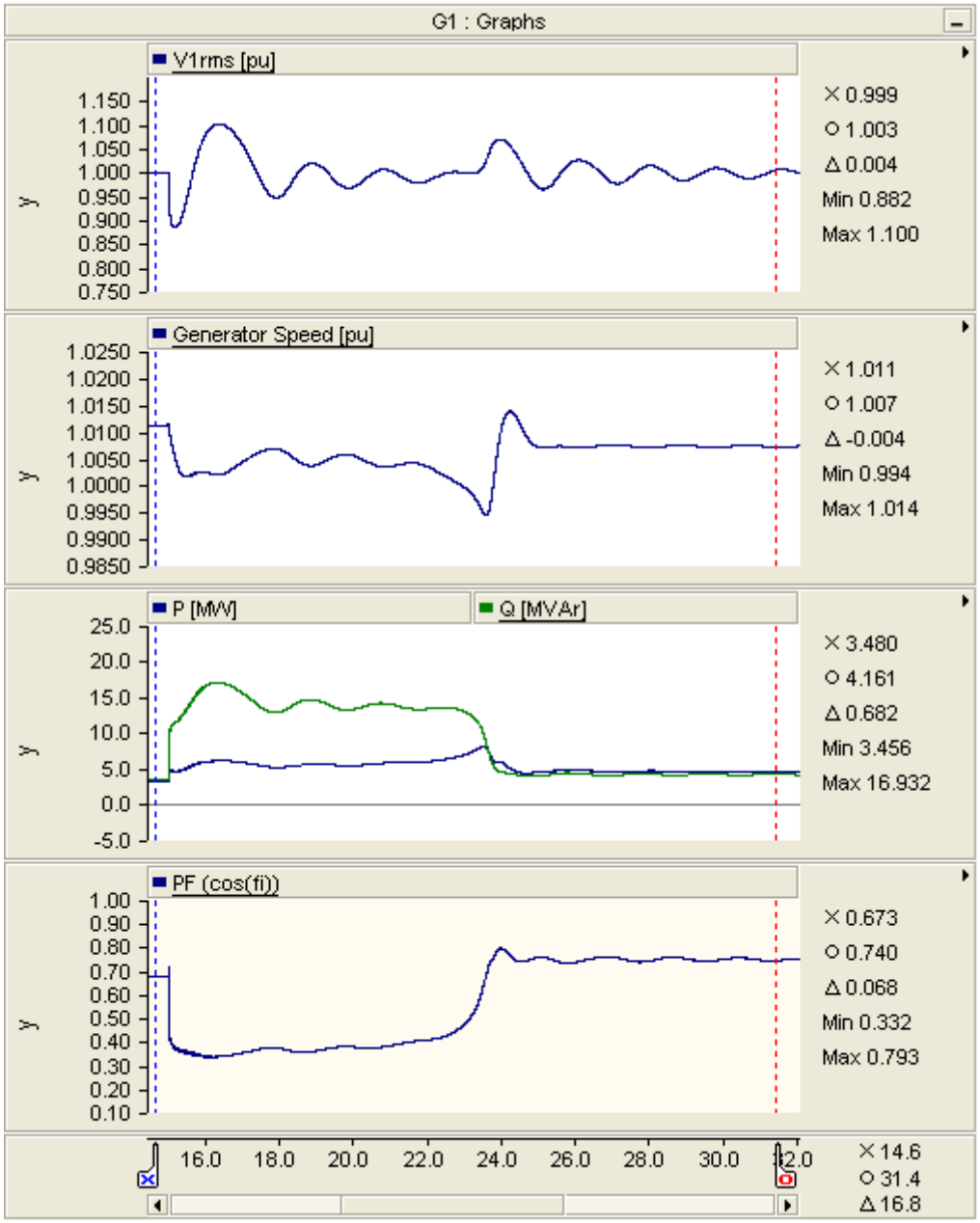

Figure 4.5 - Generator Terminal Voltage, Generator Speed, Active and Reactive Power Delivered to Grid and the Generators' Power Factor during the DOL Start Up Sequence

Comparing the results to figure 3.6, there is no evident changes in behaviour. Data has to be studied and are supplied on the next page. As seen from the tables, the changes are indeed negligible.

Table 4.1 - Gas Turbine Generator Terminal Voltage, DFIG Model Including Mutual Damping

Incident:	**Voltage [pu]:**	**Time [seconds]:**
Initial value:	0.999	15.00
Low peak:	0.882	15.18
Low peak:	0.944	17.89
Low peak:	0.966	19.88
High peak:	1.068	23.96
High peak:	1.024	26.10
High peak:	1.011	28.03

Table 4.2 - Gas Turbine Generator Speed, DFIG Model Including Mutual Damping

Incident:	**Frequency [pu]:**	**Time [seconds]:**
Initial value:	1.011	15.00
Low peak at beginning of start up:	1.001	15.49
Low peak at motor torque peak:	0.994	23.59
Stable value after start up sequence:	1.007	40.00

4.1.1.1 Discussion

The SCIG based wind turbine was not severely affected by the transient event. There were some minor rapid torque oscillations (vibrations) in the beginning of the start up sequence. Also, there was a dip in torque and power when the machine is reaccelerated.

Neither stator terminal voltage nor frequency trajectories were drastically changed from the model simulated in section 3.1.1.

4.1.2 SCIG Model Excluding Mutual Damping Coefficient

The same case as in section 4.1.1 was simulated without any mutual damping coefficient in the multi mass and shaft model.

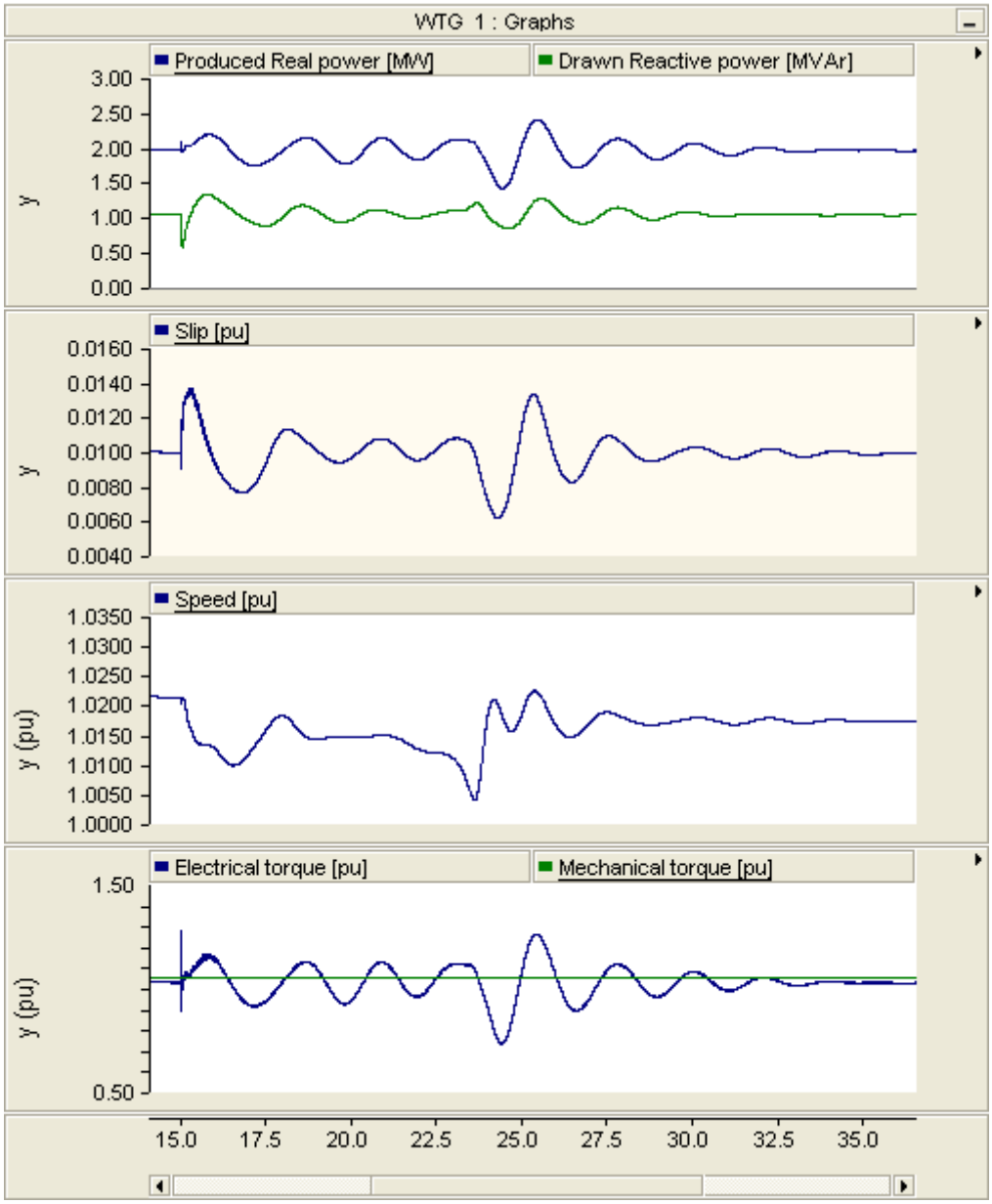

Figure 4.6 - Generator Terminal Voltage, Generator Speed, Active and Reactive Power Delivered to Grid and the Generators' Power Factor during the DOL Start Up Sequence

The observed parameter values are more oscillatory than for the case where damping was included. However, the variations in torque are slow and small enough to safely state that it will not inflict unacceptable stresses on the system.

Generator values were also observed, but were essentially unchanged from the first simulation.

5 Doubly Fed Induction Generator

Doubly fed induction generators are currently the market leading generator technology for wind turbines. This particular technology has to be studied in order to determine whether it can withstand the transient fluctuations of an offshore oil platform or not. As no standard models for such machines exist in PSCAD, it has to be developed from scratch. The next sections will cover the development of the DFIG parameters and controls used in later simulations.

The reader is referred to appendices 5 and 6 for figures, and especially to the figures A5.1, A5.6 and A5.8, which in combination gives an overview of the system and the control loops. The latest PI controller parameters were developed late in the process and are added in section 5.5.

No data or control schemes for existing doubly fed induction generators are made easily available in the public domain. Therefore the model was developed with general data. The emphasis when designing the control loops was to eliminate the disturbances made by fluctuations in voltage and frequency.

No fault ride through logic has been implemented in the DFIG's control loops.

5.1 Dimensioning and Modelling of a DFIG Based Wind Turbine Suited for Offshore Applications

Parameters for inductance, reactance and stator/rotor turns ratio for the simulated machine were found in [18]. However, this document contains no information about the sizing of the converter or other important parameters such as the converter or converter controls.

It is assumed that the power rating for a DFIG in offshore applications will be marginally higher than the rated real power output. The machine will generate additional heat when decelerating, and thus the MVA rating will limit how fast the machine can decelerate. It will also limit the amount, if any, of reactive power that can be produced trough the machine.

The rated real power should be taken as 2 MW. Parameters for the power rating (2.3 MVA) and the two mass and shaft models were unchanged from the first SCIG simulation.

Speed is chosen to vary from 0.7 to 1.3 pu.

The converters' power rating is chosen to be 700 kW, which is fairly close to 30% of the machine power rating.
Both converters are assumed to be six pulse PWMs and to use fast IGBT transistors with rated switching frequency in the range of 6-7 kHz. This is within the range of state of the art power electronics.

The transformer was given a higher impedance value in order to suppress harmonics generated by the converters.

Machine and transformer data are given in appendix 3.

5.1.1 DC Bus Voltage Level, Transformer Configuration, L Filter Parameters

The voltage level of the AC sides of the converter has to be determined in order to dimension the system properly. Voltages of the generators rotor terminals at no load can for example be found by a calculation using faraday's law of induction and knowledge about the different states, e.g. the slip, or it can be found quickly by simulating the machine at fixed speed at rated conditions with only voltage measurements connected to the rotor terminals. The figure below illustrates the results of such a test for this machine. The peak value on this machine was measured to be just about 381 kV.

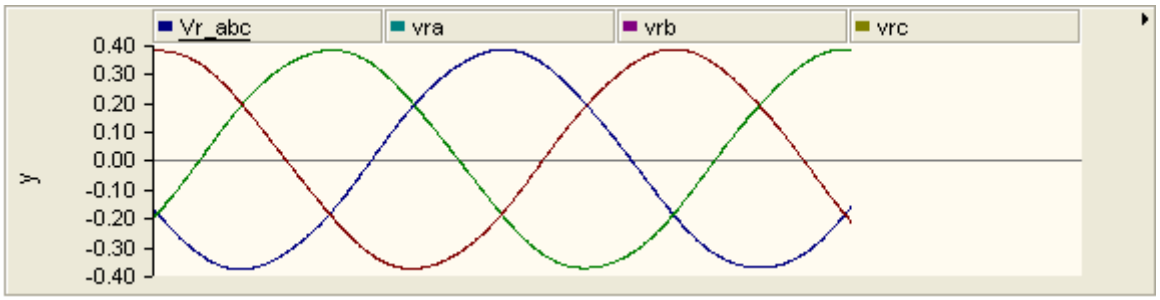

Figure 5.1 - Rotor Voltages at Rated Conditions, Open Rotor Terminals

The machine has to be able to operate at 20% overvoltage as a result of the transients on the offshore oil platform. This means that the maximal rotor voltage at no load could be taken as 457 V, i.e. the voltage increase is proportional on the stator and rotor sides. This could be calculated into a value in the peak based per unit system as follows:

$$vr = \frac{vr,peak}{vr,ref} \tag{5.1}$$

$$vr,ref = \frac{690\ V}{\sqrt{3}}\sqrt{2}\frac{1}{0.4333} = 1300.2\ V \tag{5.2}$$

$$vr = \frac{457}{1300.2} = 0.351\ pu \tag{5.3}$$

In addition, there will be a voltage drop caused by leakage fluxes and resistances when the generator delivers active or reactive power. Using the induction machine parameters from appendix 3, equations based on the fifth order model for an induction generator, we get the expressions given on the next page. Calculations are shown in detail in subsection 5.3.1.

$$v_{dr} = R_r\left(\frac{v_{qs}-R_s i_{qs}}{\omega_s L_m} - \mathrm{Bi}_{\mathrm{ds}}\right) - As\omega_s i_{qs} + C(v_{ds} - R_s i_{ds}) + A\frac{di_{ds}}{dt} \tag{5.4}$$

$$v_{qr} = -BR_r \mathrm{i_{qs}} + sC\left(v_{qs} - R_s i_{qs}\right) + As\omega_s i_{ds} + A\frac{di_{qs}}{dt} \tag{5.5}$$

Constants are:

$$\mathrm{A} = L_m - \frac{(L_m+L_s)(L_m+L_r)}{\mathrm{L_m}} = -0.56306 \tag{5.6}$$

$$\mathrm{B} = \frac{(L_m+L_s)}{\mathrm{L_m}} = 1.03715 \tag{5.7}$$

$$\mathrm{C} = \frac{(L_m+L_r)}{\mathrm{L_m}} = 1.04262 \tag{5.8}$$

Further, it is assumed that the system is in steady state (derivatives are zero), and that the machine should be able to decelerate while operating at any wind speed condition with a limit on 1.5 pu active power. This translates to -1.5 pu q-axis current. Also, the rotor converter should control the d-axis current to zero due to the marginal power rating of the machine. The d-axis voltage will be zero as a result of:

$$v_{ds} = R_s i_{ds} - \omega_s \psi_{qs} + \frac{d\psi_{ds}}{dt} = 0 - 0 + 0 = 0 \tag{5.9}$$

By studying the equations we find that the voltages will be highest at maximal positive slip. From this we get:

$$v_{dr} = R_r\left(\frac{v_{qs}-R_s i_{qs}}{\omega_s L_m}\right) - As\omega_s i_{qs} \tag{5.10}$$

$$v_{dr} = 0.019\ \left(\frac{1.15-0.0175 i_{qs}}{\omega_s 6.921}\right) - 0.56306 \cdot 0.3 \cdot \omega_s \cdot i_{qs} \tag{5.11}$$

$$v_{dr} \approx \frac{0.0027}{\omega_s} - 0.169 \cdot \omega_s \cdot i_{qs} \tag{5.12}$$

$$v_{qr} = -BR_r \mathrm{i_{qs}} + sC\left(v_{qs} - R_s i_{qs}\right) \tag{5.13}$$

$$v_{qr} = -1.03715 \cdot 0.019 \cdot \mathrm{i_{qs}} + 0.3 \cdot 1.04262\left(1.15 - 0.0175 \cdot i_{qs}\right) \tag{5.14}$$

$$v_{qr} \approx 0.0142 \cdot 1.5 + 0.3597 \tag{5.15}$$

The q-axis voltage is affected by the frequency. The magnitude will be the highest if the frequency is deviating positively. We choose a frequency of 1.1 pu which is the maximal value specified in the IEC 61892-series of standards [5].

By inserting -1.5 pu q-axis current and 1.1 pu synchronous angular velocity (same as frequency in per unit) we get:

$$v_{dr} \approx \frac{0.0027}{1.1} + 0.169 \cdot 1.1 \cdot 1.5 = 0.2813 \tag{5.16}$$

$$v_{qr} \approx -0.0142 \cdot 1.5 - 0.3597 = -0.381 \tag{5.17}$$

The rotor voltage magnitude is:

$$|v_r| = \sqrt{{v_{dr}}^2 + {v_{qr}}^2} = \sqrt{0.2813^2 + 0.381^2} = 0.4736\ pu \tag{5.18}$$

Combining this information with equation (5.2) we find that the rotor peak voltage will be within:

$$|v_r, peak, max| = 0.4736 \cdot 1300.2\ V \approx 615.77\ V \tag{5.19}$$

The maximal peak voltage for the stator side will be:

$$vs, peak, max = \frac{690\ V}{\sqrt{3}} \cdot \sqrt{2} \cdot 120\% = 676\ V \tag{5.20}$$

The small difference indicates that the DFIG could work well with a two-winding transformer and a filter to the stator bus instead of a three-winding transformer. This makes the model simpler, but still relevant.

The grid side converter may supply or consume real power. It may also deliver/consume reactive power. This could increase or decrease the voltage across the filter to the stator bus. It is further assumed that the grid side converter will either keep the power factor to unity or for voltage control. If a L filter is chosen to be 0.2 pu in a converter based pu system, the converter ac voltage will have a magnitude of:

$$vc, peak, max = \sqrt{1.2^2 + 0.2^2}\ pu \cdot \frac{690V}{\sqrt{3}} \sqrt{2} \frac{V}{pu} = 685.4\ V \tag{5.21}$$

For this model, single-level six pulse PWM converters are used. The voltage on the DC bus should be twice as high as the maximal peak AC voltage in order to avoid over modulation. Also, disturbances caused by the rotor side converter may cause the DC voltage to drop. The magnitude of such a disturbance will be dependent on the capacitance and the control loops for both converters.

To be on the safe side, the DC bus voltage is chosen to be 2.5 per unit of the stator rated AC voltage, which translates to 1408.5 V.

Figure 5.2 below illustrates an equivalent circuit of the transformer and the filter in the synchronous rotating reference frame.

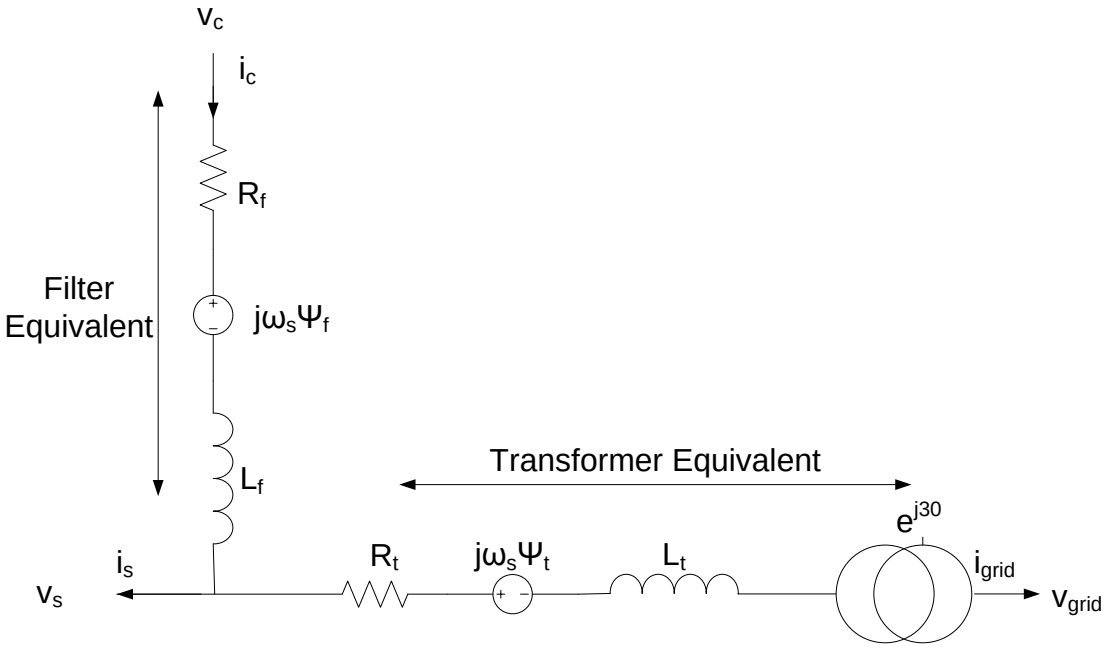

Figure 5.2 – Single Line Equivalent of the Filter and the DYn11-Wound Transformer in the Synchronous Rotating Reference Frame

Filter parameters were based on converter ratings and chosen to be:

Table 5.1 – L Filter Parameters	
Base RMS line voltage:	690 V
Converter power rating:	700 kW
Filter inductance:	0.000360827 H
Filter resistance:	0.0136028571 Ω
Filter inductance in per unit:	0.2 pu
Filter resistance in per unit:	0.02 pu

5.2 Grid Side Converter Controls

Reference is made to figure 5.2 on the previous page. In this section of the thesis a control strategy for controlling the grid side converter will be developed. The aim is to design a controller that can control active and reactive power independently, and to ensure that the wind turbine electrical system has no reactive current flowing at the point of the transformer primary terminals at rated conditions. Inspirations for the decoupled controller are taken from [17], [19], [20]. The converter is controlled as a STATCOM.

5.2.1 Decoupled Grid Side Converter Current Controls

The following equations could be developed for the system:

$$v_c = R_f i_c + j\omega_s \psi_f + \frac{d\psi_f}{dt} + v_s \tag{5.22}$$

$$v_s = R_t i_c + j\omega_s \psi_t + \frac{d\psi_t}{dt} + v_{grid} e^{-j30} \tag{5.23}$$

$$\psi_f = L_f i_c \tag{5.24}$$

$$\psi_t = L_t i_{grid} \tag{5.25}$$

$$i_{grid} = (i_c - i_s) \tag{5.26}$$

The d-axis is in phase with the grid voltage vector, further equations are in d-q-coordinates.

$$v_{dc} = R_f i_{dc} - \omega_s \psi_{qf} + \frac{d\psi_{df}}{dt} + v_{ds} \tag{5.27}$$

$$v_{qc} = R_f i_{qc} + \omega_s \psi_{df} + \frac{d\psi_{qf}}{dt} + v_{qs} \tag{5.28}$$

Inserting flux and current relations in the equations above give:

$$v_{dc} = R_f i_{dc} - \omega_s L_f i_{qc} + L_f \frac{di_{dc}}{dt} + v_{ds} \tag{5.29}$$

$$v_{qc} = R_f i_{qc} + \omega_s L_f i_{dc} + L_f \frac{di_{qc}}{dt} + v_{qs} \tag{5.30}$$

We can now put up an equation on how to control the currents independently, and for how to use the voltage source converter for current control. The aim is to eliminate disturbances caused by the controller for the perpendicular voltage. We configure the grid side converter voltage reference in d and q axes, given by v_{dc} and $v_{qc,}$ to be a sum of an active (controllable) and a passive (decoupling) part:

$$v_{dc} = v_{dc,control} + v_{dc,decoupling} \tag{5.31}$$

$$v_{qc} = v_{qc,control} + v_{qc,decoupling} \tag{5.32}$$

By choosing:

$$v_{dc,decoupling} = -\omega_s L_f i_{qc} + v_{ds} \tag{5.33}$$

$$v_{qc,decoupling} = \omega_s L_f i_{dc} + v_{qs} \tag{5.34}$$

We get:

$$v_{dc,control} = R_f i_{dc} + L_f \frac{di_{dc}}{dt} \tag{5.35}$$

$$v_{qc,control} = R_f i_{qc} + L_f \frac{di_{qc}}{dt} \tag{5.36}$$

The equations above are Laplace transformed:

$$L_f i_{dc} \boldsymbol{S} + R_f i_{dc} = v_{dc,control} \tag{5.37}$$

$$L_f i_{qc} \boldsymbol{S} + R_f i_{qc} = v_{qc,control} \tag{5.38}$$

Reshaping the equations above and inserting per unit values for the L filter we get:

$$i_{dc} = \frac{v_{dc,control}}{0.2\boldsymbol{S}+0.02} \tag{5.39}$$

$$i_{qc} = \frac{v_{qc,control}}{0.2\boldsymbol{S}+0.02} \tag{5.40}$$

Since the currents contain harmonics, a low pass filter with cut off frequency of 1000 Hz is chosen for the feedback. This will not significantly reduce the performance. This low

pass filter could also resemble smoothing of discontinuous but rapid measurements. The transfer functions are equal and were modelled in SIMULINK as illustrated in figure 5.3.

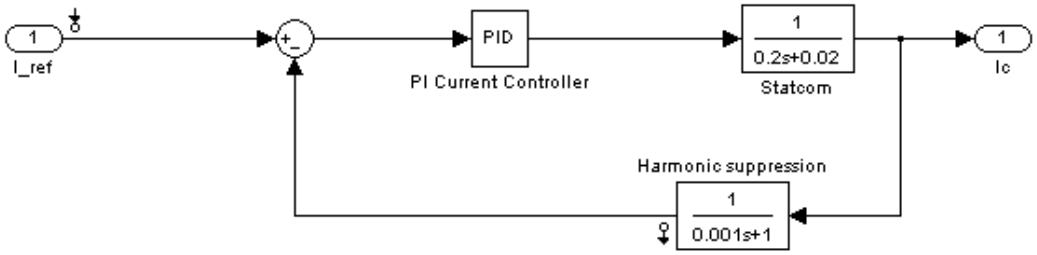

Figure 5.3 - Transfer Function for Both Grid Side Converter Currents

Subsequently, the PI controller in the figure above was graphically tuned using the SIMULINK SISO design tool. The focus was to get the closed loop step response to be as fast as possible with minimal overshoot and critical damping. The open loop Bode plot from the current references to the current will not be altered if the voltage and frequency changes. Figure 5.4 illustrates the step response to the left and the open loop Bode plot to the right.

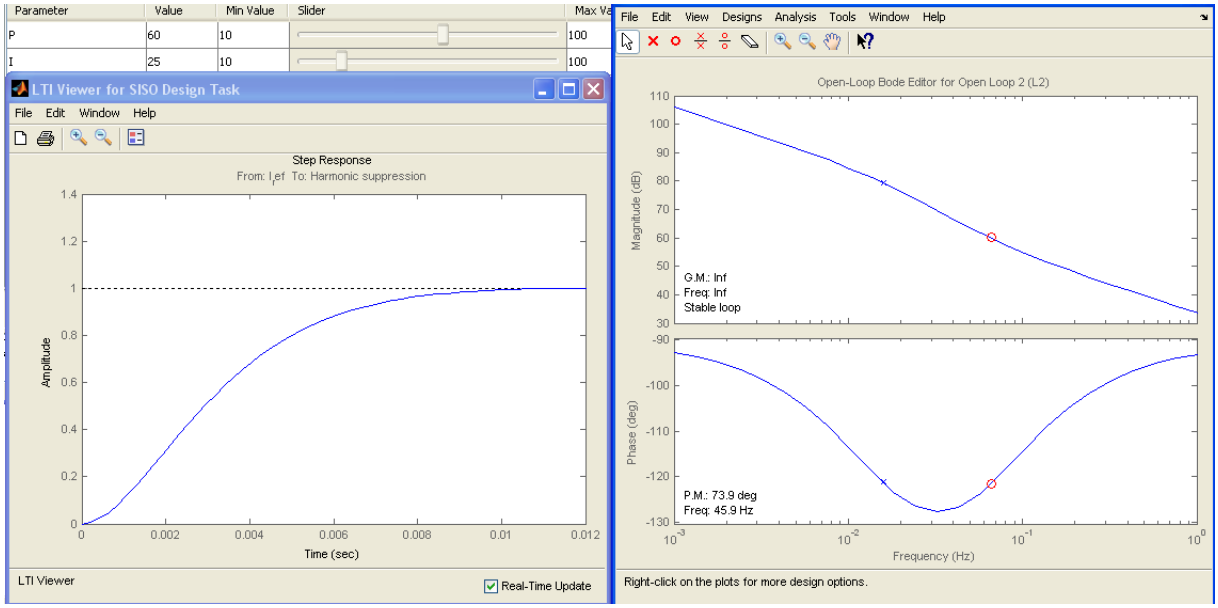

Figure 5.4 - Graphical Tuning of the Converter Current PI Controllers.

With proportional gain of 60 and integral time constant of 0.04 seconds the current can be controlled for a 1 pu step in just 10 milliseconds! The gain margin is infinite and the phase margin is 73.9 degrees at 45.9 Hz cut off frequency. Further increments in gain or decreases in integral time constant were found to create overshoots without speeding up the time response.

As a comparison, the energy stored in a 10000 µF capacitor bank at the chosen voltage level of 1408.5 V is 9919.36 J. This translates to 14.2 milliseconds of the converter rated power. Voltage control has to be very fast in order to achieve a stable voltage at all conditions.

The control loops will be detuned if filter parameters are changed due to heat, skin effect or saturation. In the final model such changes were made by varying the resistance and inductance values to the double of the original, and to zero. The changes had minor effects, and the control loops were stable.

5.2.2 DC Bus Voltage Control

The d-axis current should be used to control the DC bus voltage. Positive current for the DC side and the AC side was chosen to be out of the capacitor bank. The following power balance is valid for the peak value based per unit system (rotor side converter neglected):

$$i_{dc}v_{dc} + i_{qc}v_{qc} = i_{DC}v_{DC} \tag{5.41}$$

$$i_{DC} = -C\frac{dv_{DC}}{dt} \tag{5.42}$$

The size of the capacitor bank was determined by trial and error to be 10000 µF. This choice was made in order to get the DC voltage controller to be as fast as it needs to stabilise the voltage when the rotor side converter disturbs the system. The large size also reduces the voltage ripple, which, when fed trough the control loops, could contribute to disturbances.

$$C = \frac{10000 \cdot 10^{-6} F}{2\pi 60 rad/s \frac{690^2\, V}{700000\, W}} = 2.5641\ pu \tag{5.43}$$

Equations (5.41) and (5.42) are combined:

$$i_{dc}v_{dc} + i_{qc}v_{qc} = -Cv_{DC}\frac{dv_{DC}}{dt} \tag{5.44}$$

Further, the state equation for DC voltage could be written:

$$v_{DC}\frac{dv_{DC}}{dt} = \frac{-(i_{dc}v_{dc}+i_{qc}v_{qc})}{C} \tag{5.45}$$

DC voltage measurement was chosen to be filtered with a low pass filter with 2000 Hz cut off frequency in order to reduce the controller disturbances from the DC voltage ripple. The voltage regulator system was modelled in SIMULINK, q-axis states were neglected as they are not part of the open or closed loop from voltage reference to voltage measurement signal.

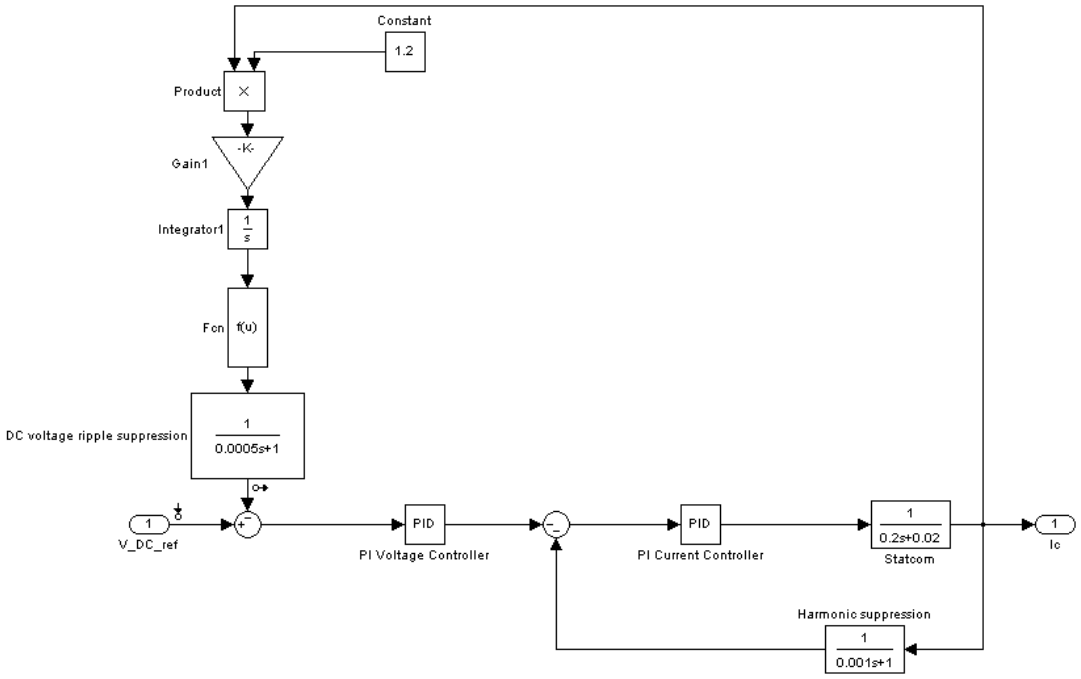

Figure 5.5 - Transfer Function for Optimization of DC Voltage PI Controller

SIMULINK was configured to linearise the system for a DC voltage reference of 2.5. The d-axis voltage was fixed to be 1.2 pu at the input of the energy equation, this value will give the highest gain in the control loop. Again, SIMULINK SISO design tool was used for graphical tuning. Closed loop step response and open loop Bode plot for the DC voltage are illustrated in figure 5.6 on the next page.

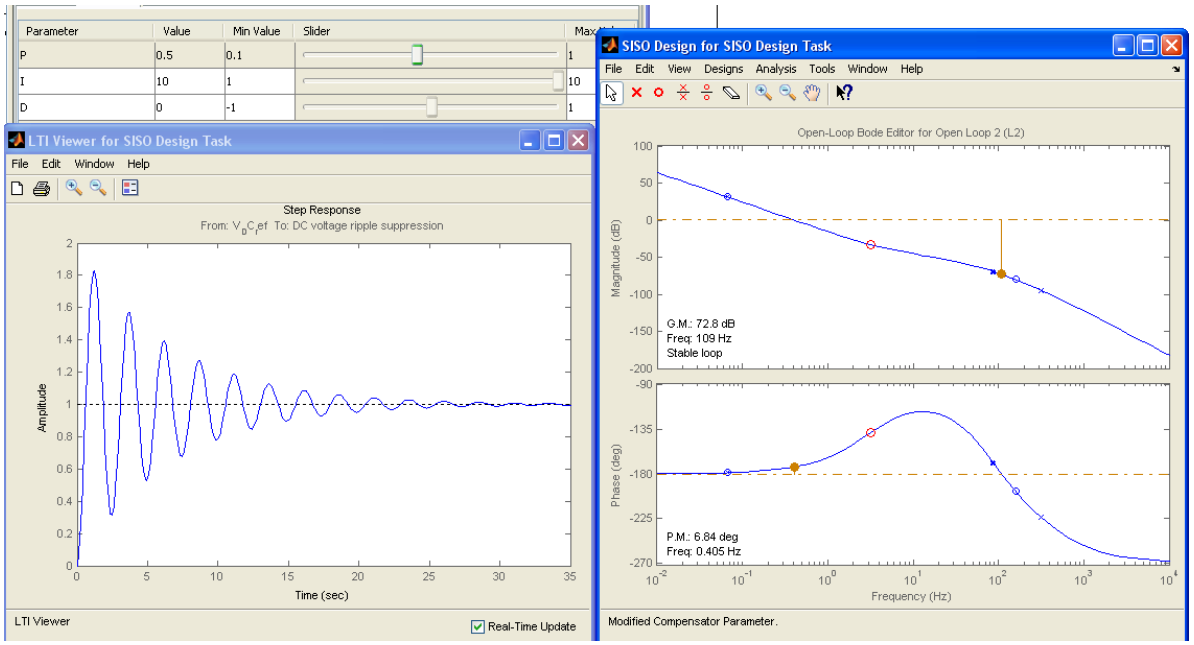

Figure 5.6 - Graphical Tuning of the DC Voltage PI Controller

Proportional gain of 0.5 was found to be acceptable, and the integral time constant is 0.1 seconds. The control loop has to have a marginal phase margin in order for the integral part to be fast enough to compensate for q-axis and rotor converter real power disturbances. Gain margin was found to be 72.8 dB and phase margin 6.84 degrees.

Later, during trial and error, the DC voltage low pass ripple suppression filter was replaced with a fourth order Butterworth filter with the same cut off frequency (2 kHz). This made no apparent difference in the stability of the control loop but reduced the gain of the DC voltage ripple and thus also the harmonics.

The filter, converter and controllers were tested without switching in PSCAD and connected to a perfect voltage source. Frequency and voltage variation had no apparent effect on the AC current or DC voltage controls. This simple model is not described further in this report. Results show no disturbances from one current regulator to the other. The testing of the current controllers is depicted below, and time span in the figure was one second. Inputs to the regulators were manually controlled by sliding value selectors.

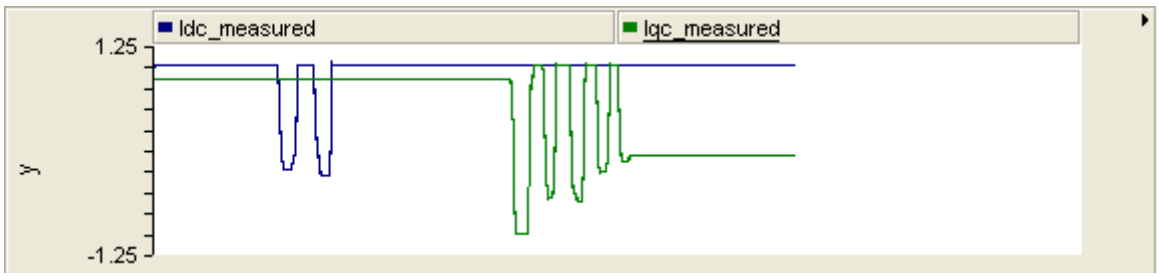

Figure 5.7 – Unfiltered Measurement Results from the Testing of Current Controllers

5.2.3 Choice of Angular Reference for the Grid Side Converter

An expression on how to find the angular difference between the stator and the grid voltage vectors is one possibility for how to control the reactive power delivered to the grid. If the grid voltage vector is chosen as the rotating reference, the reactive current is expressed by:

$$i_{q,grid} = (i_{qc} - i_{qs}) \tag{5.39}$$

One method for determining the grid voltage angle by a recursive function was experimentally found to be inadequate. The method is briefly described in appendix 5.

Other ways for calculating the grid voltage vector's angular position from the two current measurements and the voltage measurement was explored, but were found to be reliant on steady state conditions. The conclusion is that the grid voltage has to be measured.

The preferred choice is to measure the voltage at the oil platform gas turbine generators' terminal. This measurement is at the point of common coupling for all wind turbines if several units were to be installed. It is assumed that modern fibre optic communication will transport the measured signals without significant delay. It is also convenient that such measurement could be used for voltage control, an option that will be explored in later sections.

When the voltage vector is measured, the angular position could be found by a PLL as described in section 2.1. This quantity could again be used as an input in the park transform matrix in order to find the magnitude of d and q axis vectors for voltages and currents.

5.2.4 Voltage Control

In section 5.6.2 an AC voltage control strategy for the grid side converter is tested. The control strategy was found experimentally. Gas turbine generator bus voltage is measured, smoothed trough a low pass filter with cut off frequency 50 Hz, and subsequently compared to the reference of 1 pu voltage.

A gain of 100 was found to be acceptable, which means that the reference for reactive current will be 1 pu if the voltage deviates 0.01 pu. The q-axis converter current reference is limited to ±1 pu, producing or consuming the rated current of reactive power in any event. Any d-axis current will in this case lead to a total current vector magnitude that is higher than the rated value. The philosophy in this case is that the over current is low and is produced during a very limited time.

5.3 Rotor Side Converter Controls

For the rotor side converter it is normal practice to refer the equations to the stator flux, and to control the rotor voltages. However, as the stator currents are measured in order for the grid side converter to control the reactive power output of the wind turbine, it could be shown that it is also an option to control the wind turbine stator currents. Inspiration to the decoupling was taken from [21].

5.3.1 Decoupled Stator Current Controller

The reader is referred to section 2.1 and 2.3 for figures and explanation. Equations are referred to peak value based per unit system.

Stator flux linkages:

$$\psi_{ds} = (L_m + L_s)i_{ds} + L_m i_{dr} \tag{5.40}$$

$$\psi_{qs} = (L_m + L_s)i_{qs} + L_m i_{qr} \tag{5.41}$$

Rotor flux linkages:

$$\psi_{dr} = (L_m + L_r)i_{dr} + L_m i_{ds} \tag{5.42}$$

$$\psi_{qr} = (L_m + L_r)i_{qr} + L_m i_{qs} \tag{5.43}$$

Stator voltage equations:

$$v_{ds} = R_s i_{ds} - \omega_s \psi_{qs} + \frac{d\psi_{ds}}{dt} \tag{5.44}$$

$$v_{qs} = R_s i_{qs} + \omega_s \psi_{ds} + \frac{d\psi_{qs}}{dt} \tag{5.46}$$

Rotor voltage equations:

$$v_{dr} = R_r i_{dr} - s\omega_s \psi_{qr} + \frac{d\psi_{dr}}{dt} \tag{5.47}$$

$$v_{qr} = R_r i_{qr} + s\omega_s \psi_{dr} + \frac{d\psi_{qr}}{dt} \tag{5.48}$$

The d-axis is oriented in the direction of the stator flux, which gives:

$$\psi_{qs} = 0 \tag{5.49}$$

$$\frac{d\psi_{qs}}{dt} = 0 \tag{5.50}$$

Stator voltages from (5.44) and (5.45), and the relationships in (5.49) and (5.50) are used to calculate the flux and flux derivative:

$$\frac{d\psi_{ds}}{dt} = v_{ds} - R_s i_{ds} \tag{5.50}$$

$$\psi_{ds} = \frac{v_{qs} - R_s i_{qs}}{\omega_s} \tag{5.51}$$

The following constants will be used to simplify further calculations:

$$\mathrm{A} = L_m - \frac{(L_m + L_s)(L_m + L_r)}{\mathrm{L_m}} = \mathrm{L_m}(1 - \mathrm{BC}) \tag{5.52}$$

$$\mathrm{B} = \frac{(L_m + L_s)}{\mathrm{L_m}} \tag{5.53}$$

$$\mathrm{C} = \frac{(L_m + L_r)}{\mathrm{L_m}} \tag{5.54}$$

Stator flux linkages from (5.40) and (5.41), and the relationship in (5.49) give the following relation between stator and rotor currents. The constant B is introduced.

$$i_{dr} = \frac{\psi_{ds} - (L_m + L_s)\mathrm{i_{ds}}}{L_m} = \frac{\psi_{ds}}{L_m} - \mathrm{Bi_{ds}} \tag{5.55}$$

$$i_{qr} = \frac{-(L_m + L_s)\mathrm{i_{qs}}}{L_m} = -\mathrm{Bi_{qs}} \tag{5.56}$$

Rotor flux equations (5.42) and (5.43) can now have rotor currents substituted with stator currents:

$$\psi_{dr} = (L_m + L_r)\left(\frac{\psi_{ds}}{L_m} - \mathrm{Bi_{ds}}\right) + L_m i_{ds} = C\,\frac{v_{qs} - R_s i_{qs}}{\omega_s} + A i_{ds} \tag{5.57}$$

$$\psi_{qr} = (L_m + L_r) i_{qr} + L_m i_{qs} = A i_{qs} \tag{5.58}$$

Rotor flux equations (5.42) and (5.43) are derived:

$$\frac{d\psi_{dr}}{dt} = (L_m + L_r)\left(\frac{\frac{d\psi_{ds}}{dt}}{L_m} - \mathrm{B}\frac{di_{ds}}{dt}\right) + L_m\frac{di_{ds}}{dt} = C(v_{ds} - R_s i_{ds}) + A\frac{di_{ds}}{dt} \tag{5.59}$$

$$\frac{d\psi_{qr}}{dt} = -(L_m + L_r)\mathrm{B}\frac{\mathrm{di_{qs}}}{\mathrm{dt}} + L_m\frac{di_{qs}}{dt} = A\frac{di_{qs}}{dt} \tag{5.60}$$

The rotor voltage equations (5.47), (5.48) can now be simplified by inserting results from equations (5.49) to (5.60). We end up with:

$$v_{dr} = R_r\left(\frac{v_{qs} - R_s i_{qs}}{\omega_s L_m} - \mathrm{Bi_{ds}}\right) - As\omega_s i_{qs} + C(v_{ds} - R_s i_{ds}) + A\frac{di_{ds}}{dt} \tag{5.61}$$

$$v_{qr} = -BR_r\mathrm{i_{qs}} + sC\left(v_{qs} - R_s i_{qs}\right) + As\omega_s i_{ds} + A\frac{di_{qs}}{dt} \tag{5.62}$$

To decouple the current control, we configure the rotor voltage reference in d and q axes given by v_{dr} and v_{qr} to be a sum of an active (controllable) and a passive (decoupling) part:

$$v_{dr} = v_{dr,control} + v_{dr,decoupling} \tag{5.63}$$

$$v_{qr} = v_{qr,control} + v_{qr,decoupling} \tag{5.64}$$

The parameters and values included in the expression for decoupling voltage were chosen to make the control loops linear and decoupled from each other. Variable parameters such as slip cannot be a part of the control voltage equation.

By choosing:

$$v_{dr,decoupling} = R_r\left(\frac{v_{qs} - R_s i_{qs}}{\omega_s L_m}\right) - As\omega_s i_{qs} + Cv_{ds} \tag{5.65}$$

$$v_{qr,decoupling} = sC\left(v_{qs} - R_s i_{qs}\right) + As\omega_s i_{ds} \tag{5.66}$$

We end up with:

$$v_{dr,control} = -(\mathrm{B}R_r + CR_s)i_{ds} + A\frac{di_{ds}}{dt} \tag{5.67}$$

$$v_{qr,control} = -\,BR_r\mathrm{i_{qs}} + A\frac{di_{qs}}{dt} \tag{5.68}$$

Equations (5.67) and (5.68) are Laplace transformed:

$$\mathrm{i_{ds}} = \frac{-v_{dr,control}}{(\mathrm{B}R_r + CR_s - A\,\boldsymbol{S})} \tag{5.69}$$

$$\mathrm{i_{qs}} = \frac{-v_{qr,control}}{(\,BR_r - A\,\boldsymbol{S})} \tag{5.70}$$

Values for the constants are calculated:

$$\mathrm{A} = L_m - \frac{(L_m+L_s)(L_m+L_r)}{\mathrm{L_m}} = -0.56306 \tag{5.71}$$

$$\mathrm{B} = \frac{(L_m+L_s)}{\mathrm{L_m}} = 1.03715 \tag{5.72}$$

$$\mathrm{C} = \frac{(L_m+L_r)}{\mathrm{L_m}} = 1.04262 \tag{5.74}$$

Finally we insert values into equations (5.69) and (5.70):

$$\mathrm{i_{ds}} = \frac{-v_{dr,control}}{(0.03795 + 0.56306\,\boldsymbol{S})} \tag{5.75}$$

$$\mathrm{i_{qs}} = \frac{-v_{qr,control}}{(0.0197 + 0.56306\boldsymbol{S})} \tag{5.76}$$

These expressions were implemented in SIMULINK and the PI controllers were graphically tuned. However, the decoupling for a machine will never be perfect and therefore the cut off frequency for the open loop should be lower than the resonant frequency of the system. This frequency is close to the synchronous frequency. By experimenting back and forth between a PSCAD model without switching and SIMULINK the results presented on the next page were found to be acceptable.

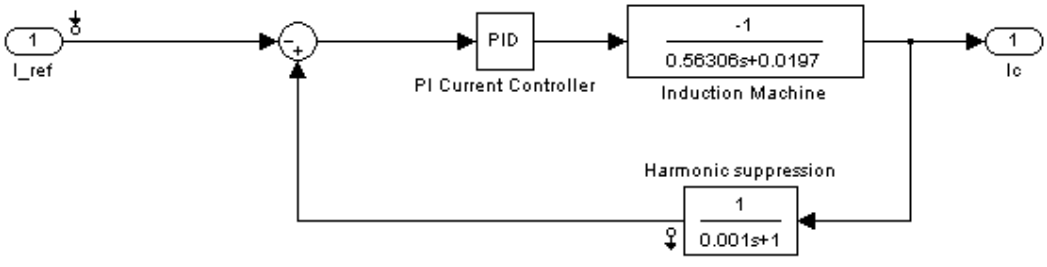

Figure 5.8 - Stator Current Controller Q-axis Transfer Function

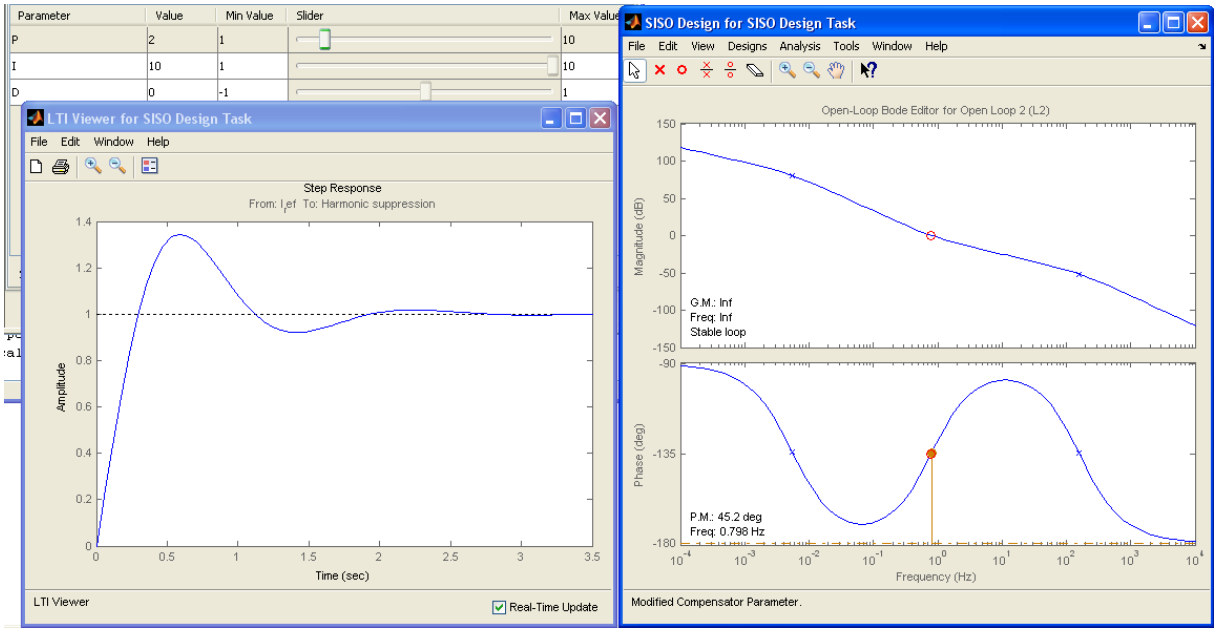

Figure 5.9 - Step Response Plot and Bode Plots for the Stator Q-axis Current Controller

For proportional gain of 2 and integral time constant of 0.1 seconds, the gain margin is infinite and the phase margin is 45.2 degrees at cut off frequency 0.789 Hz. During tests it was verified that the integral gain is high enough to eliminate effects of disturbances in steady state.

Substituting quantities from q-axis with d-axis parameters, the d-axis transfer function was modelled. Figure 5.10 illustrates the result:

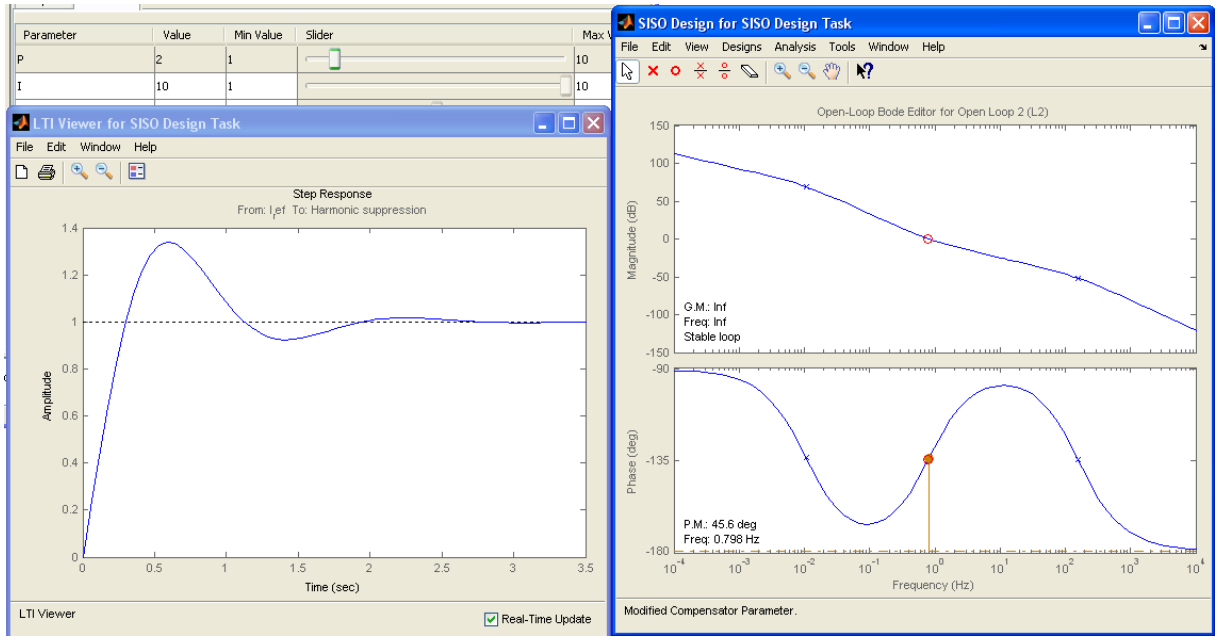

Figure 5.10 - Step Response Plot and Bode Plots for the Stator D-axis Current Controller

For equal gain and integral time constant as the q-axis (2, 0.1 s), the d-axis system's gain margin was found to be infinite, and the phase margin 45.6 degrees at cut off frequency 0.798 Hz.

5.3.2 Speed Controller

Although the wind turbine was tested with constant torque and not varying wind conditions, the tracking of optimal speed was important for determining how the electrical torque and real power output will behave. The speed controller could also have been modelled in SIMULINK by known equations for the torque, but for this case it was fairly easy to find acceptable values by varying parameters directly in PSCAD.

The philosophy behind the controller is to keep tracking of optimal speed acceptably fast, but with low enough gain not to change current reference in the case of a wind gust. Also, the change rate of the speed reference should be limited in order for the rotor's d-axis current not to have sudden step changes and thereby cause severe disturbances for the DC bus voltage controller. The gain value found was a trade-off between the tracking of optimal speed point, the ability to withstand wind gusts and the limits given by the DC bus voltage controller.

The d-axis current reference, or the torque reference in a later case, is given by a PI controller for the speed. The change rate on the speed reference is limited to 0.1 pu per second, and the speed deviation is put trough a controller with proportional gain set to 20 and integral time constant set to 0.05 seconds.

An example of the resulting behaviour is illustrated in figure 5.11 the next page.

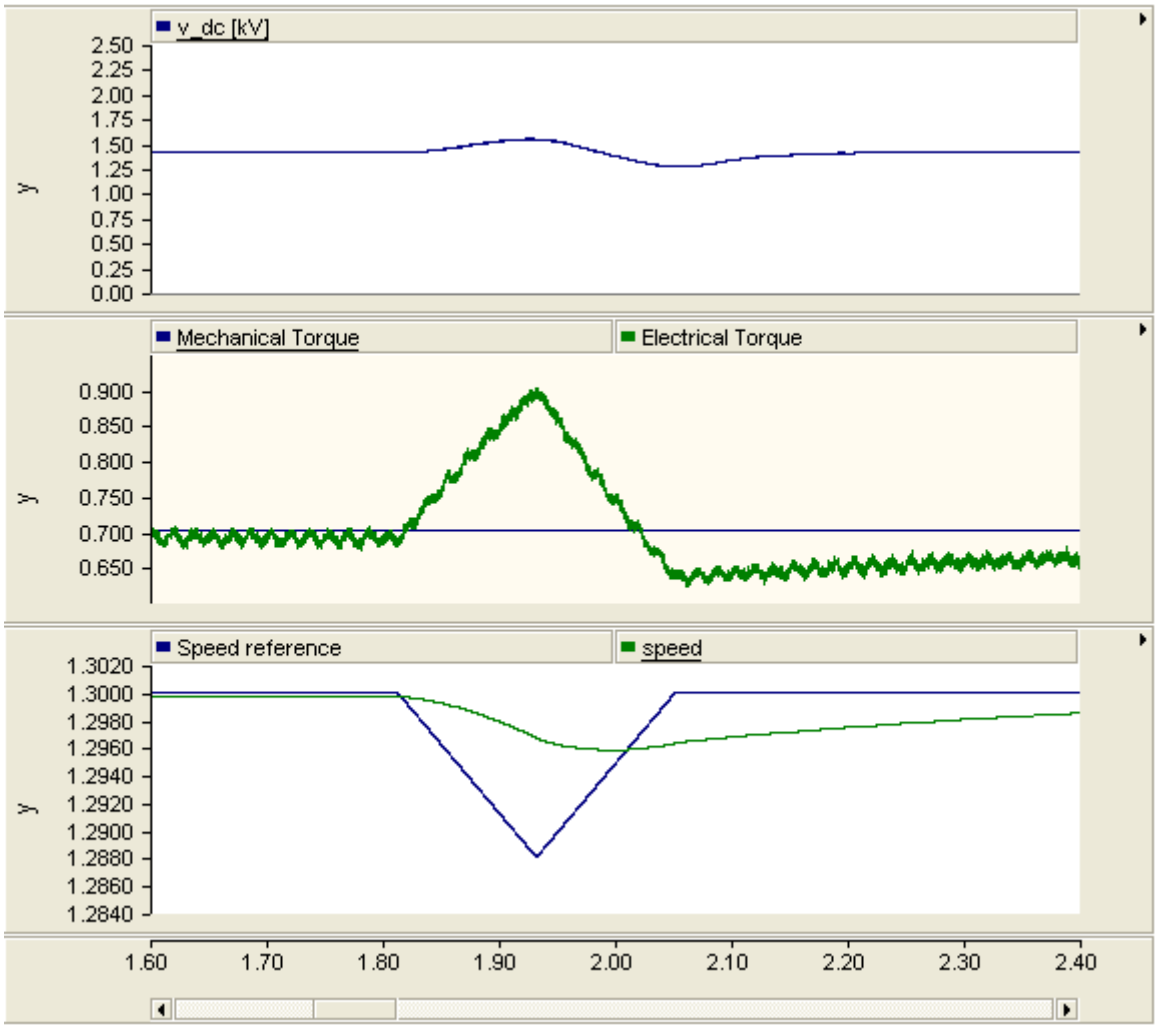

Figure 5.11 - Dc Bus Voltage, Torques, Speed Reference and Speed While Changing the Speed Reference

As illustrated in the picture, the torque changes gently and the speed does not deviate significantly from the reference in steady state. However, the DC-bus voltage is affected by the rotor d-axis current. Electrical torque is disturbed by harmonics and 60 Hz oscillations. The sources of the 60 Hz oscillations were investigated but not found. These disturbances are believed to be caused by either having an offset in the angular calculations, or due to zero sequence currents in the rotor circuit. However, the latter option seems improbable since the machine is modelled with the PSCAD standard model which should be symmetrical.

5.3.3 Induction Generator Reactive Power Control

The stator q-axis current will be controlled to zero for all simulations. This will prevent any reactive current and hereby also limit heat build up if the generator has a marginal MVA rating.

5.3.4 Stator Flux Feed Forward

As shown by equations in section 2.3, given that the system is referred to the stator flux, the electrical torque of an induction generator could be expressed by:

$$T_{el} = i_{qs}\psi_{ds} \tag{5.77}$$

The electrical torque is used for speed control. The equation can be reshaped to:

$$i_{qs} = \frac{T_{el}}{\psi_{ds}} \tag{5.78}$$

We now have a relation that could be used for feeding forward voltage disturbances. This can hopefully make the real power output of the wind turbine constant during transient events. The stator voltage drop will be sensed one step earlier in the control cascade as there is no need for speed deviations before any action made.

By inserting measureable quantities the electrical torque reference can be translated into a current reference by applying the relation:

$$i_{qs,ref} = \frac{T_{el,ref}}{\left(\frac{v_{qs} - R_s i_{qs}}{\omega_s}\right)} \tag{5.79}$$

The idea is to use the speed deviation for torque control and subsequently feeding forward the stator flux to make a current reference. Reference is made to the control loop schematics of appendix 5, section A 5.1.

The technique behaved well during simulations, and no modifications from the current control strategy had to be made. However, if the speed control loop had been given a much higher gain there will be less need for a stator flux feed forward. This option will be rougher on mechanical components and also lead to significantly higher power fluctuations in the event of wind gusts.

A stator flux feed forward could also be made for rotor current controlled machines by applying calculations developed from the fifth order model of the induction machine.

5.4 Results from Initial Tests for the DFIG model

The DFIG model was modelled as described by appendices 5 and 6, and tested directly towards a perfect voltage source. By manually controlling sliding value selectors the DFIG could be tested for all thinkable combinations of occurrences. The tested events were combinations of:

- Voltage transients
- Frequency transients
- Acceleration / Deceleration
- Speed (and thus also slip) from 0.7 to 1.3 times synchronous speed
- Mechanical torque variation

The system behaved well for all events, but tests confirmed that there are still issues to be resolved before the model could be said to be perfect. Findings were:

- The system is stable at all conditions.
- Developed techniques for dynamic modulation are working brilliantly.
- Stator flux feed-forward made the generator deliver constant power under slow transients.
- The control loops for the grid side converter have a too high cut off frequency, and hence they are amplifying some disturbances, producing a range of lower harmonics than the switching frequency.
- Changes in torque or voltage disturb the DC voltage control. For any real application, this could be resolved by feed forward expressions for instantaneous real power in the grid converter q-axis and for both rotor converter axes. Also, the capacitor bank could be made larger and thus the DC voltage control gain could be higher. A lower integral time constant would also be helpful here.
- There is a discrepancy between the mechanical and electrical torque outputs in PSCAD. Deviation is about 1% at steady state. This issue was investigated but not resolved.
- Electrical torque contains 60 Hz fluctuations. It is believed that the problem is caused by either an angular miscalculation, by the decoupling voltage components or by the PSCAD model itself. The issue was not resolved. The magnitude of this disturbance is varying from 0.04 pu in transient conditions to 0.01-0.02 pu in stationary conditions. As the wind force will vary in real applications, the wind turbine will never have stationary conditions.
- Most of the major problems could be solved by applying control theory. However, there is little benefit in making the test model perfect as it is based on fictive parameters.
- The gain of the speed control is quite high. Wind gusts could affect the short term power output.

5.4.1 Example Results from Tests

By applying the FFT tool in PSCAD to an unfiltered a-phase current measurement, the total and individual harmonic production was investigated. In the figure below, the 97th and 101st harmonics are the most prevalent (odd neighbour harmonics to the switching harmonic). The switching frequency was chosen to be 99 times the measured frequency for both converters, as described in appendix 6. This choice was made on purpose to avoid tripled harmonics. Switching of the two converters is shifted in time, as described by the same appendix. There is also a production of lower harmonics caused by the control loops themselves.

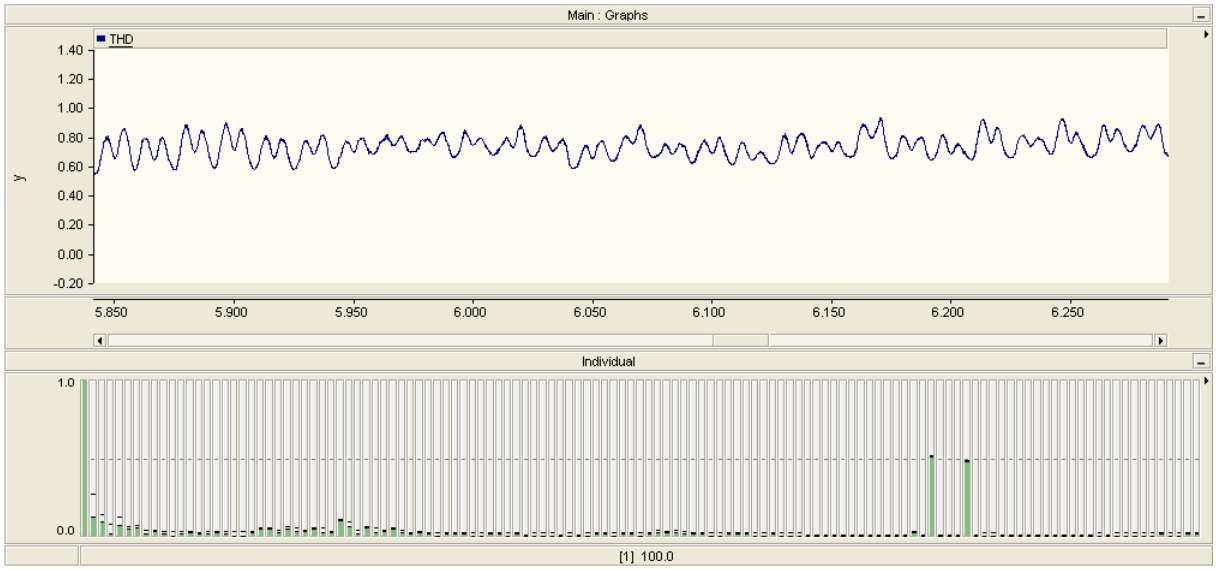

Figure 5.12 – THD in % and Harmonic Spectrum

Total harmonic distortion of the currents to the platform utility grid was measured to be in the range from 0.6% to 2% at close to rated conditions. When producing less power the THD rises for natural reasons as the base frequency component looses magnitude.

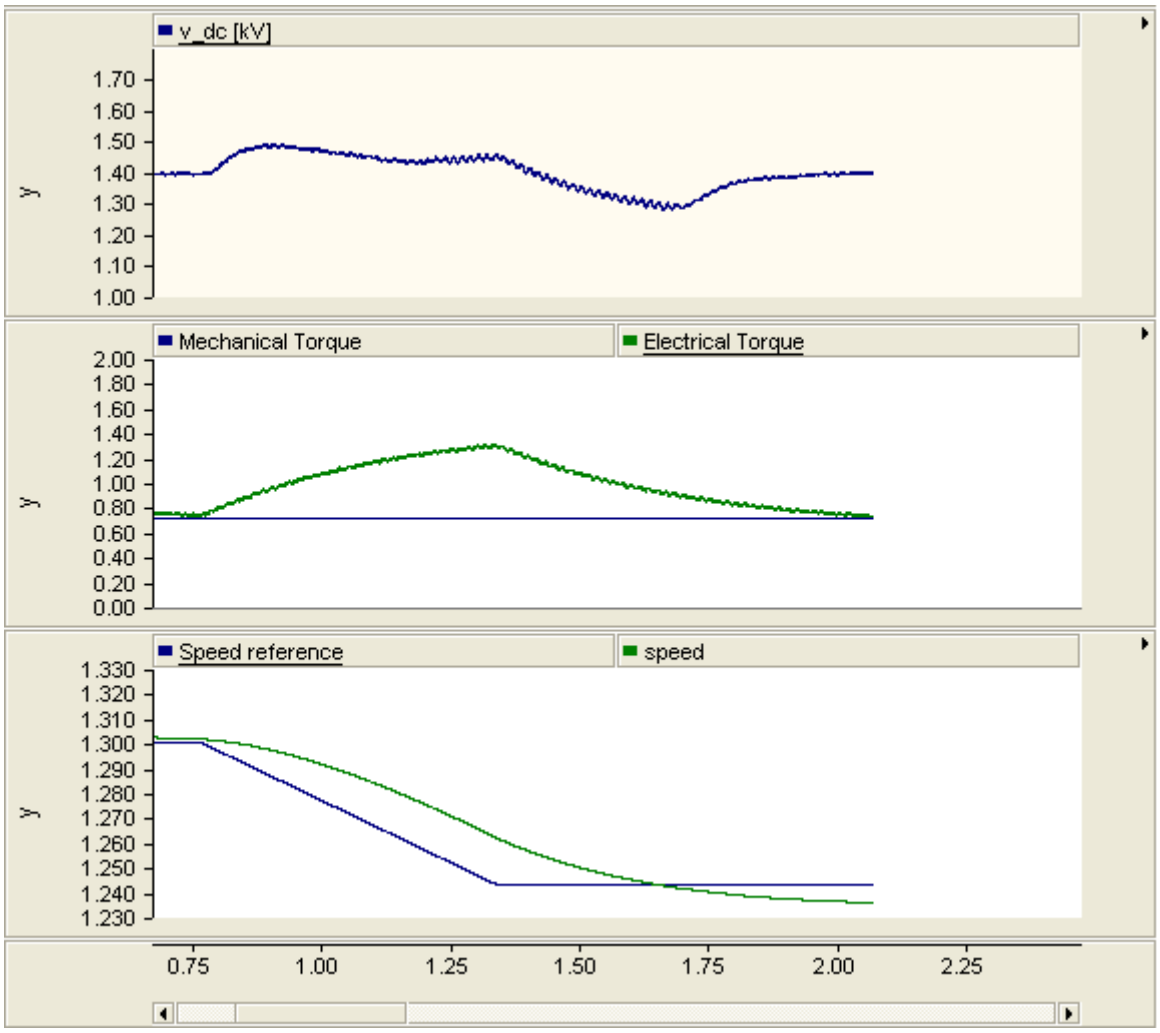

Figure 5.13 - Example of Deceleration Test, Stator Voltage 1.2 pu, Frequency 1.05 pu

As illustrated above there are quite large disturbances in the DC voltage when the machine changes state from keeping a fixed speed to decelerating etc.

5.4.2 Suggested Solutions to Observed Problems with DFIG Model

- DC voltage needs to be more stable. One solution could be to increase the size of the capacity bank, and possibly to alter the properties of both the cascaded control loops in order to achieve better performance.
- The gain of the current controls for the grid side converter could be reduced somewhat in order to dampen disturbances more effectively
- A stator flux oriented rotor current controlling rotor converter model could be developed to see if the oscillating torque problem is caused by the strategy of controlling stator currents.
- More advanced control theory with feed forwards of power transport by rotor converter and grid converter q-axis current should be implemented.

5.5 Modifications of Controller Parameters

As a result of thorough testing, several of the suggested solutions from the previous section were developed. Firstly reductions of the stator current controller gains were experimentally found to provide a better damping for the 60 Hz oscillations.

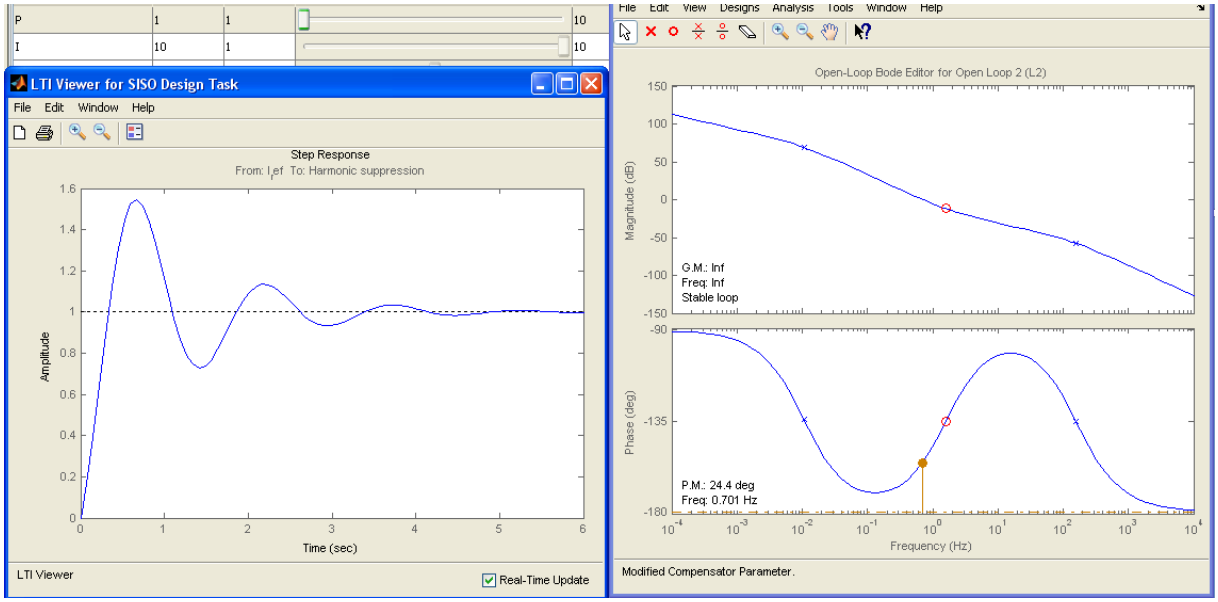

Figure 5.14 - Final Stator D-axis Current Controller Time Response and Bode Plot

With a gain of 20 and an integral time constant of 0.01 s, the phase margin was lowered to 24.4 degrees at cut off frequency 0.701 Hz. As depicted below, the phase margin of the q-axis controller was lowered to 24 degrees at the same cut off frequency and with the same gain and time constant.

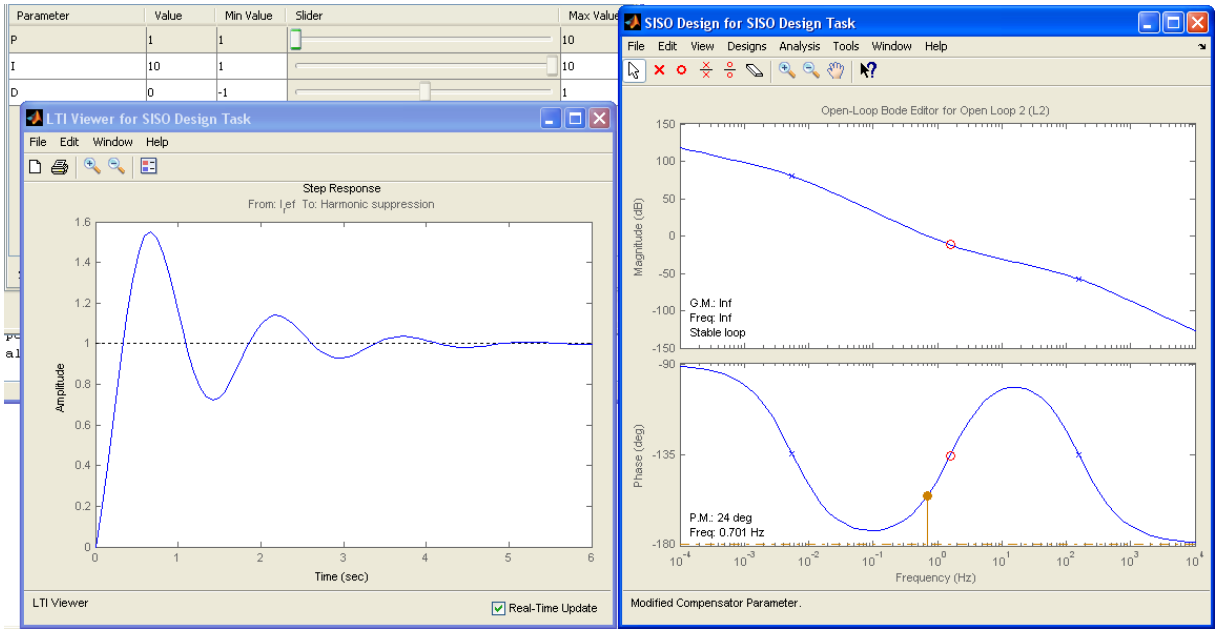

Figure 5.15 - Final Stator Q-axis Current Controller Time Response and Bode Plot

The gains of the grid side converter current controls had to be lowered to further dampen distortions and the harmonics generated.

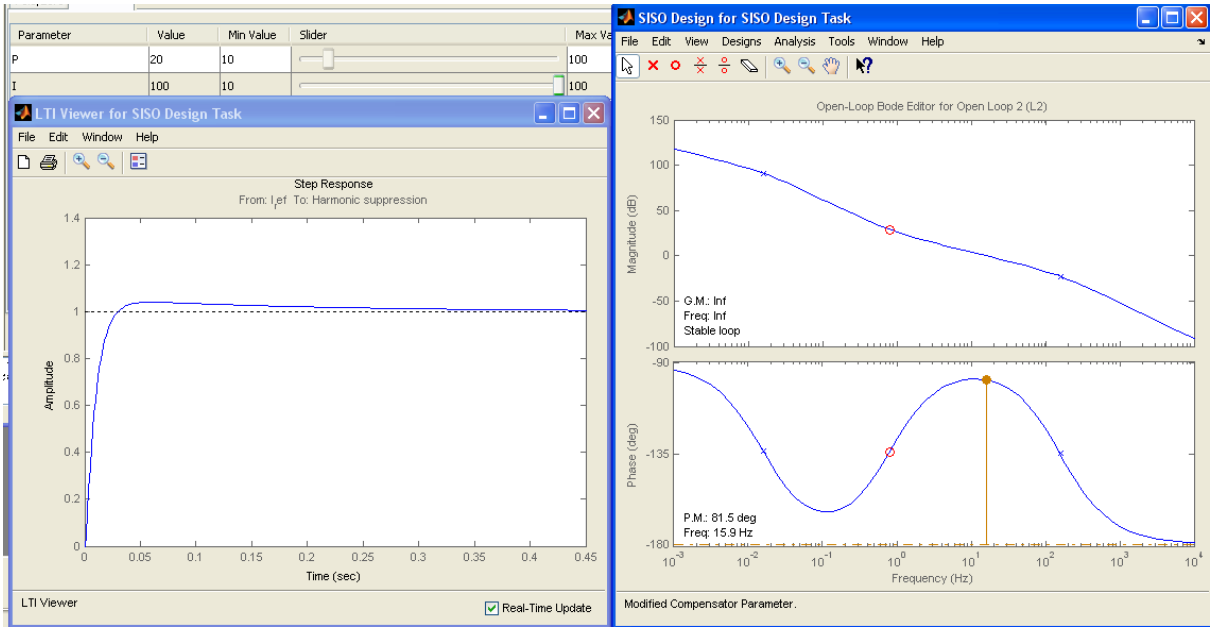

Figure 5.16 - Final Grid Side Converter Current Controllers' Time Response and Bode Plot

With a gain of 20 and an integral time constant of 0.01 s, the gain margin was found to be infinite and the phase margin was found to be 81.5 degrees at cut off frequency 15.9 Hz. These settings greatly reduced the grid side converter's production of harmonics proven earlier in section 5. Harmonics with frequencies lower than the switching frequency were almost non-existent with the new settings.

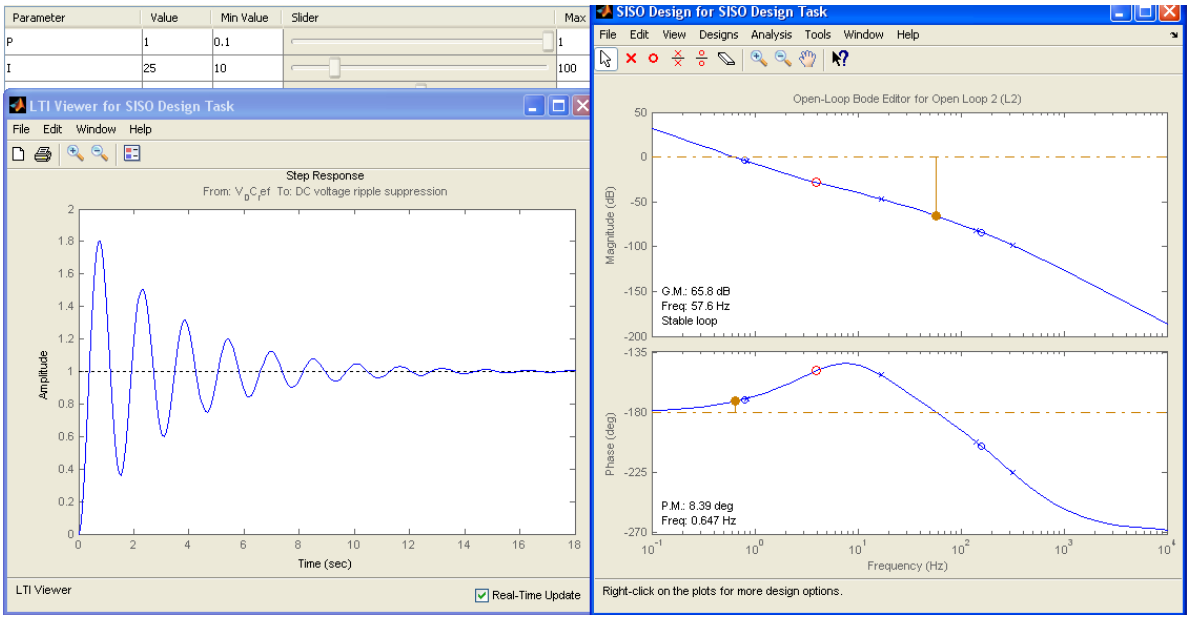

Figure 5.17 - Final DC Voltage Controller Time Response and Bode Plot

The gain for the voltage controller was increased to 1 and the integral time constant lowered to 0.04 s. The gain margin was found to be 67.8 dB and the phase margin was 8.39 degrees at cut off frequency 0.647 Hz. According to the Bode plots, it should be possible to further increase the DC voltage controller gain without any problem. However, this gave a distorted DC voltage in PSCAD. The cause of this problem was not resolved.

The lowered integral time constant helped to eliminate most of the problems previously discovered. The DC voltage is much less disturbed by transitions from steady state to acceleration or deceleration of the generator etc.

5.6 Simulations: DFIG Based Wind Turbine

Simulations were carried out for the DFIG based wind turbine developed previously in this section. The controller parameters found in section 5.5 were used. The figure on the next page illustrates important findings from the simulation without stator flux feed forward or reactive AC voltage compensation controller.

5.6.1 DFIG Model without Stator Flux Feed Forward or Reactive AC Voltage Compensation

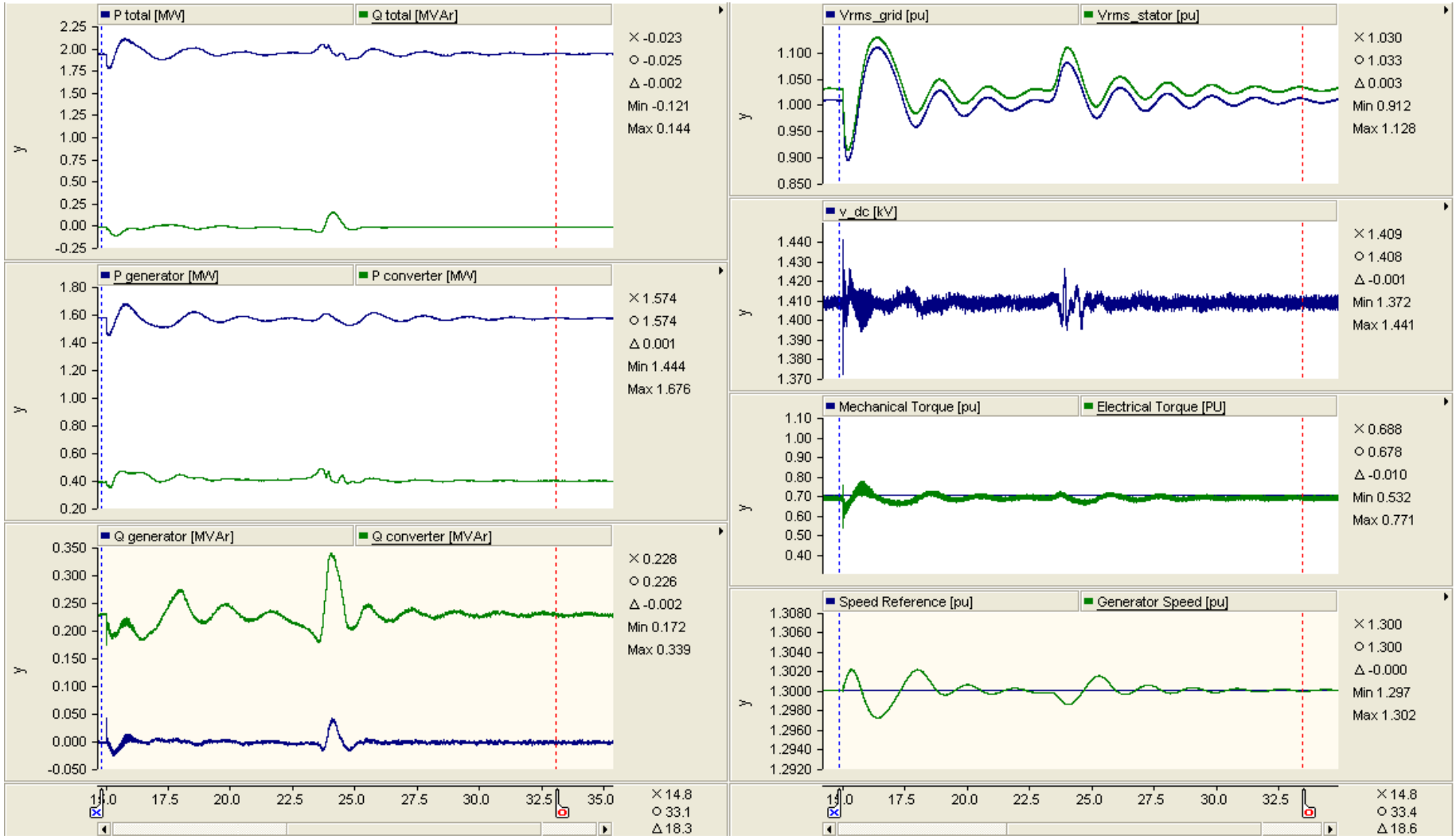

Figure 5.18 - Important DFIG Parameters Measured Throughout the DOL Start Up Sequence, Model without Stator Flux Feed Forward or Reactive AC Voltage Compensation

As seen from figure 5.18 on the previous page, the controllers were able to keep up with the disturbances without any problems. However, there were some small deviations in the total real and reactive power delivered. The measured electrical torque behaved fairly well without any major oscillations (which could cause vibrations). Speed deviation was insignificant due to low variations in electrical torque. DC voltage was kept well within acceptable levels.

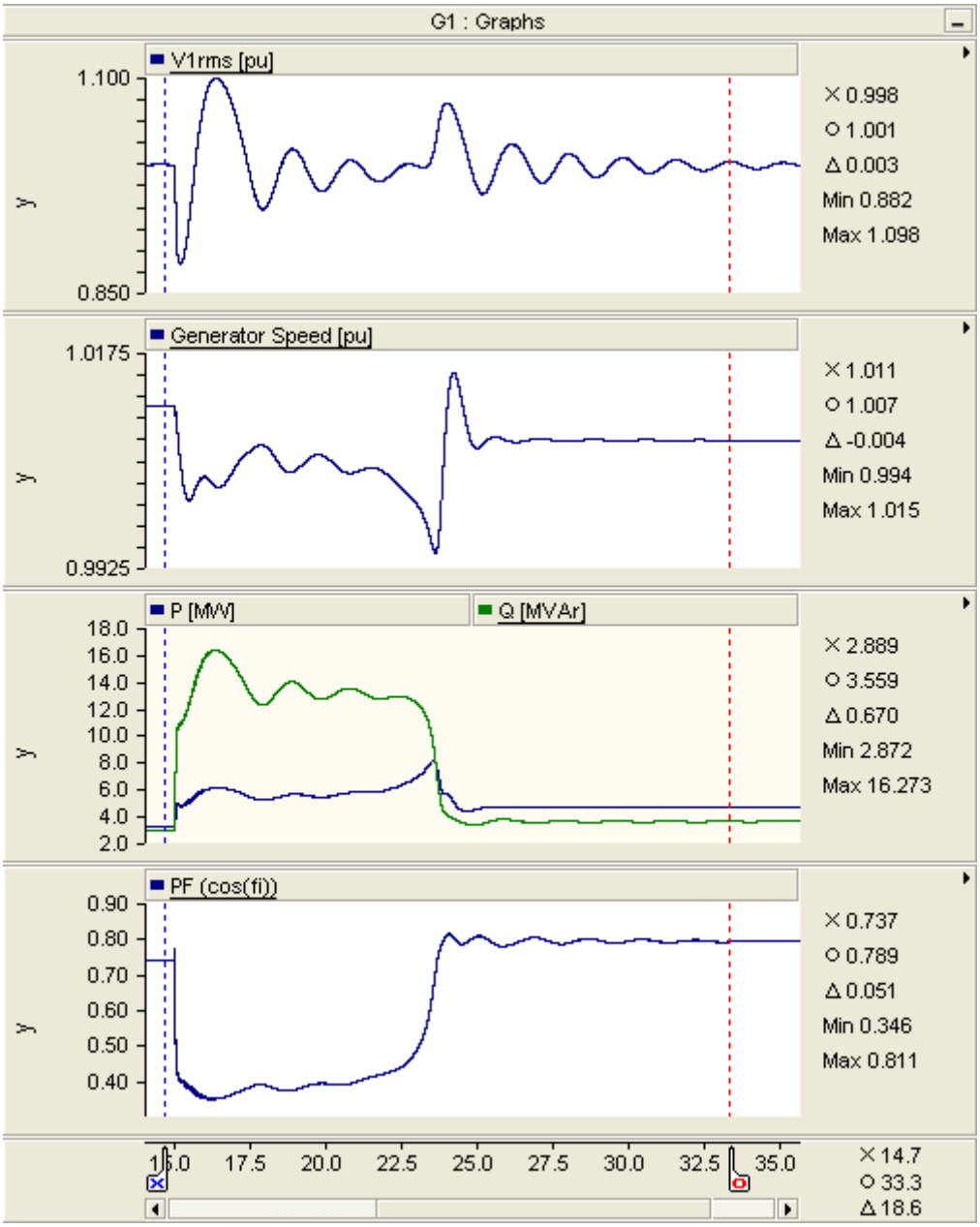

Figure 5.19 – Gas Turbine Generator Terminal Voltage, Generator Speed, Active and Reactive Power Delivered to Grid and the Generators' Power Factor during the DOL Start Up Sequence

Figure 5.19 illustrates how important parameters for gas turbine generators' behaviour also were measured. Changes from previous readings were insignificant, but are given by tables on the next page.

Table 5.1 - Gas Turbine Generator Terminal Voltage, DFIG Test without Flux Feed Forward or Reactive AC Voltage Compensation

Incident:	**Voltage [pu]:**	**Time [seconds]:**
Initial value:	0.997	15.00
Low peak:	0.882	15.18
Low peak:	0.946	17.88
Low peak:	0.967	19.67
High peak:	1.069	24.00
High peak:	1.021	26.12
High peak:	1.010	28.00

Table 5.2 - Gas Turbine Generator Speed, DFIG Test without Flux Feed Forward or Reactive AC Voltage Compensation

Incident:	**Speed [pu]:**	**Time [seconds]:**
Initial value:	1.011	15.00
Low peak at beginning of start up:	1.000	15.45
Low peak at motor torque peak:	0.994	23.59
Stable value after start up sequence:	1.007	40.00

The addition of the DFIG based wind turbine did not have a significant effect on the power system behaviour as a whole. Voltage and frequency measured at the gas turbine generators' terminals were virtually unchanged.

5.6.2 DFIG Model with Stator Flux Feed Forward and Reactive AC Voltage Compensation

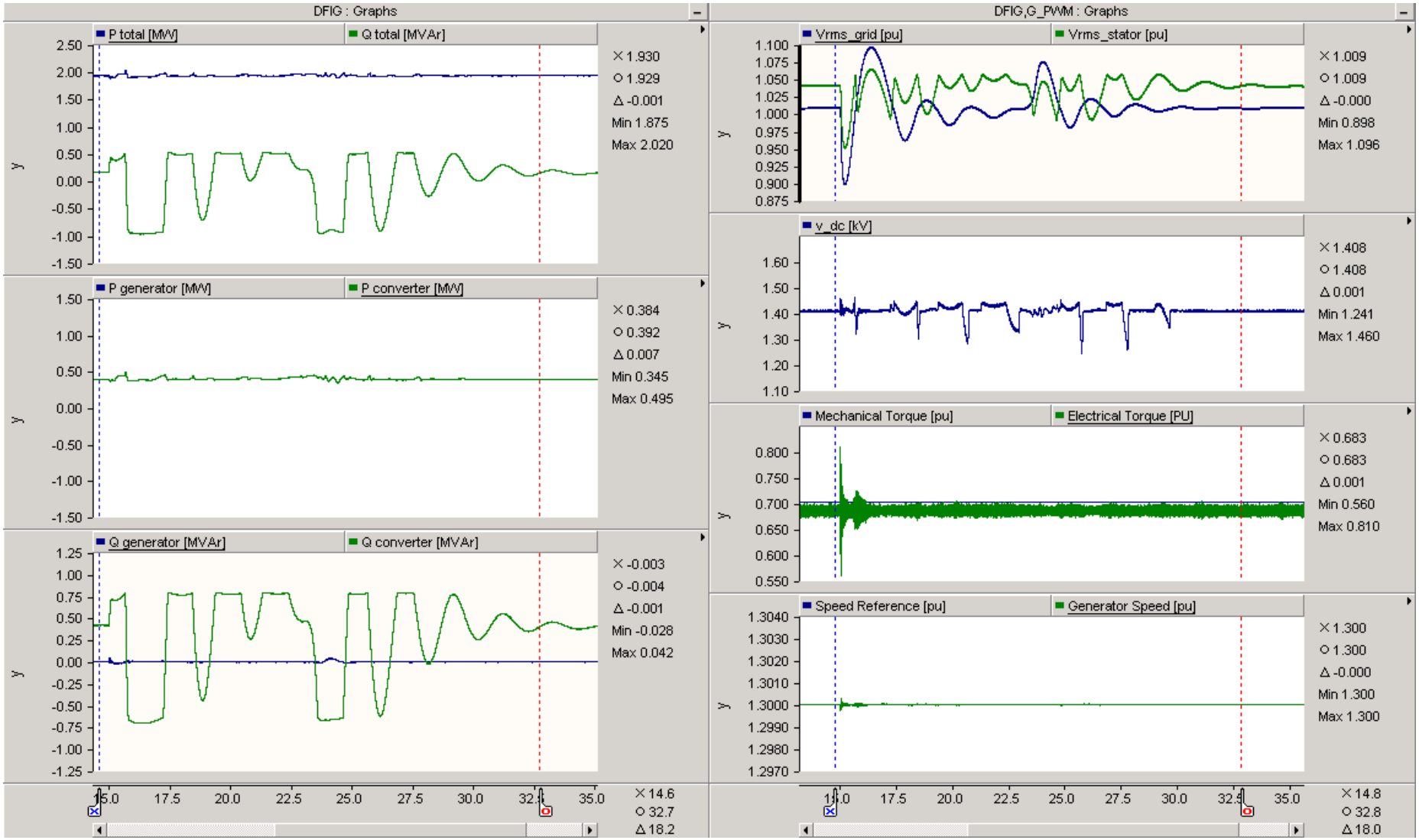

Figure 5.20 - Important DFIG Parameters Measured Throughout the DOL Start Up Sequence, Model with Stator Flux Feed Forward and Reactive AC Voltage Compensation

The stator flux feed forward and AC voltage control terms were added to the model without any changes. However, the voltage increase across the transformer and the grid side converter L filter was not taken into account, and thus the grid side controller ran into problems caused by over modulation. As illustrated in figure 5.20, the DC voltage was disturbed significantly by this. Time did not allow resolving this problem. An easy solution would be to increase the DC voltage or to alter the turn ratio of the transformer. Since this did not inflict material disturbances on the other parameters measured, no further simulations were made.

As illustrated in the left side of figure 5.20, the stator flux feed forward term makes the wind turbine stable. However, there was an instance of small oscillations in the electrical torque at the beginning of the start up sequence. These were quickly dampened. The AC voltage control was very fast and compensated for the variations in the voltage at the gas turbine terminals.

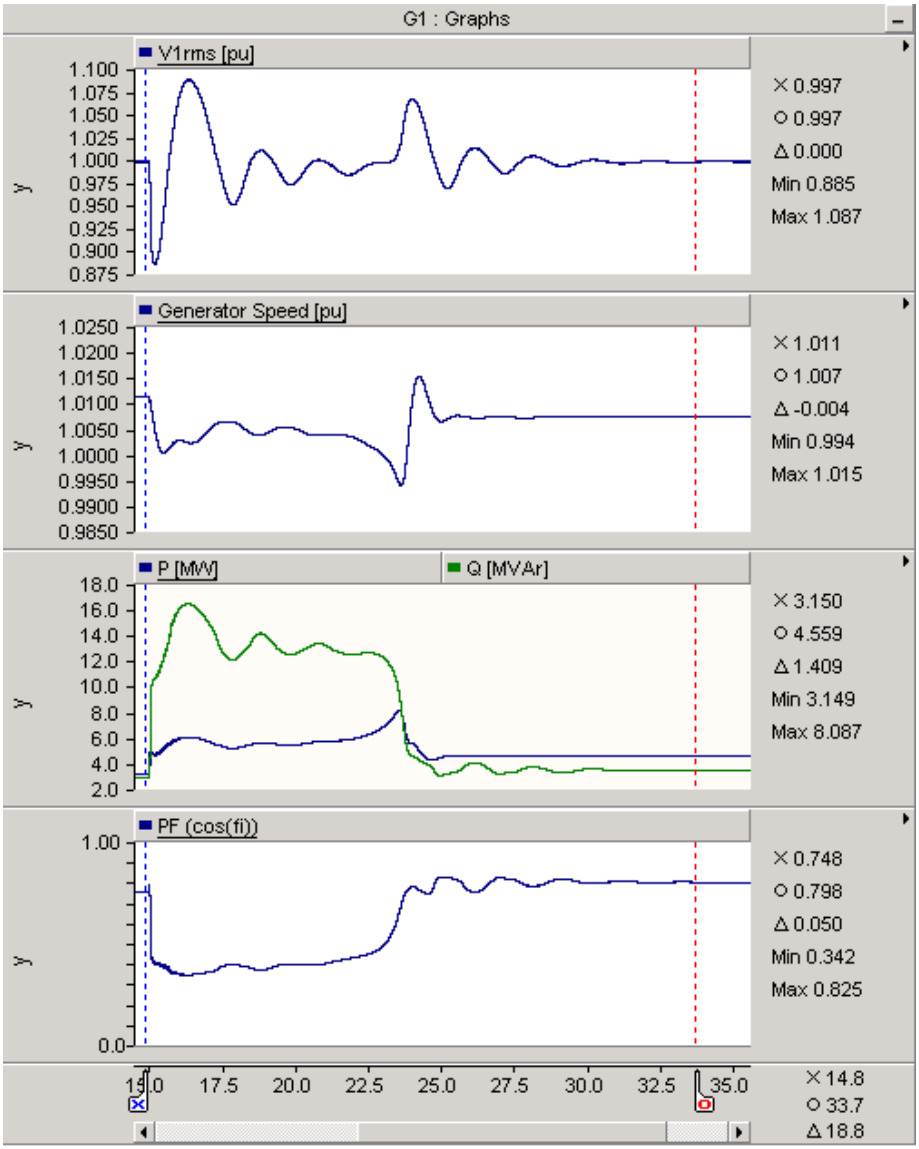

Figure 5.21 - Gas Turbine Generator Terminal Voltage, Generator Speed, Active and Reactive Power Delivered to Grid and the Generators' Power Factor during the DOL Start Up Sequence

Table 5.3 - Gas Turbine Generator Terminal Voltage, DFIG Test with Flux Feed Forward and Reactive AC Compensation

Incident:	**Voltage [pu]:**	**Time [seconds]:**
Initial value:	0.997	15.00
Low peak:	0.885	15.16
Low peak:	0.959	17.87
Low peak:	0.973	19.76
High peak:	1.066	24.00
High peak:	1.012	26.12
High peak:	1.003	28.12

Table 5.4 - Gas Turbine Generator Speed, DFIG Test with Flux Feed Forward and Reactive AC Voltage Compensation

Incident:	**Speed [pu]:**	**Time [seconds]:**
Initial value:	1.011	15.00
Low peak at beginning of start up:	1.000	15.45
Low peak at motor torque peak:	0.994	23.59
Stable value after start up sequence:	1.007	40.00

As seen from the tables, the changes from the other cases were almost insignificant. However there were a slight damping in the voltage oscillation of the power system, and it is expected to reach steady state faster than without any AC voltage control loop of the DFIG.

The DFIG was not expected to alter the frequency response of the power system as the power output is completely stable. It is questionable whether the stator flux feed forward is a valuable addition to the DFIG wind turbine speed control loop or not.

6 Discussion

The modelled squirrel cage induction generator based wind turbine was, as anticipated, affected by the fluctuations in frequency and voltage. It has been shown by calculations and figures that the response to an event where voltage and frequency are reduced or increased simultaneously will be difficult to foresee due to conflicting properties. This makes it hard to determine a worst case scenario for the electrical load situation on the offshore oil platform during the transient event. It could be that the modelled wind turbine had given a more dynamic response with a different load situation.

Converters made for offshore applications need to withstand grid fluctuations. It was shown in section 5.1.1 that converter DC voltage has to be higher than for onshore applications in order to avoid overmodulation. The speed control loop and the DC voltage control loop are found to be nonlinear. If linearised, both of these control loops will have highest gains when the voltage is at the highest and thus also the lowest gain margins. Similarly, they will have the lowest phase margins when the voltage is at its lowest. This process is not shown in further detail.

During simulations it was found that the modelled doubly fed induction generator based wind turbine had no problems to withstand the transient events. However, the inclusion of an AC voltage reactive compensator controller made the DC voltage controller run into problems caused by overmodulation. This could be resolved by redesigning the DFIG system, and by taking the voltage increase across the transformer and the grid side converter L filter into account.

The modulation scheme of the doubly fed induction generator is shown in appendix 6. It features a variable switching frequency generated by the PLL angular output and also a compensation for DC voltage variations.

The strategy of controlling the stator voltages instead of the rotor voltages could have affected the results. It is possible that the 60 Hz oscillations in electrical torque could be eliminated by using the more conventional control strategy. The reason why the latter strategy is more frequently used than the other has not been found. If a rotor current controlling strategy gives better precision, faster controls or better damping it would be relatively easy to develop a stator flux feed forward term based on the fifth order model of the induction machine. Also, the relations found between stator and rotor currents could be used to generate inputs for the grid side converter reactive power control loop. If so, this addition would not represent a need for additional current measuring equipment.

7 Conclusion

None of the modelled generators experienced problems with the disturbances caused by the electromechanical transient fluctuations. Based on the behaviour of the DFIG's grid side converter, it is believed that the result would be the same for a wind turbine with full frequency conversion. Variable speed wind turbines are expected to remain controllable throughout electromechanical transient fluctuations such as for the simulated case.

The stator flux feed forward term stabilised the power output of the doubly fed induction generator. However, the impact on the power system's response was minimal and there is probably no material value of such an addition to the control loop. Detailed studies of the stator flux feed forward term should provide insight for resolving other impacts on the doubly fed induction machine behaviour.

The variable switching frequency ensures an acceptable control over generated harmonics. Also, the variable DC voltage modulation scheme significantly improved the converters behaviour if subjected to disturbances in the DC voltage. This is well illustrated by figure 5.20 where the DC voltage is disturbed and where none of the other controllers were materially affected by these disturbances.

Although the AC voltage compensator controller was imperfect it demonstrated how fast such a control scheme is able to account for voltage deviations.

The high peak values for the voltage at the gas turbine generators' terminals were plotted. Findings were taken from the end of the start up sequence. The figure below depicts a comparison between the voltage peaks with and without reactive voltage compensation. From the figure it is evident that the DFIG not only reduces the voltage transients but also helps to dampen and stabilise the system. The effect is expected to be higher with the addition of higher reactive capability, e.g. by adding more DFIG based wind turbines or wind turbines with full frequency conversion.

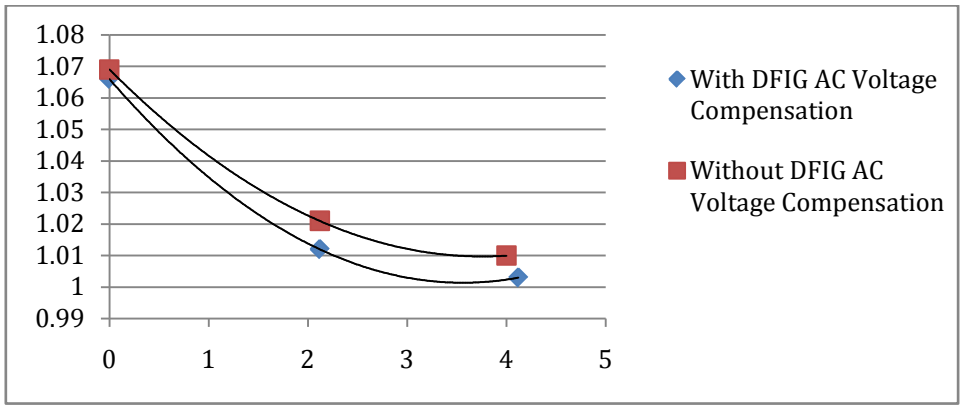

Figure 7.1 - Comparison of Voltage at Gas Turbine Generators' Terminals with and without AC Voltage Compensation

Finally, the measured parameters from the gas turbine generators indicate that all of the modelled wind turbines have minimal impact on the behaviour of the power system as a whole. The gas turbine generators are the most important dynamic component of the modelled power system.

8 Future Work

For the modelled doubly fed induction generator it was found that the reactive voltage compensation controller caused overmodulation from the grid side converter. A solution to this problem is proposed: The system needs to be redesigned and the voltage increase across the transformer and the grid side converter L filter needs to be taken into account. Relevant actions are to alter the turn ratio of the transformer, to limit the reactive compensation or to increase the DC voltage level.

Control schemes for a rotor current controlled DFIG wind turbine could be developed and the behaviour could be compared to a model with stator current control schemes. If such a control strategy provides better behaviour from the doubly fed generator it is expected to also be stable for the simulated events.

There are a lot of unresolved questions regarding the addition of wind turbines to an offshore oil platform utility grid. Among these is how the system will behave throughout a fault situation.

The DOL start up sequences of large motors require large amounts of reactive power to be produced, and thus it seems necessary that gas turbine generators are kept running throughout such events. A study could discover whether it would be possible to stop these generators after such a planned transient event.

Also, the efficiency of gas turbines will be lowered when they run with lower load situations. The wind power generated is somewhat unpredictable, and thus it seems necessary to keep gas turbine generators running as a reserve. A study should seek to determine how these properties of the power system affect the economic and environmental benefits of adding wind turbines.

9 Bibliography

1. **The Norwegian Ministry of Petroleum and Energy; The Norwegian Petroleum Directorate.** *FACTS - The Norwegian Petroleum Sector - 2009.* 2009. ISSN: 1502-5446.

2. **Statens Forurensningstilsyn.** Kvotepliktig utslipp av klimagasser i 2008. *SFT.NO.* [Online] [Cited: 5 06 2009.] http://www.sft.no/artikkel___43613.aspx?cid=3346.

3. **Nord Pool.** Emissions - Carbon Contracts. *NordPool.com.* [Online] [Cited: 12 06 2009.] http://www.nordpool.com/en/asa/Markets/Emissions/EUACER2/.

4. **NPD, NVE, Ptil, SFT.** *Kraft fra land til norsk sokkel.* 2008.

5. **International Electrotechnical Commision.** *IEC 61892-1:2001 - Mobile and fixed offshore units - Electrical installations.* s.l. : British Standard, 2002.

6. **Vestas Wind Systems A/S.** *Electrical Data - V90 3MW 60Hz - Item no: 950027.R1.* 2005.

7. **Blaabjerg, Frede and Chen, Zhe.** *Power Electronics for Modern Wind Turbines.* s.l. : Morgan & Claypool Publishers, 2006. ISBN: 1-59829-032-0.

8. **Alexandra Bech Gjørv, Statoil Hydro.** Presentation: The world's first large scale floating wind turbine. [Online] [Cited: 02 05 2009.] http://www.statoilhydro.com/en/NewsAndMedia/News/2008/Downloads/StatoilHydro%20Hywind%20English%20presentation.pdf.

9. **Stig M. Svalheim, Lyse.** Presentation: Offshore Wind Power. [Online] [Cited: 02 05 2009.] http://www.power-cluster.net/Portals/6/documents/General/Kick%20off%20Stavanger/Svalheim_2008-09-22.pdf.

10. **Ackermann, Thomas.** *Wind Power in Power Systems.* s.l. : John Wiley & Sons Ltd., 2005. ISBN: 0-470-85508-8.

11. **Næss, Bjarne Idsøe.** *Operation of Wind Turbines with Doubly Fed Induction Generators During and After Line Voltage Distortions, Thesis for the degree of Philosophiae Doctor.* s.l. : Norwegian University of Science and Technology, 2008. ISBN: 978-82-471-1211-3.

12. **The Institute of Electrical and Electronics Engineers, Inc.** *IEEE Std. 1110-2002 - IEEE Guide for Synchronous Generator Modeling Practices and Applications in Power System Stability Analyses.* 2003. ISBN: 0-7381-3481-3.

13. **Kundur, P.** *Power System Stability and Control.* s.l. : McGraw-Hill Inc., 1994. ISBN: 978-0-07-035958-1.

14. **Machowski, J., Bialek, J. W. and Bumby, J. R.** *Power System Dynamics - Stability and Control.* s.l. : John Wiley & Sons Ltd., 2008. ISBN: 978-0-470-72558-0.

15. **Manitoba HVDC Research Centre.** *PSCAD On-Line Help System.*

16. **Mohan, Ned.** *Advanced Electric Drives.* s.l. : MNPERE, 2001. ISBN: 0-9715292-0-5.

17. **Marvik, Jorun Irene.** *Masteroppgave - Stabilitet i vindpark med asynkrongeneratorer.* s.l. : NTNU, 2004.

18. **Tao Sun, Zhe Chen, Frede Blaabjerg.** *Flicker Study on Variable Speed Wind Turbines With Doubly Fed Induction Generators.* s.l. : IEEE Transactions on Energy Conversion, Vol 20, No. 4, December 2005, 2005.

19. **C. Schauder, H. Mehta.** *Vector Analysis and Control of Advanced Static VAR Compensators.* 1993. IEEE Proceedings-C, Vol 140, No 140, July 1993.

20. **Marvik, Jorun I., et al.** *Control of a Wind Turbine with a Doubly Fed Induction Generator after Transient Failures.* 2004. Paper for NORPIE 2004.

21. **Bjørgum, Torstein.** *Hovudoppgåve - Dobbeltmata asynkronmaskin, Analyse av maskindynamikk.* s.l. : NTNU, 2004.

22. **The Institute of Electrical and Electronics Engineers, Inc.** *IEEE Std. 421.5-2005 - IEEE Recommended Practice for Excitation System Models for Power System Stability Studies.* 2006. ISBN: 0-7381-4786-9.

23. —. *IEEE Std. 421.5-1992 - IEEE Recommended Practice for Excitation System Models for Power System Stability Studies.* 1992. ISBN 1-55937-218-4.

24. **Yee, Soon Kiat, Milanovic, Jovica V. and Hughes, F. Michael.** *Overview and Comparative Analysis of Gas Turbine Models for System Stability Studies.* s.l. : IEEE Transactions On Power Systems Vol. 23 NO. 1. February 2008, 2008.

25. **Nexans Norway.** TSLE-O 12kV3x1x 50AQ. *Nexans Norway.* [Online] [Cited: 10 05 2009.] http://www.nexans.no/eservice/Norway-no_NO/navigateproduct_540078376/TSLE_O_12kV3x1x_50AQ.html.

Appendix 1 - Configuration of the Offshore Oil Platform Case Model

The figure A1.1 gives a visual overview of the electrical configuration on an offshore oil platform. The next pages will be used to cover the model in more detail. As the PSCAD model has been split up into modules, the detailing will follow a similar pattern. The figure below illustrates a screenshot from PSCAD, giving a graphical overview of how the electrical system has been modelled.

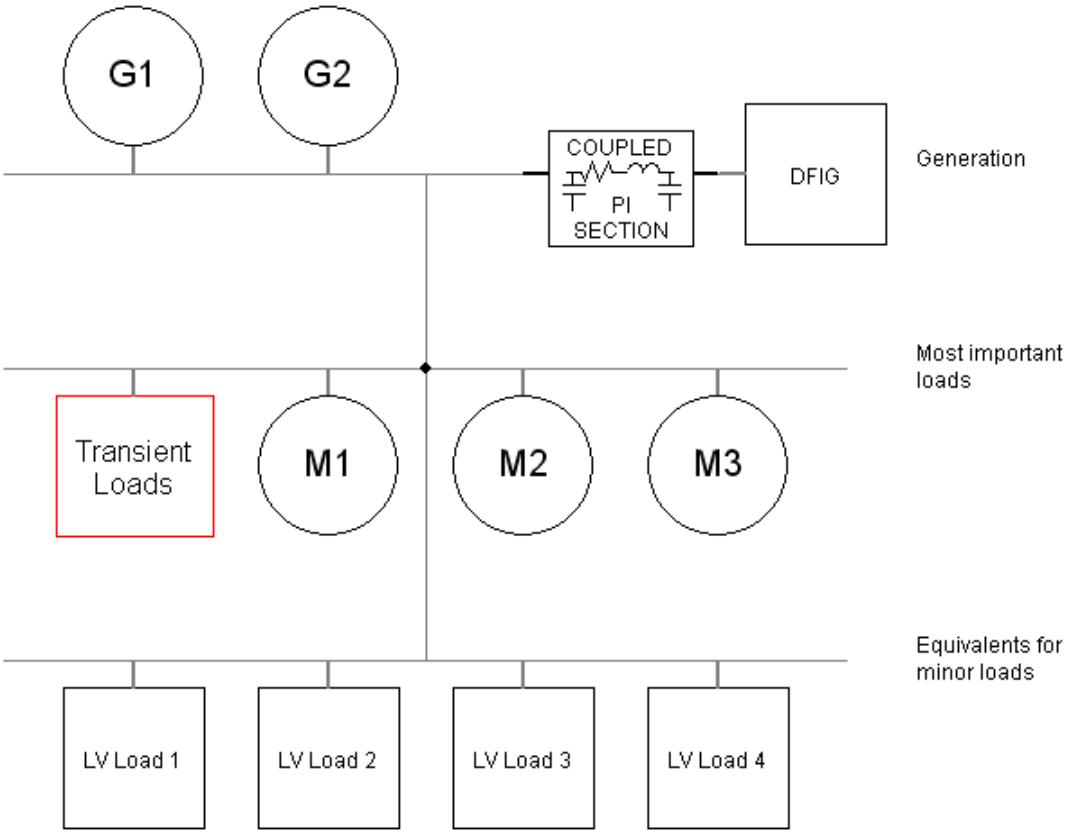

Figure A1.1 - Overview of the Offshore Oil Platform Electrical System Modules Used in PSCAD Simulations

The case model consists of the following modules:

- G1, G2 – 12.45 MW gas turbine generators
- Transient load models, e.g. start up model of produced water injection pump
- M1 – Two water injection pumps
- M2 – Two sea water lift pumps
- M3 – A cooling pump
- Equivalents for minor loads, e.g. heating, lighting, control systems and auxiliary
- Optional wind turbine generator attached by subsea cable (covered in other sections)

A 1.1 - Modelling of the Gas Turbine Generators:

In order to simulate the behaviour of synchronous machines it is important to include models of the voltage regulator, the excitation system and the governor as well as the physical properties of the machine itself. Figure A1.2 illustrates the configuration of the generator modules in the simulated PSCAD case.

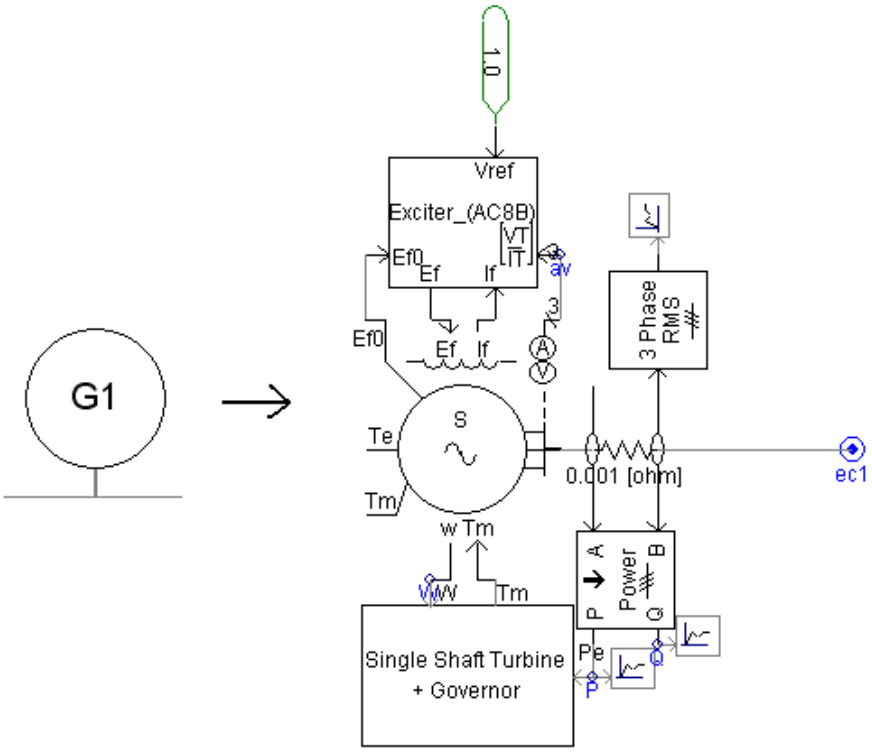

Figure A1.2 -Overview of the Generator Model in PSCAD

The G1 and G2 modules consist of three interconnected models: the generator, the turbine/governor and the voltage regulator. The next few pages will be used to cover the properties and the modelling for each of these models.

A 1.1.1 - The Synchronous Generator

The synchronous generator model was selected from the PSCAD Master Library, and the parameters were adjusted to fit properties given in table A1.1 and by calculations on the next pages.

As load flow calculations are impossible to conduct in PSCAD the start up routine was modified. This means that the generator starts with rated voltage, rated speed and 10 MW power output. This last setting should ensure that the generators start off with a rotor angle above zero and hereby minimize oscillations. The start up fluctuations will need to calm down prior to undertaking any of the measurements or important system configuration changes.

Table A1.1 – Physical Properties of the Gas Turbine Generators	
Voltage rating:	11 kV
Power rating:	12.45 kW
Rated power factor:	0.8
Number of poles:	4
Moment of inertia:	1285 kgm^2 (lumped)
Number of Q-axis damper windings:	0
Unsaturated reactance values (60 Hz):	
Armature leakage reactance Xl:	0.10 pu *
Direct axis synchronous reactance Xd:	1.057 pu
Quadrature axis synchronous reactance Xq:	0.504 pu
Direct axis transient reactance X'd:	0.175 pu
Direct axis subtransient reactance X''d:	0.107 pu
Quadrature axis subtransient reactance X''q:	0.176 pu
Time constants:	
Armature time constant Ta:	0.125 s
Direct axis transient open time constant T'do:	6.35 s
Direct axis subtransient open T.C.: T''do:	0.02944 s **
Quadrature axis subtransient open T.C. T''qo:	0.07358 *s* ***
Direct axis subtransient short circuit T.C T''d:	0.018 s
Quadrature axis subtransient short circuit T.C. T''q:	0.037 s

* Estimated based on typical values found in [13] page 153 and the knowledge that this value should be lower than any of the other reactances.

** Estimated based on the relationship found in [14] page 139:

$$T''do \cong T''d \ \frac{X'd}{X''d} = 0.018 \frac{0.175}{0.107} \ s = 0.02944 \ s \qquad \text{(A1.1)}$$

*** Estimated based on the relationship found in [14] page 139 and a typical value for X'q knowing that it should be higher than both X'd and X''q but lower than Xq, and looking at the typical relation between X'q and X'd from [14] page 138:

$$T''qo \cong T''q \ \frac{X'q}{X''q} \approx T''q \ \frac{2X'd}{X''q} = 0.037 \frac{2 \cdot 0.175}{0.176} \ s = 0.07358 \ s \quad \text{(A1.2)}$$

From the information given in table A1.1 it is possible to calculate the values needed for the PSCAD model. The symbols used in equations A1.3 to A1.8 represent the following quantities:

H – Inertia constant
Sr – Rated apparent power
Pr – Rated active power
cosφ – Rated power factor
j – Moment of inertia
ω_m – Synchronous mechanical speed
ω_s – Synchronous electrical speed
p – Number of poles in the synchronous generator
Vln – RMS line-to-neutral voltage
Vll – RMS line-to-line voltage
Ir – Rated RMS current

The model needs the inertia constant H. This could be found using the following relations:

$$H = \frac{0.5 J \omega_m{}^2}{Sr} \quad \text{(A1.3)}$$

$$Sr = \frac{Pr}{cos\varphi} \quad \text{(A1.4)}$$

$$\omega_m = \omega_s \frac{2}{p} = 2\pi f \frac{2}{p} \quad \text{(A1.5)}$$

By combining the equations A1.3-A1.5 we get:

$$H = \frac{cos\varphi \cdot 0.5 \cdot j \cdot \omega_m{}^2}{Pr} = \frac{0.8 \cdot 0.5 \cdot 1285 \ kgm^2 \cdot (\pi \cdot 60 \ rad/s)^2}{12450 \ kW} = 1.46688 \ s \quad \text{(A1.6)}$$

In addition, the RMS line-to-neutral voltage is found by:

$$Vln = \frac{Vll}{\sqrt{3}} = \frac{11 \ kV}{\sqrt{3}} = 6.3508 \ kV \quad \text{(A1.7)}$$

Rated RMS current is found by:

$$Ir = \frac{\sqrt{3} \cdot Pr}{3 \cdot Vll \cdot \cos\varphi} = \frac{12450\ kW}{\sqrt{3} \cdot 11kV \cdot 0.8} = 0.8168\ kA \quad \text{(A1.8)}$$

For iron loss resistance, the value pre-existing in the PSCAD Master Library model is used. This value is 300 pu, and is so high that it will have minimal implications on the generators dynamic behaviour.

The generator neutral is grounded trough a fairly large resistance. This is arbitrarily chosen to be 40 pu. This value will not inflict the behaviour of the synchronous generator in the simulations as no fault situations will be simulated.

The armature leakage reactance Xl is implemented in the model by setting the Potier reactance at the same value as Xl in table A1.1, and by setting the air gap factor to 1. This factor is scaling the relationship between the armature leakage reactance and the Potier reactance as shown by the equation below:

$$Xl = Xp \cdot AGF \quad \text{(A1.9)}$$

No saturation data for the generator was included. The model should be sufficiently accurate without this data. Due to the large amount of reactive power that the generators have to supply during the start up sequence of a large squirrel cage motor, the model would clearly have been even more accurate with this data supplied. However, the main purpose of this particular model is to generate a frequency and voltage response that will be within the vicinity of what could be expected from a medium sized offshore oil platform electrical system.

A 1.1.2 - The Automatic Voltage Regulator and Excitation System

IEEE Std. 421.5-2005 [22] is a major source for excitation system models used in dynamic simulations. The type of excitation system used in an offshore gas turbine generator is most often, if not always, of the brushless type. To model this kind of a system the use an IEEE AC-series model is needed. The AC8B model is used for the simulations conducted in this thesis.

A model for the excitation system AC8B is already included in the PSCAD Master Library, and it can be edited to match specifications given by the user. As seen by figures A1.3 and A1.4 on the next page, there is a difference between the transfer function schematics from the IEEE standard and the PSCAD excitation system model. A field current

measurement is not included in the simulated model. The reason for this is that the PSCAD model is based on the previous standard IEEE Std. 421.5-2002 [23] and is not updated to the new specifications. However, the new standard would not have had major implications on the simulated results. In addition, the updated standard [22] states that, for a digitally controlled voltage regulator, the parameters K_C and K_D in figure A1.3 could be set to zero, and thus the impacts of the field current can be neglected.

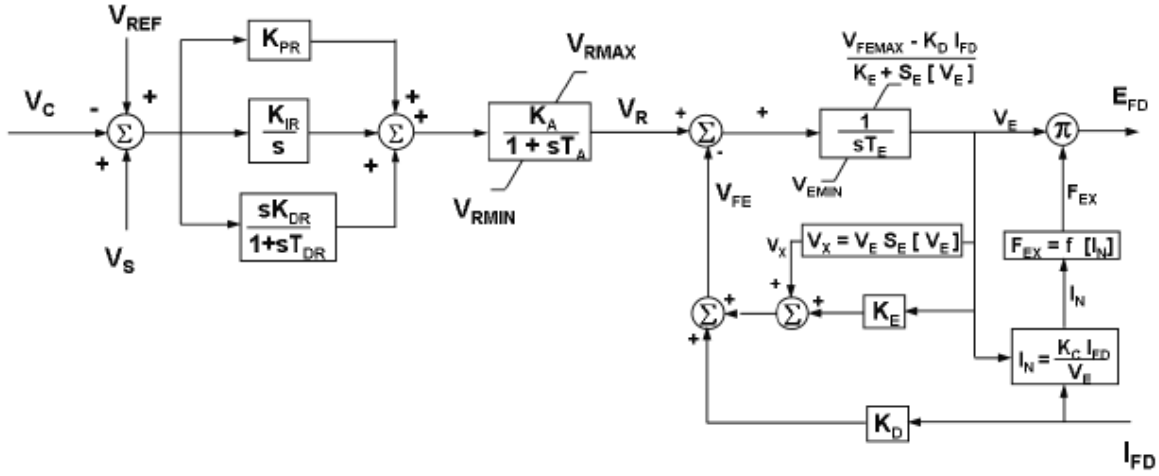

Figure A1.3 - Type AC8B Alternator-Rectifier Excitation System as Presented in IEEE Std. 421.5-2005

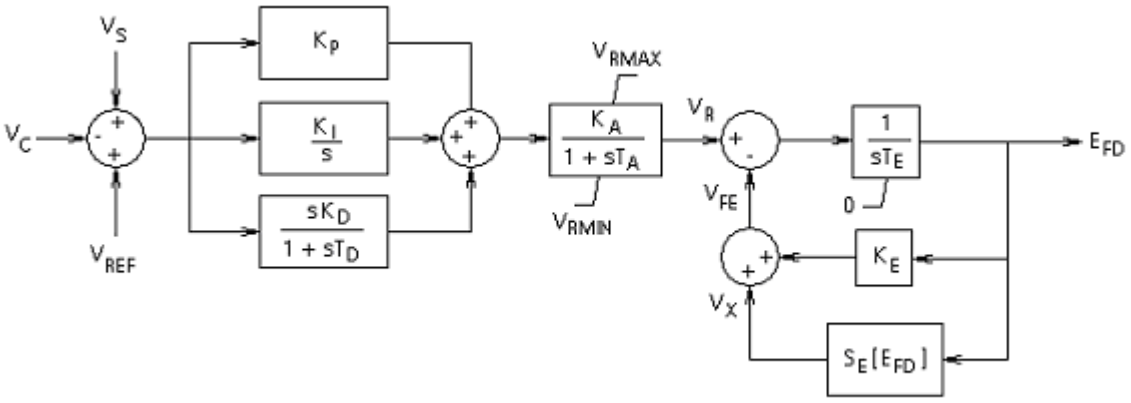

Figure A1.4 - Type AC8B Alternator-Rectifier Excitation System as Presented by PSCAD On-Line Help System

Section 1.1 in the latest version of IEEE Std. 421.5 [22] states that the models of excitation systems are valid for all voltage levels and for frequency deviations of up to ±5% from rated. This is exactly the same as the deviation limits in the IEC 61892-series of standards [5]. Therefore the models will be valid for simulations of the electrical systems of both mobile and fixed offshore units.

The following parameter values have been used for the voltage controller and excitation mechanism:

Table A1.2 – Voltage Regulator and Excitation System Parameters	
Proportional gain, K_P:	84
Integral gain K_I:	5
Derivative gain K_D:	10
Voltage regulator maximum output, $V_{Rmax:}$	51
Voltage regulator minimum output, $V_{Rmin:}$	0
Voltage regulator gain, $K_{A:}$	1
Voltage regulator time constant, $T_{A:}$	0 s
Exciter field time constant, $T_{E:}$	1 s
Exciter constant, $K_{E:}$	1
Saturation at 75% ceiling voltage, S_E(Efd1):	0.51 pu
75% ceiling voltage, Efd1:	6.2 pu
Saturation at 100% ceiling voltage, S_E(Efd2):	5.21 pu
100% ceiling voltage, Efd2:	8.3 pu

A 1.1.3 - The Gas Turbines and Governors

It is essential to have a good model of the gas turbine and the governor to predict the generator's behaviour and the frequency deviation of the power system. The IEEE paper "Overview and Comparative Analysis of Gas Turbine Models for System Stability Studies" [24] is one of the best sources available for explanations of different gas turbine and governor models. The model used in this simulation is illustrated in figure A1.5 on the next page.

Gas turbine governors have several control loops affecting their behaviour. This particular model contains a frequency and a temperature override control mode. This means that if the gas turbine runs too hot, the frequency control loop will be overridden and the gas turbine governor will remain in temperature override control mode until the measured temperature of the gas turbine reaches an acceptable level.

Normally, the governor operates in frequency control mode. The per unit speed of the generator is measured and compared to a reference speed; the deviation is magnified by a gain and used as an input for the fuel controller. Further, the model replicates the behaviour of the combustion process and turbine mechanics before an output torque is applied to the generator model (discussed in previous sections).

Since the PSCAD model and the governor have different per unit bases, the measured power input is converted into an active power based per unit system. In the end, the output torque is transferred into an apparent power based per unit system.

The air flow set point does not vary in this model, but could be used as an input in advanced control schemes where inlet guide vanes are operated. The guide vanes are operated to keep a sufficiently high temperature in order to lower emissions in part load operation.

The governors are operated in droop mode during the simulations in order to avoid problems with load sharing. This is assumed to be the normal mode of operation for the simulated system.

Unfortunately, PSCAD is not always cooperative when it comes to rotating transfer function blocks. The text on the time-delay and the low pass function (the real pole) in the temperature measurement does appear to be upside down in the figure on the next page.

All the parameters used in this model are found on the next two pages.

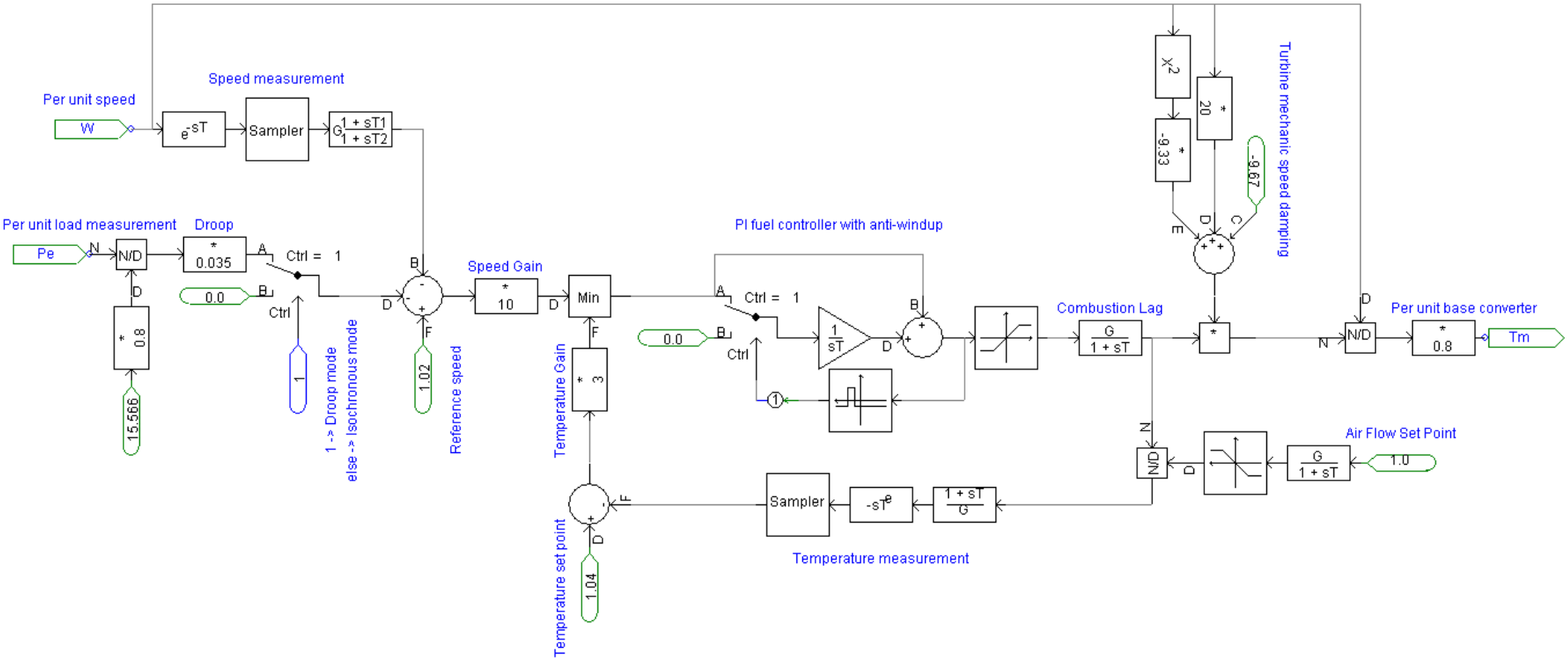

Figure A1.5- The Gas Turbine and Governor Transfer Function

Correction: the temperature measurement control loop figures are flipped upside down by PSCAD, it should be a first order low pass function in series with a time-delay and a sampler.

The following parameter values are used in the governor and gas turbine transfer functions:

Table A1.3 – Gas Turbine and Governor Transfer Function Parameters	
Speed measurement:	
Transport delay time constant:	0.04 s
Sampling frequency:	33.3333 Hz
Lead-Lag gain, G:	1
Lead time constant, T1:	0.65 s
Lag time constant, T2:	0.15 s
Droop function:	
Per unit base for active power:	15.566 x 0.8 MW
Droop:	0.035 (or 3.5%)
Operating mode:	Droop mode
Temperature measurement:	
Low pass gain, G:	1
Low pass time constant, T1:	0.5 s
Sampling frequency:	33.3333 Hz
Controller:	
Reference speed:	1.02 (higher than 1 because of droop)
Temperature set point:	1.04
Speed gain:	10
Temperature gain:	3
Fuel controller proportional gain:	1
Fuel controller integral time constant T:	0.3 s
Upper fuel controller limit:	1.1
Lower fuel controller limit:	-0.7 (negative because of turbine dynamics)
Gas turbine dynamics:	
Combustion lag gain:	1
Combustion lag time-constant:	0.3
Turbine mechanic speed damping:	$-9.33\omega^2 + 20\omega - 9.67$ (PU speed input)
Per unit base converter:	0.8
The air flow function is inactive during the simulations and can be neglected.	

A 1.2 - Transient Loads

The transient loads of the power system have to be modelled. Figure 4.6 illustrates that there are three different loads modelled for this power system. By controlling which loads are open and which are closed it is possible to simulate different transients. The most important load is the dynamic model of the squirrel cage motor of the M1 type. The other two are fixed resistance and fixed reactance loads (not fixed power and reactive power as PSCAD visualises it). The fixed resistance load could be used to better isolate the frequency response of the system, whereas the fixed reactance could force an instantaneous voltage drop.

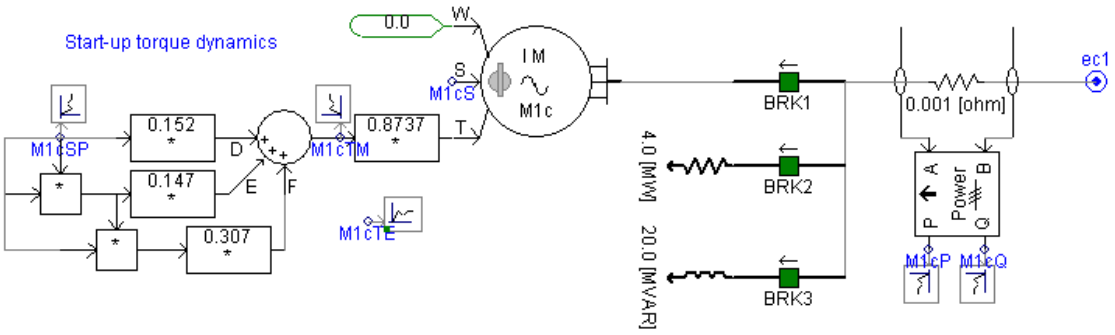

Figure A1.6 - Dynamic Models of the Transient Loads

Throughout the start up sequence of the produced water injection pump the water will be forced trough a closed loop. This ensures that the torque will be low enough for the machinery to accelerate before it gets overheated. The curve-fitted torque function is:

$$T_{mech} = (0.307\omega_m{}^3 + 0.147\omega_m{}^2 + 0.152\omega_m) \cdot 0.8737 \qquad \text{(A1.10)}$$

There are several methods for modelling the start up sequence of squirrel cage induction motors. Most of the large motors have a huge variation in parameter values during the start up due to changes in flux, flux paths and the skin effect. The options in PSCAD are to model this by making a two-caged rotor or by using the EMTP type 40 model. The latter model is based on current-speed and torque-speed characteristics and is therefore simpler to generate. Because of this, the EMTP type 40 model is chosen.

Motor model parameters will be found in table A1.4 on the next page.

Table A1.4 – M1 Type Motor Start Up Parameters	
Rated voltage:	11 kV
Rated power on shaft:	4600 kW
Coefficient of efficiency:	0.96
Rated power factor:	0.90
Rated slip:	0.011 pu
Synchronous speed:	3600 rpm
Start up current divided by rated current:	4.16 pu
Moment of inertia:	178 kgm^2 (lumped)
Start up time:	8.75 s (in rated conditions)
Calculated/estimated additional parameters for PSCAD:	
Rated RMS phase voltage:	6.35085 kV *
Rated RMS phase current:	0.27944 kA *2
Base angular frequency:	376.991 rad/s *3
Number of poles:	2 *4
Starting torque at rated conditions:	0.6 (typical data)
Maximum torque:	1.9 (typical data)
EMTP Type 40 design ratio:	0.60 *5

* Found by:

$$V_{LN} = \frac{V_{LL}}{\sqrt{3}} = \frac{11\ kV}{\sqrt{3}} = \ 6.35085\ \text{kV} \tag{A1.11}$$

*2 Found by:

$$I_R = \frac{P}{3 \cdot \cos\varphi \cdot \eta \cdot V_{LN}} = \frac{\sqrt{3} \cdot 4600}{3 \cdot 0.90 \cdot 0.96 \cdot 11} = \ 0.27944\ \text{kA} \tag{A1.11}$$

*3 Found by:

$$\omega_s = 2\pi f = 2\pi 60\ {}^{rad}/_{S} = 376.991\ {}^{rad}/_{S} \tag{A1.12}$$

*4 Found by relation in (A1.5).

*5 After all the other parameters were established, the “design ratio” parameter for this model had to be estimated. PSCAD calculates a two-cage motor model from this value, which gives a relationship between the reactance and resistance values of the two cages. Unfortunately the PSCAD On-Line Help System [15] does not reveal exactly how this process works.

It seems like a good idea to tune this parameter until the machine accelerates as fast as the given start up time. A small benchmark model is set up in order to do this. The machine is accelerated connected to an ideal three phase voltage source at rated conditions. With a design ratio value of 0.60 we get a result with virtually no error in start up time.

In figure A1.7 below the torque-speed characteristic is logged throughout the start up sequence. The difference between electrical torque (green) and mechanical torque (blue) leads to an acceleration of the rotor. This lasts until the speed reaches a certain level where the two characteristics are in equilibrium. The curve for electrical torque looks a bit pointy, but still plausible.

On the other half of the figure it can be observed that the motor draws quite a lot of reactive power during the start up. This will cause the voltage of the entire platform utility grid to drop until the automatic voltage regulators of the gas turbine generators makes up for it. Also, the machine draws almost 8.4 MW of active power during the start up. It is important to have a bit of extra capacity from the gas turbines before attempting such a start up in order to avoid compromising the stability of the power system.

Further, it has been measured that the machine reaches its speed in 8.72 seconds and that the powers reaches steady state in 8.8 seconds. This is very close to the 8.75 seconds we attempted to tune the machine parameters to match.
The power factor throughout the start up has been calculated by means of the relationship:

$$\cos\varphi = \cos\left(\tan^{-1}\left(\frac{Q}{P}\right)\right) \tag{A1.13}$$

Figure A1.7 is included in order to illustrate how real time calculations can be done in PSCAD. The rightmost symbol illustrates that the value is logged to a graph frame. The inputs M1aQ and M1aP are reactive and active power respectively.

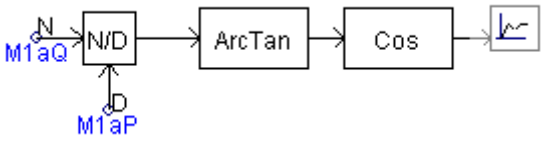

Figure A1.7- Calculation of Power Factor in PSCAD

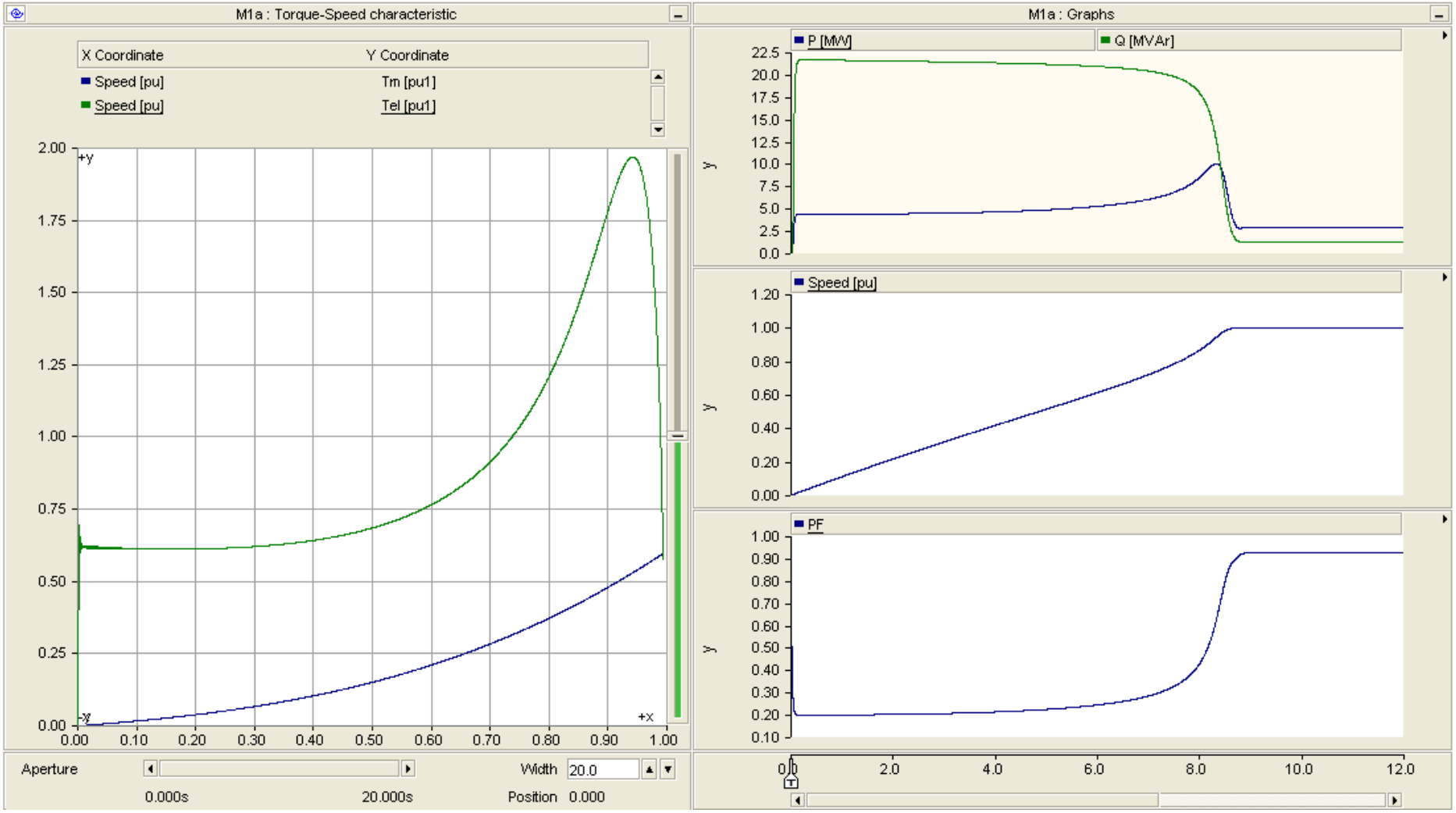

Figure A1.8 – Torque-Speed Characteristic, Powers, Speed and Power Factor for the Produced Water Injection Pump at Rated Conditions

A 1.3 - Dynamic Load Models for Loads Connected Prior to Transient Events

In order to investigate how the offshore oil platform power system behaves throughout the simulated events, it is crucial to include the dynamics of the loads that are connected (hot) to the power system before the transient event takes place. The majority of loads in an offshore utility grid are squirrel cage motors. As seen from figure 3.1 in section 3, this also applies to the load situation for the simulated case. Figure A1.1 illustrates how the system has been modelled by the use of PSCAD sub modules.

A 1.3.1 - M1 Type Motors

There are two motors of the M1 type running prior to the transient events that are simulated. To get the models as accurate as possible the explicit data format will be used. This means that the equivalent circuit parameters have to be supplied. PSCAD does not allow modelling of a squirrel cage induction generator with only one rotor cage, but this restriction is overcome by setting the second cage reactance and resistance very high. 10000 pu is arbitrarily chosen for these values.

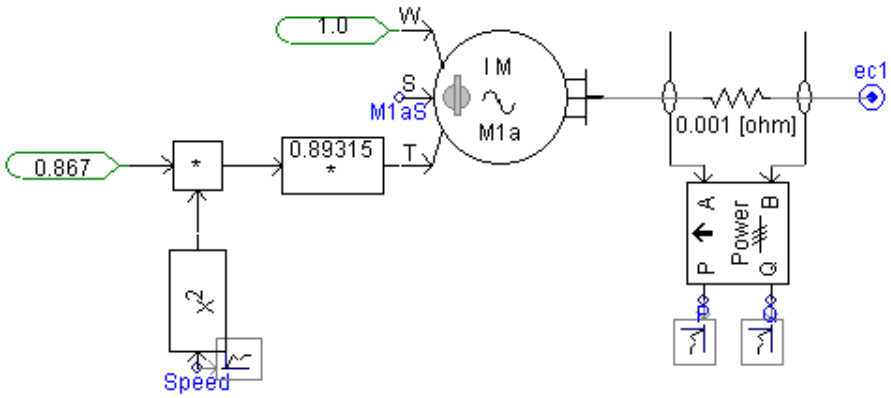

Figure A1.9 - The Most Important Contents of the M1 Module in PSCAD

The mechanical torque characteristic is different from the start up characteristic where water is running in a closed loop. Mechanical torque as function of speed is given by:

$$T_{mech} = 0.89315(0.867\omega_m{}^2) \tag{A1.14}$$

The factor inside the parenthesis determines the shaft torque as a function of speed squared. The factor 0.89315 transfers the torque from a shaft power based per unit system into a motor apparent power PU system as calculated by (A1.15).

$$\frac{T_{base}}{0.867\omega_m{}^2} = \frac{\cos\varphi \cdot \eta}{(1-s_{rated})^3} = \frac{0.90 \cdot 0.96}{(1-0.011)^3} = 0.89315 \tag{A1.15}$$

This relation was based on:

$$P_m = \omega_m T_m = \omega_m {\omega_m}^2 0.867 \tag{A1.16}$$

$$P_m = T_{base} \cdot \omega_s \cdot \cos\varphi \cdot \eta \tag{A1.17}$$

$$\omega_{m,rated} = \omega_s(1 - s_{rated}) \tag{A1.18}$$

Such that:

$$0.867{\omega_s}^3(1 - s_{rated})^3 = T_{base} \cdot \omega_s \cdot \cos\varphi \cdot \eta \tag{A1.19}$$

From equation (A1.19) we get (A1.15).

Also, the model type requests the per unit moment of inertia calculated by:

$$J = 2H = \frac{cos\varphi \cdot \eta \cdot j \cdot {\omega_s}^2}{Pm} = \frac{0.90 \cdot 0.96 \cdot (1 - s_{\text{rated}}) \cdot 178 \cdot (2\pi 60)^2}{4600000}\,\text{s} = 4.7516\ \text{s} \tag{A1.20}$$

The two machines are modelled as one by setting the number of coherent machines parameter to 2. According to [15] this will make the machine look like two machines by multiplying the currents.

The motor model input marked W sets a fixed speed at 1 pu and the input S is controlled by releasing the rotor from this speed during the initialization process of the simulation.

Table A1.5 gives the parameters used for the two M1 type motors running prior to the transient event. For some of the calculations the reader is referred to section A1.2 which covered a start up model of the same motor.

Table A1.5 – M1 Type Motor Parameters for Machines Running Prior to Transient Event	
Rated voltage:	11 kV
Rated power on shaft:	4600 kW
Coefficient of efficiency:	0.96
Rated power factor:	0.90
Rated slip:	0.011 pu
Synchronous speed:	3600 rpm
Moment of inertia:	178 kgm^2 (lumped)
Stator resistance:	0.0138998 pu
First cage resistance:	0.017345 pu
Second cage resistance:	10000 pu (avoiding second cage effect)
Stator leakage reactance:	0.11731 pu
Rotor cage reactance:	0.160963 pu
Second cage reactance:	10000 pu (avoiding second cage effect)
Magnetizing reactance:	4.17783 pu
Mechanical damping:	0.00 (neglected)
Calculated/estimated additional parameters for PSCAD:	
Saturation:	Disabled
Rated RMS phase voltage:	6.35085 kV
Rated RMS phase current:	0.27944 kA
Base angular frequency:	376.991 rad/s
Per unit moment of inertia:	4.7516 s (see eq. (A1.20))
Number of coherent machines:	2

A 1.3.2 - M2 Type Motors

The two sea water lift pumps are modelled by the same method as M1. Therefore, it does not seem necessary to explain every calculation of the parameters. An important difference between the two models is that M2 is connected via a step down transformer. Also, the motors are of an especially slim design which makes their moment of inertia low.

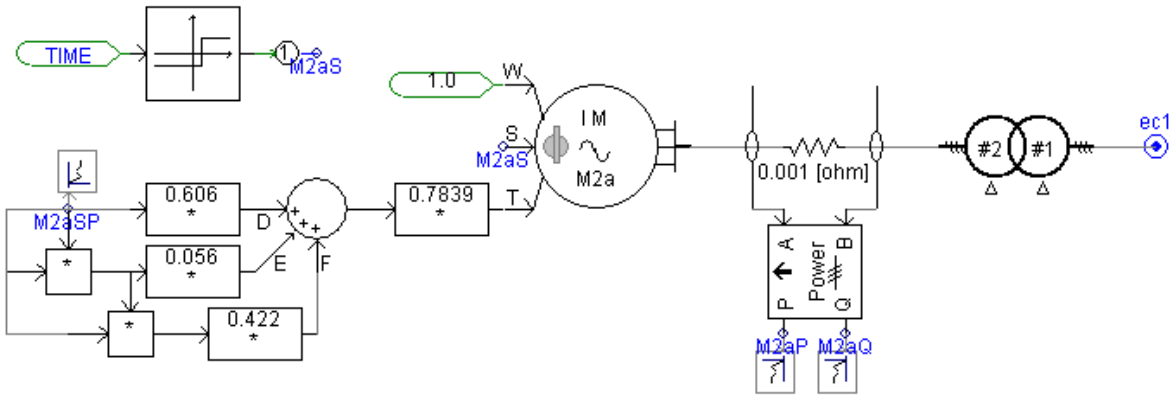

Figure A1.10 - The Most Important Contents of the M2 Module in PSCAD

As seen from the figure, the mechanical torque as function of mechanical speed is:

$$T_{mech} = (0.606\omega_m{}^3 + 0.056\omega_m{}^2 + 0.422\omega_m) \cdot 0.7839pu \tag{A1.21}$$

The factor 0.7839 scales the torque from a shaft power based per unit system to a machine apparent power based PU system.

$$T_{mech} = \frac{T_{mech,mpu} \cdot \cos\varphi \cdot \eta}{(1-s_{rated})} = \frac{T_{mech,mpu} \cdot 0.82 \cdot 0.94}{(1-0.017)} = T_{mech,mpu} 0.7839\ pu \tag{A1.22}$$

Here, the parameter "number of coherent machines" is set to two in order to speed up simulations. This is the same as for the M1 model. However, the transformer parameters have to be transformed into a new equivalent. We choose to model the transformer as if it is twice as large. This makes it necessary to recalculate the per unit values in order for the transformer resistance and reactance to have the same values in ohm as before.

$$\frac{Z_{base}}{Z_{base,equivalent}} = \frac{S_{base,equivalent}}{S_{base}} = 2 \tag{A1.23}$$

Table A1.6 – M2 Transformer Parameters	
Base transformer model:	
Transformer rating:	1.6 MVA
Winding 1 voltage:	11 kV
Winding 2 voltage:	6.8 kV
Positive sequence leakage reactance:	0.0413 pu
Copper losses:	0.0075 pu
Saturation enabled:	NO
Equivalent transformer model:	
Transformer rating:	3.2 MVA
Winding 1 voltage:	11 kV
Winding 2 voltage:	6.8 kV
Positive sequence leakage reactance:	0.0826 pu
Copper losses:	0.0150 pu
Saturation enabled:	NO

Table A1.7 – M2 Type Motor Parameters	
Rated voltage:	6.6 kV
Rated power on shaft:	600 kW
Coefficient of efficiency:	0.94
Rated power factor:	0.82
Rated slip:	0.017 pu
Synchronous speed:	1800 rpm
Moment of inertia:	8 kgm^2 (lumped)
Stator resistance:	0.0169414 pu
First cage resistance:	0.0176637 pu
Second cage resistance:	10000 pu (avoiding second cage effect)
Stator leakage reactance:	0.122297 pu
Rotor cage reactance:	0.183446 pu
Second cage reactance:	10000 pu (avoiding second cage effect)
Magnetizing reactance:	2.47441 pu
Mechanical damping:	0.00 (neglected)
Calculated/estimated additional parameters for PSCAD:	
Saturation:	Disabled
Rated RMS phase voltage:	3.8105118 kV
Rated RMS phase current:	0.0680934 kA
Base angular frequency:	376.991 rad/s
Per unit moment of inertia:	0.35895 s
Number of coherent machines:	2

A 1.3.3 - M3 Type Motor Model

The cooling pump marked M3 is also connected to the 11 kV bus. It is modelled in the same manner as M1 and M2.

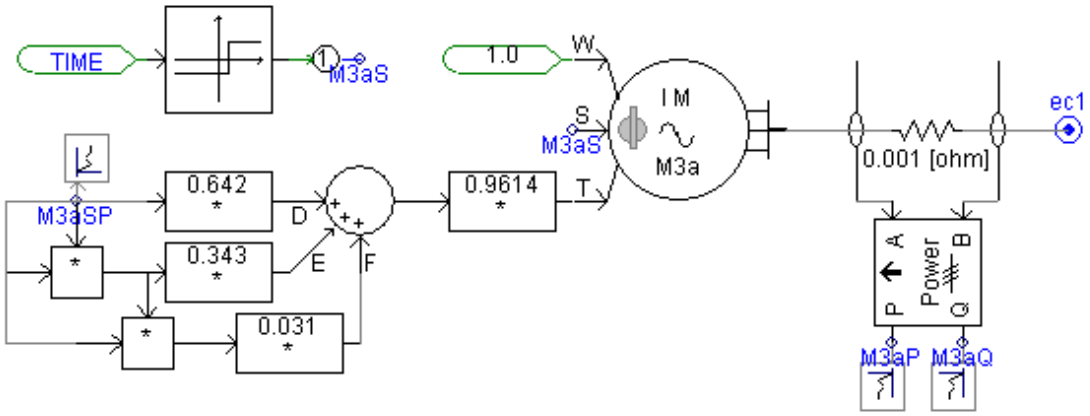

Figure A1.12 - The Most Important Contents of the M3 Module in PSCAD

As seen from the figure, the mechanical torque as function of mechanical speed is:

$$T_{mech} = (0.642{\omega_m}^3 + 0.343{\omega_m}^2 + 0.031\omega_m) \cdot 0.9641\ pu \qquad \text{(A1.24)}$$

The factor 0.9641 scales the torque from a shaft power based per unit system to a machine apparent power based PU system.

$$T_{mech} = \frac{T_{mech,mpu} \cdot \cos\varphi \cdot \eta}{(1 - s_{rated})} = \frac{T_{mech,mpu} \cdot 0.84 \cdot 0.95}{(1 - 0.017)} = T_{mech,mpu} 0.9614\ pu \qquad \text{(A1.25)}$$

Table A1.8 on the next page lists the machine parameters. For some of the parameter calculations the reader is referred to the methods used in other parts of this appendix, particularly section A 1.3.1. Repetition of these should not be necessary here.

Like all the other motors running prior to the transient events, the speed is fixed to 1 pu at the simulation start up, and the rotor is configured to spin freely during the initialization process.

Table A1.8 – M3 Type Motor Parameters	
Rated voltage:	11 kV
Rated power on shaft:	300 kW
Coefficient of efficiency:	0.95
Rated power factor:	0.84
Rated slip:	0.017 pu
Synchronous speed:	1800 rpm
Moment of inertia:	13.5 kgm^2 (lumped)
Stator resistance:	0.0271654 pu
First cage resistance:	0.0176994 pu
Second cage resistance:	10000 pu (avoiding second cage effect)
Stator leakage reactance:	0.084278 pu
Rotor cage reactance:	0.111417 pu
Second cage reactance:	10000 pu (avoiding second cage effect)
Magnetizing reactance:	2.33276 pu
Mechanical damping:	0.00 (neglected)
Calculated/estimated additional parameters for PSCAD:	
Saturation:	Disabled
Rated RMS phase voltage:	6.350852961 kV
Rated RMS phase current:	0.023020346 kA
Base angular frequency:	376.991 rad/s
Per unit moment of inertia:	1.254212 s
Number of coherent machines:	1

A 1.3.4 - Equivalents for Minor Loads

The four equivalents for the minor loads are equal. They represent the remainder of the electrical machines connected to the utility system as well as heating, lighting, UPS supply, control equipment etc. A platform could have thousands of lighting fixtures.

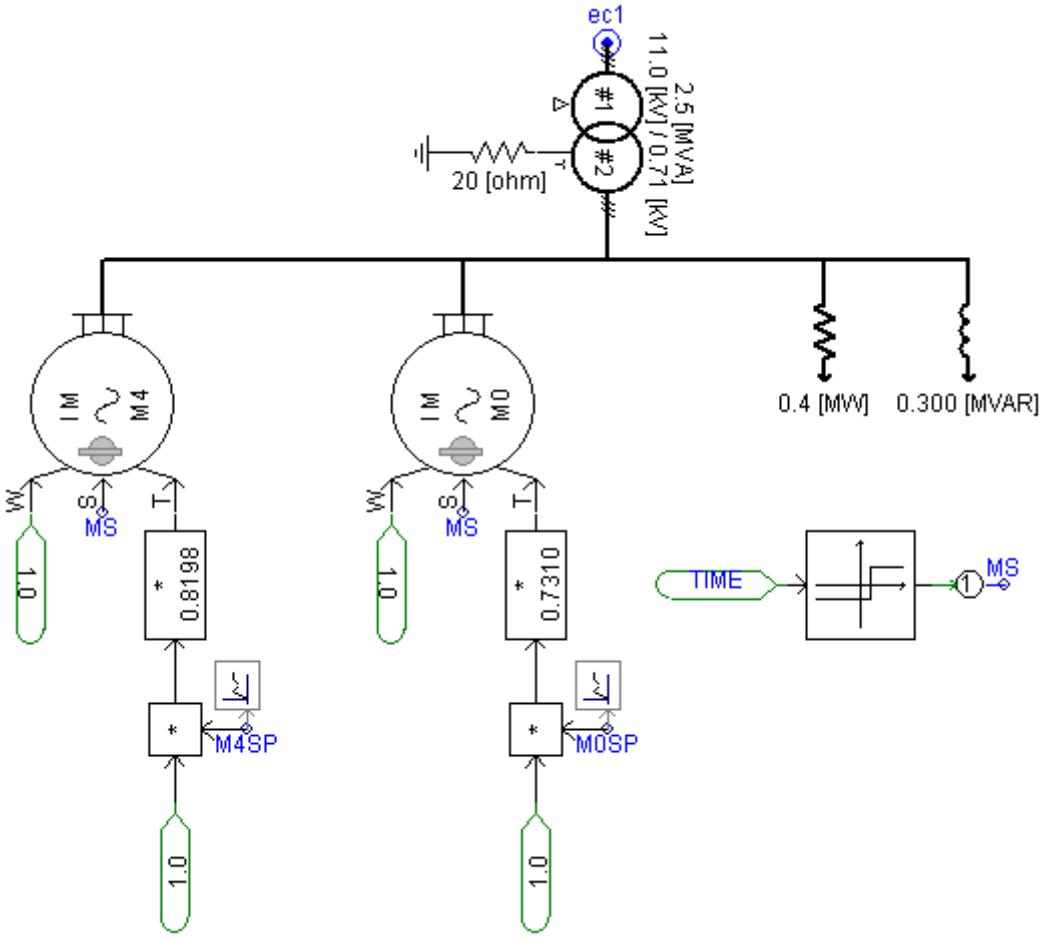

Figure A1.12 - The Main Contents of the PSCAD Module for the Minor Load Equivalents

Table A1.9 – Transformer Parameters	
Base transformer model:	
Transformer rating:	2.5 MVA
Winding 1 voltage:	11 kV
Winding 2 voltage:	0.71 kV
Positive sequence leakage reactance:	0.10 pu
Copper losses:	0.009 pu
Saturation enabled:	NO

M4 is the largest motor on the low voltage buses. The mechanical torque as function of mechanical speed is:

$$T_{mech} = 0.8198\omega_m \, pu \tag{A1.24}$$

The factor 0.8198 scales the torque from a shaft power based per unit system to a machine apparent power based PU system.

$$T_{mech} = \frac{T_{mech,mpu} \cdot \cos\varphi \cdot \eta}{(1-s_{rated})} = \frac{T_{mech,mpu} \cdot 0.85 \cdot 0.95}{(1-0.015)} = T_{mech,mpu} 0.8198 \, pu \tag{A1.25}$$

The remainder of the calculations are conducted based on theory previously presented. EMTP type 40 data model is chosen; the model is based on typical current-speed and torque-speed curves. The machine was simulated connected to a perfect voltage source in order to tune the torque-speed curve to get the start up time within an acceptable level. The model was tuned like the start up model in A1.2, but the design ratio was left to be 1.

Table A1.10 – M4 Type Motor Parameters	
Rated voltage:	0.690 kV
Rated power:	300 kW
Coefficient of efficiency:	0.95
Rated power factor:	0.85
Rated slip:	0.015 pu
Start up current divided by rated current:	8 pu
Per unit moment of inertia:	1.5 s (lumped, typical)
Start up time:	3 s (typical)
Calculated/estimated additional parameters for PSCAD:	
Rated RMS phase voltage:	0.3983717 kV
Rated RMS phase current:	0.3108630 kA
Base angular frequency:	376.991 rad/s
Number of poles:	4
Starting torque at rated conditions:	0.7 (typical data)
Maximum torque:	3 (typical data)
EMTP Type 40 design ratio:	1 (from simulated model at rated conditions)

M0 is an equivalent for the remainder of the low voltage motor loads. It is tuned to behave like a group of smaller squirrel cage motors. The mechanical torque as function of mechanical speed is:

$$T_{mech} = 0.7310\omega_m \, pu \tag{A1.24}$$

The factor 0.8198 scales the torque from a shaft power based per unit system to a machine apparent power based PU system.

$$T_{mech} = \frac{T_{mech,mpu} \cdot \cos\varphi \cdot \eta}{(1-s_{rated})} = \frac{T_{mech,mpu} \cdot 0.80 \cdot 0.90}{(1-0.015)} = T_{mech,mpu} 0.7310 \, pu \tag{A1.25}$$

EMTP type 40 data model is chosen; the model is based on typical current-speed and torque-speed curves. The machine was simulated connected to a perfect voltage source in order to tune the torque-speed curve to get the start up time within an acceptable level. The process was equal to the one of machine type M4.

Table A1.11 – M0 Type Motor Parameters	
Rated voltage:	0.690 kV
Rated power:	800 kW
Coefficient of efficiency:	0.90
Rated power factor:	0.80
Rated slip:	0.015 pu
Start up current divided by rated current:	7 pu
Per unit moment of inertia:	1 s (lumped, typical)
Start up time:	1 s (typical)
Calculated/estimated additional parameters for PSCAD:	
Rated RMS phase voltage:	0.3983717 kV
Rated RMS phase current:	0.9297106 kA
Base angular frequency:	376.991 rad/s
Number of poles:	4
Starting torque at rated conditions:	1.5 (typical data)
Maximum torque:	3 (typical data)
EMTP Type 40 design ratio:	1 (from simulated model at rated conditions)

The remainder of the equivalent load model is a fixed resistance and a fixed reactance. PSCAD calculates the parameters based on information about the rated voltage level. Each of the four equivalents is configured to draw 400 kW active power and 300 kVAr reactive power at rated conditions.

A 1.3.5 - Cable model

A cable from the offshore oil platform to a wind turbine will either be an umbilical cable with fibre optics included, or a normal subsea type of cable. The length of the cable is assumed to be at least one kilometre. As it is hard to obtain physical data for these applications, data for a XLPE cable found in [25] will be used in the simulations.

Table A1.12 – Cable Parameters	
Conductor material:	Aluminium
Isolation material:	Extruded PEX
Conductor cross sectional area:	50mm^2
Rated voltage:	12 kV
DC resistance at 20 °C:	0.641 ohm/km
Reactance at 50 Hz:	0.13 ohm/km
Capacitance phase-earth:	0.22 µF/km
Max load in earth at 15 °C:	185 A
Data supplied to PSCAD model:	
Model chosen:	Coupled PI section *
Line rated frequency:	60 Hz
Line length:	1000 m (arbitrarily chosen)
Positive sequence resistance:	0.000641 ohm/m *2
Positive sequence reactance:	0.000156 ohm/m *3
Positive sequence capacitive reactance:	12.05719 Mohm·m *4
PSCAD model is configured to estimate zero sequence data from positive sequence data. This will not affect these specific simulations as no earth fault will be modelled.	

* The PSCAD model named coupled PI-section has its name from the shape of the Greek character Π. This shape is very similar to a model with earth capacitance impedances at each end of the line. Figure A1.1 illustrates how the model looks like in PSCAD. Figure A1.13 on the next page is added to explain the model in further detail.

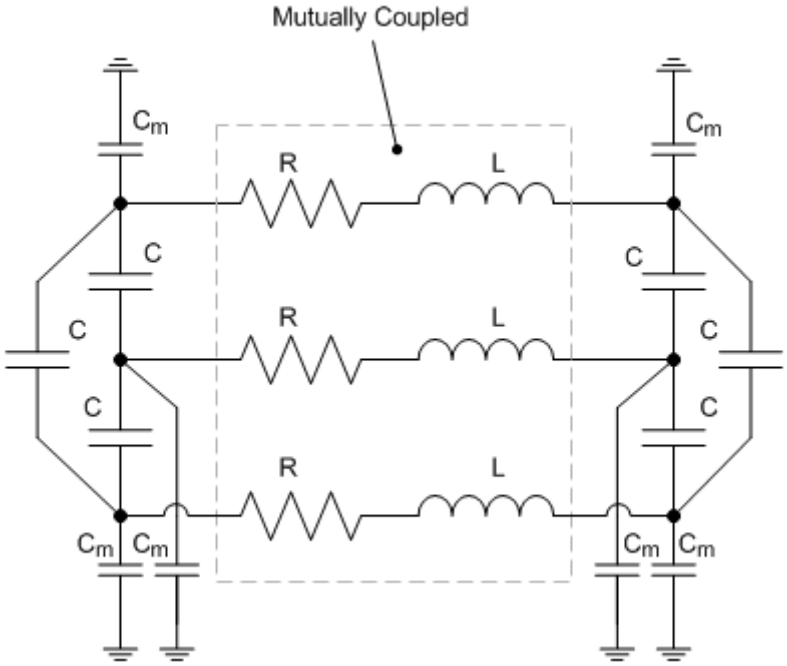

Figure A1.13 - Coupled PI section circuit equivalent as presented by PSCAD

*2 Estimated by DC resistance per kilometre divided by 1000 m/km.

*3 Estimated by:

$$X = \omega L \tag{A1.26}$$

$$X_{60} = \frac{2\pi f_{60} L}{2\pi f_{50} L} X_{50} = \frac{50\ \text{Hz}}{60\ \text{Hz}} \cdot \frac{0.13\ \text{ohm/km}}{1000\ \text{m/km}} = 0.000156\ \text{ohm/m} \tag{A1.27}$$

*4 Estimated by:

$$-Xc = \frac{1}{\omega_s C} = \frac{1}{2\pi f_s C} = \frac{1}{2 \cdot \pi \cdot 60Hz \cdot \frac{0.22}{1000} \cdot 10^{-6}\ F/m} = 12.05719\ Mohm\ m \tag{A1.28}$$

Appendix 2 - SCIG Based Wind Turbine Parameters

Table A2.1 – Parameters Used For SCIG Based Wind Turbine	
Rated voltage:	690 V
Rated power:	2.3 MVA
Synchronous speed:	1800 rpm
Blade & hub inertia constant:	2.5 s
Generator inertia constant:	0.5 s
Shaft spring constant:	42 pu
Turbine self damping:	0.008 pu
Generator self damping:	0.008 pu
Mutual damping:	160 pu
Stator resistance:	0.01 pu
First cage resistance:	0.01 pu
Second cage resistance:	10000 pu (avoiding second cage effect)
Stator leakage reactance:	0.1 pu
Rotor cage reactance:	0.1 pu
Second cage reactance:	10000 pu (avoiding second cage effect)
Magnetizing reactance:	3 pu
Calculated/estimated additional parameters for PSCAD:	
Saturation:	Disabled
Rated RMS phase voltage:	0.3983716 kV
Rated RMS phase current:	1.9245013 kA
Base angular frequency:	376.9911 rad/s
Number of coherent machines:	1

Table A2.2 – Transformer Parameters	
Base transformer model:	
Transformer rating:	2.5 MVA
Winding 1 voltage:	11 kV
Winding 2 voltage:	0.69 kV
Positive sequence leakage reactance:	0.10 pu
Copper losses:	0.01 pu
Saturation enabled:	NO

Appendix 3 - DFIG Based Wind Turbine Parameters

Table A3.1 – Parameters Used For DFIG Based Wind Turbine	
Rated voltage:	690 V
Rated power:	2.3 MVA
Synchronous speed:	1800 rpm
Rated speed zone:	0.7-1.3 pu
Blade & hub inertia constant:	2.5 s
Generator inertia constant:	0.5 s
Shaft spring constant:	42 pu
Turbine self damping:	0.008 pu
Generator self damping:	0.008 pu
Mutual damping:	160 pu
Stator resistance:	0.0175 pu
Rotor resistance:	0.019 pu
Stator leakage reactance:	0.2571 pu
Rotor reactance:	0.295 pu
Magnetizing reactance:	6.921 pu
Stator/Rotor turns ratio:	0.5
Calculated/estimated additional parameters for PSCAD:	
Saturation:	Disabled
Base angular frequency:	376.9911 rad/s
Number of coherent machines:	1

Table A3.2 – Transformer Parameters	
Base transformer model:	
Transformer rating:	2.5 MVA
Winding 1 voltage:	11 kV
Winding 2 voltage:	0.69 kV
Positive sequence leakage reactance:	0.15 pu
Copper losses:	0.02 pu
Saturation enabled:	NO

Appendix 4 - Experimental Recursive Angle Calculation that was Found Inadequate

Reference is made to section 5.2 where the controls for the grid side converter are discussed. A goal for the converter q-axis voltage control can be to eliminate any transfer of reactive power between the wind turbine and the offshore oil platform's local utility grid. In such a case the angular difference between the stator voltage and the reference voltage must be measured. In the case below this is the voltage at the transformer's primary terminals.

Based on figure 5.2 and calculations from section 5.2 we have:

$$|v_s|e^{j\varphi-30} = R_t(i_c - i_s) + j\omega_s\psi_t + \frac{d\psi_t}{dt} + |v_{grid}|e^{-j30} \quad \text{(A 5.1)}$$

Neglecting the derivative part, the equations should still be valid for steady state. The grid voltage is assumed to be 1 pu, and the cable model was removed during the experiment. Flux is replaced with current:

$$|v_s|e^{j\varphi} = R_t(i_c - i_s) + j\omega_s L_t(i_c - i_s) + 1 \quad \text{(A 5.2)}$$

On d-q coordinate form:

$$v_{ds} = R_t(i_{dc} - i_{ds}) - \omega_s L_t(i_{qc} - i_{qs}) + 1 \quad \text{(A 5.3)}$$

$$v_{qs} = R_t(i_{qc} - i_{qs}) + \omega_s L_t(i_{dc} - i_{ds}) \quad \text{(A 5.4)}$$

$$\varphi = \tan^{-1}\left(\frac{R_t(i_{qc}-i_{qs})+\omega_s L_t(i_{dc}-i_{ds})}{R_t(i_{dc}-i_{ds})-\omega_s L_t(i_{qc}-i_{qs})+1}\right) \quad \text{(A 5.5)}$$

$$|v_{grid}| = v_{ds} - R_t(i_{dc} - i_{ds}) + \omega_s L_t(i_{qc} - i_{qs}) \quad \text{(A 5.6)}$$

Lastly, the angle φ was used as part of an input in the park transforms for finding d-and q-axis quantities.

Note that (A 5.5) will only be valid in steady state and that voltage and current derivatives will disturb the result. The estimated angle will differ from the actual angle under transient voltage conditions.

The angle estimate is recursive in the sense that the output is dependent on the input. This method was experimentally used for the grid side converter, but was found to be highly inaccurate. All results deviated greatly from what was expected, and they were worse than using the stator voltage as the rotating reference even at rated conditions.

Appendix 5 - Modelling of DFIG Wind Turbine

The DFIG system that was developed in section 5 was modelled in PSCAD. The figure below illustrates an outline of the setup. Converters and controls are included in sub modules.

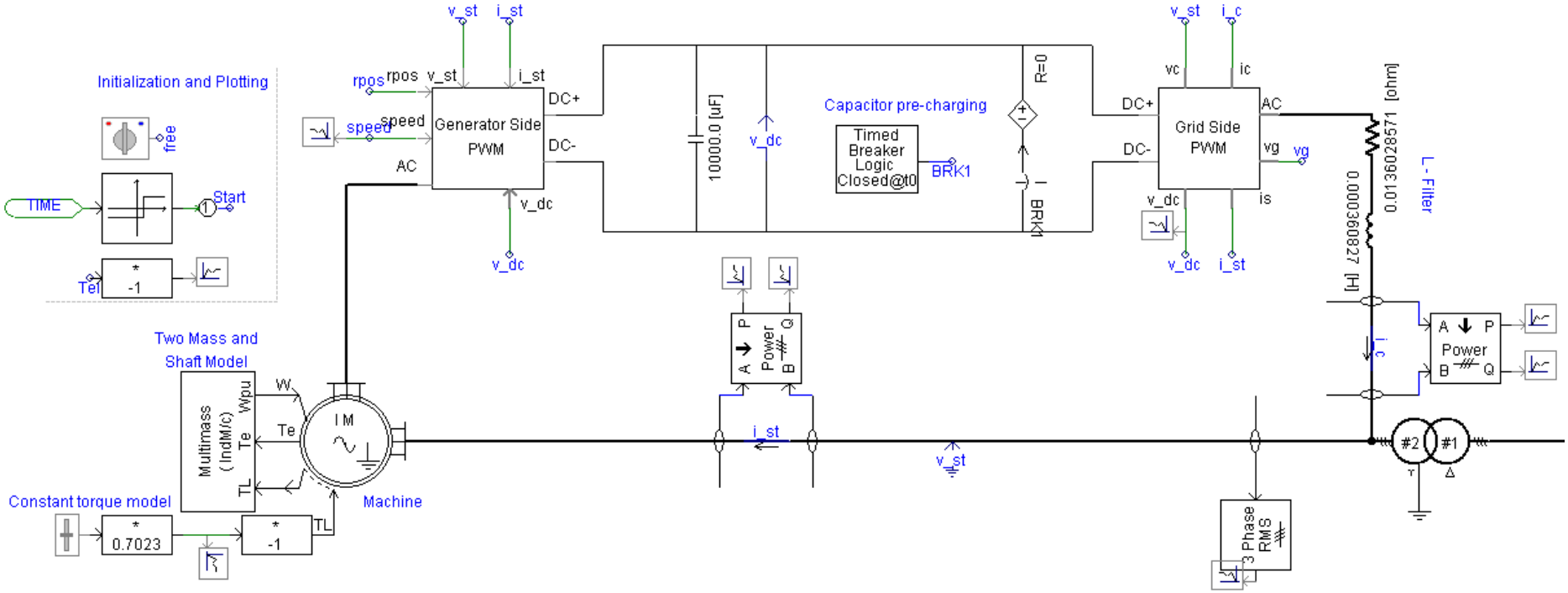

Figure A 5.1 - Overview of the Modelled DFIG System

Text marked in blue is either signal labels or descriptions. Capacitor is pre-charged by the use of a perfect DC voltage source which switches off at T=0. Generator is similarly started at fixed speed and released quickly after T=0.

A 5.1 - Rotor Side Converter

As illustrated in figure A5.1, there are multiple inputs to the rotor side converter module. In addition to the DC and AC electrical wires there are inputs for rotor position, speed, stator voltages, stator currents and lastly the DC Voltage. The reason for measuring the DC voltage is to scale the modulated signal as described in appendix 6.

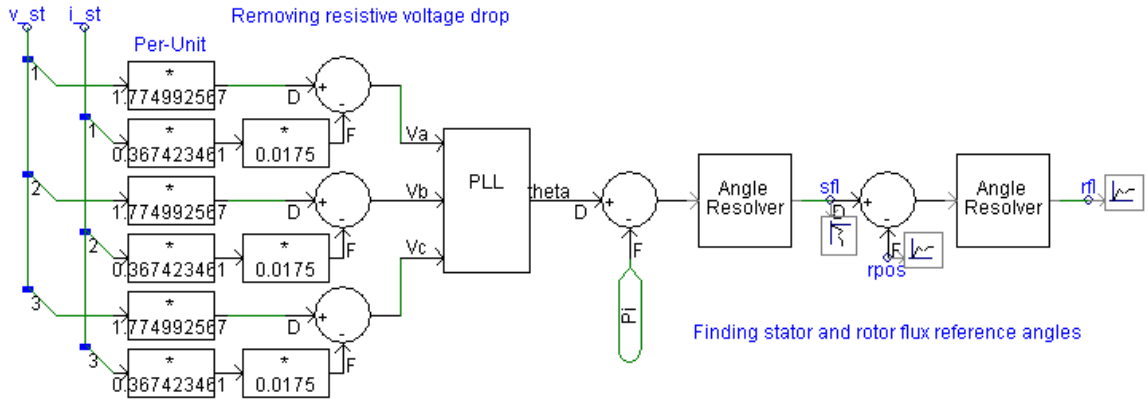

Figure A5.2 - Finding the Rotor Side Converter Reference Angles

Firstly, the position of the stator flux is found by letting the PLL track the stator voltage with the resistive voltage drop removed. PI radians are removed from the PLL angular output in order to find the flux, which is lagging 90 degrees behind the voltage vector. As shown in section 2.1 the PLL signal is 90 degrees ahead of the voltage vector. In order to find the rotor flux position, the position of the rotor's a-phase flux vector is removed.

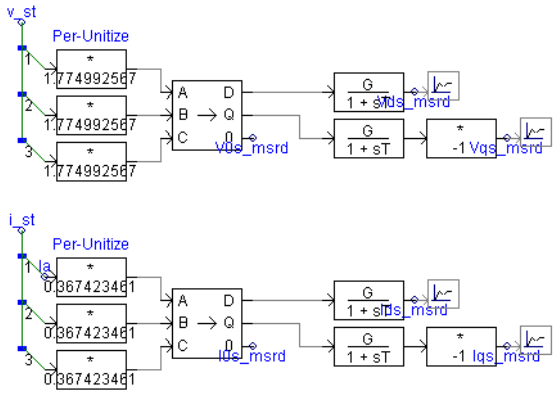

Figure A5.3 – Synchronously Referring Voltage and Current Measurements

The stator voltages and currents measured are converted into per unit values before they are converted into the d-q-reference system using the stator flux position marked "sfl" in figure A5.2. Subsequently they are filtered by using a low pass filter with 1000 Hz cut off frequency. This filter is added to suppress harmonics in the control loops and to delay the measurements so that they are not unrealistically fast. In a real application the measurements would be sampled digitally with a rate of several kHz.

Lastly the q-axis values are inverted since the q-axis in the park transform matrix from PSCAD Master Library is referred in the opposite direction of what is chosen for the control loops. The reader is referred to chapter 2.1 for details.

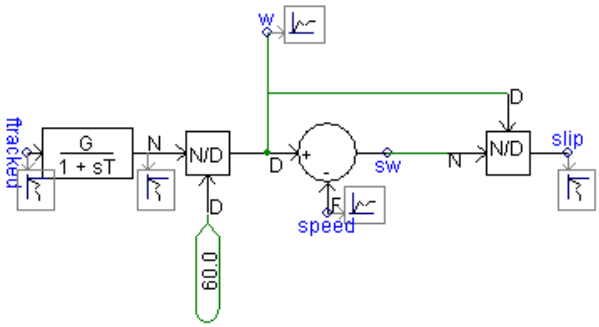

The PLL tracked frequency output is smoothed by using a low pass filter with 1000 kHz and converted into per unit. Per unit rotor speed is removed in order to find the per unit slip-synchronous velocity product and the slip.

Figure A5.4 - Per Unit Frequency, Slip and Slip-Synchronous Speed Product Measurements

Further, the decoupling rotor voltages for the stator current controls are found as described in section 5.3.1. Branches multiplied with zero were only used for testing the machine with open rotor circuit at fixed speed, and for comparing the measured with the calculated values.

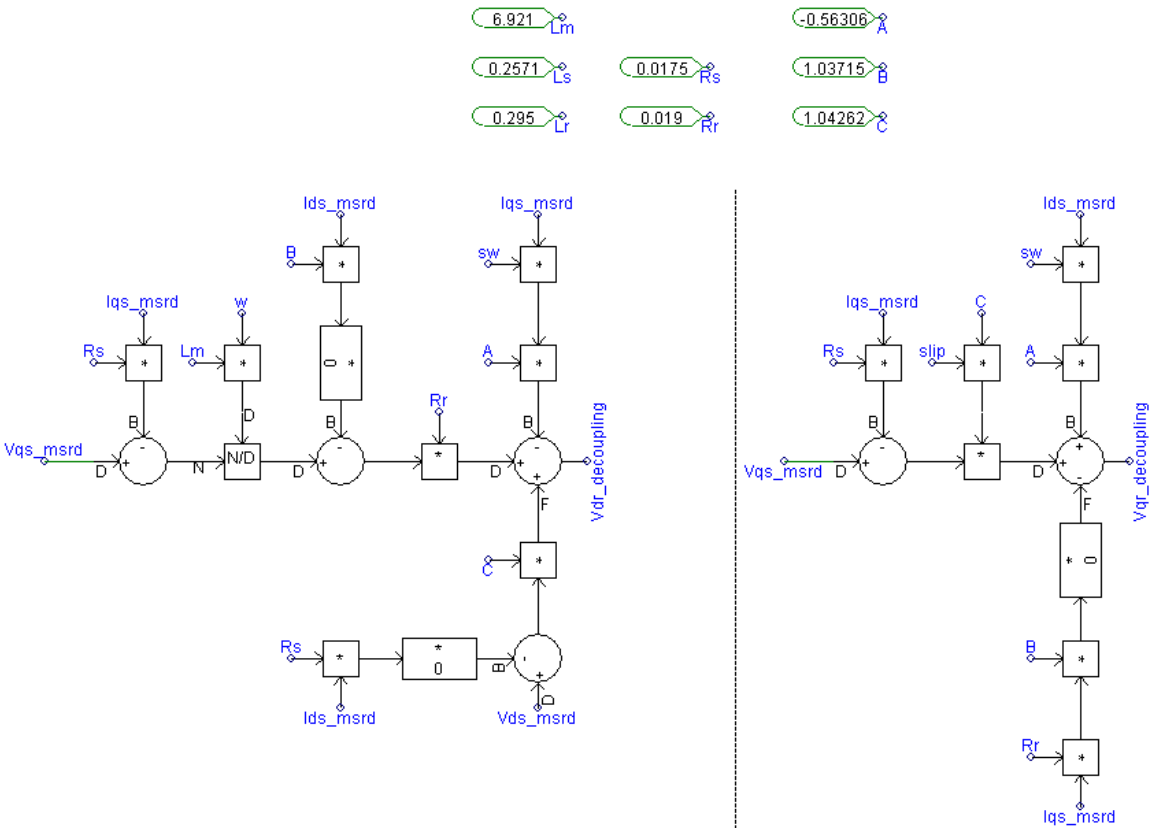

Figure A5.5 - Stator Current Decoupling as Shown In PSCAD

The decoupling rotor voltages are added to the control voltages as illustrated on the next page.

Below is a figure of the rotor side converter control loop. The d-axis flux feed forward is not included in the first simulation so that the speed controller only gives a current reference. For a real application the q-axis current reference should be limited. Controller gains and integral time constants were altered before final simulations. See section 5.5.

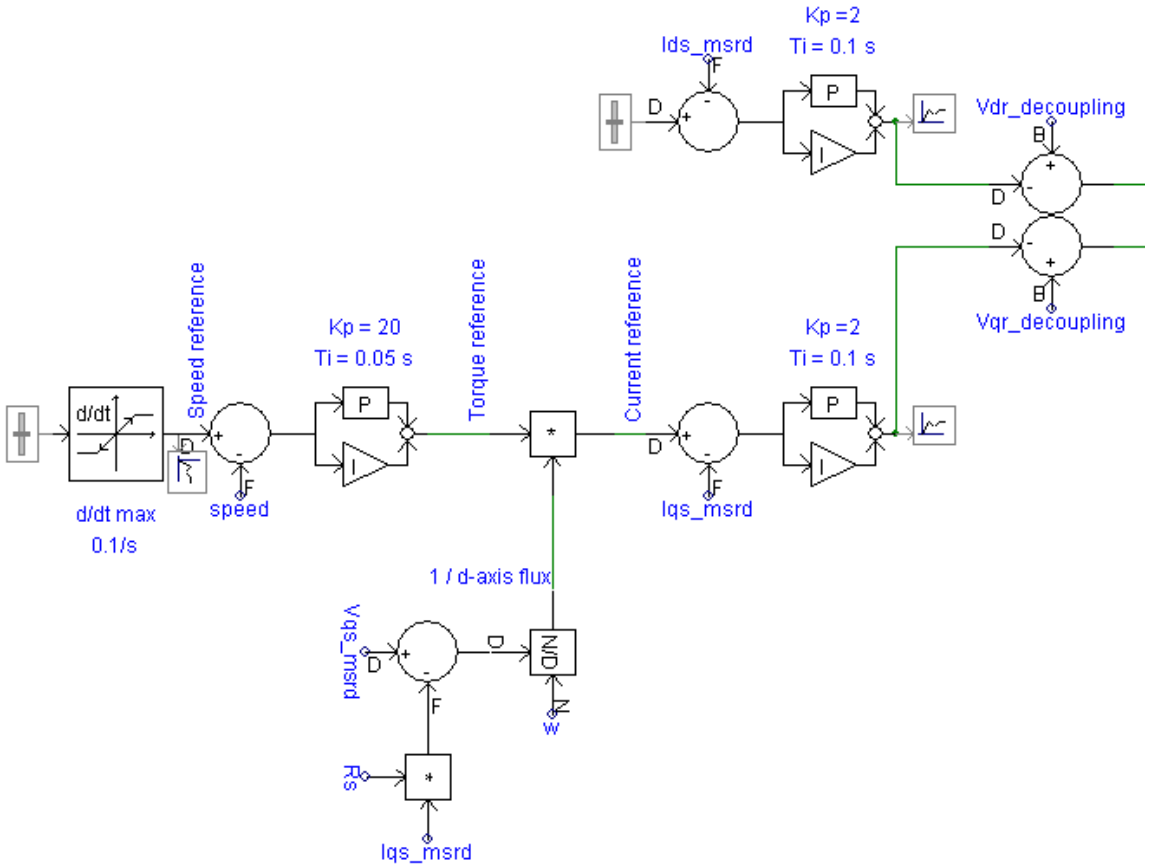

Figure A5.6 - Overview of the Rotor Side Converter Control Loops

Lastly, the voltage signals were scaled appropriately using methods described in appendix 6.

A 5.2 - Grid Side Converter

As depicted in figure A 5.1 there are several inputs to the grid side converter module. In addition to the AC and DC electrical wires, there are measurement signals for oil platform gas turbine generator bus voltages, stator voltages, stator currents, converter currents and DC voltage.

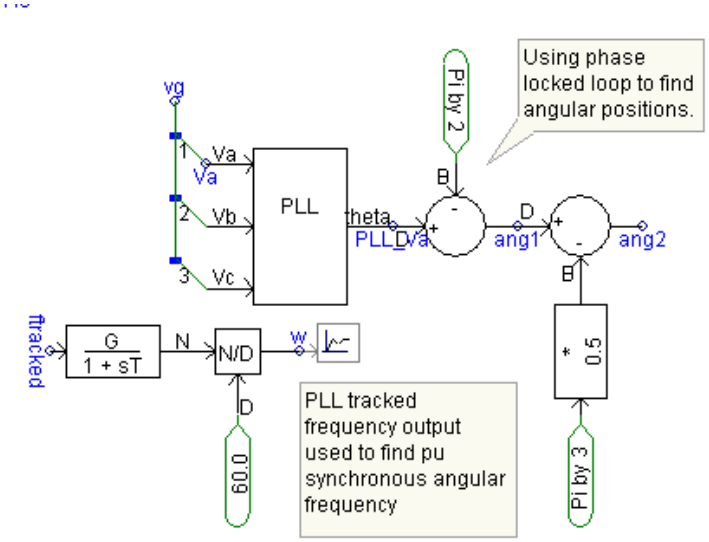

The angular position of the gas turbine generator bus voltage vector is found directly by subtracting 90 degrees from the PLL signal. For stator quantities the reference is adjusted 30 degrees more to account for the DYn11-wound transformer.

Per unit frequency is found by PLL output and smoothed.

Figure A5.7- Finding Grid Side Converter Angular Reference and Per Unit Synchronous Frequency

Further, the measurements are processed in the same manner as for the rotor side converter. All measurements are per-unitized, converted to synchronous rotating quantities and filtered through low pass filters with 1000 Hz cut off frequency. The reference for the gas turbine generator bus is marked “ang1” in the figure, and “ang 2” is the reference for all other rotating quantities.

Subsequently, the measured quantities were treated by the control loops depicted on the next page.

Below is a figure of the rotor side converter control loop. The generator bus voltage controller was not included in the first simulations of the DFIG (the current reference for total q-axis current was set to zero). Controller gains and integral time constants were altered before final simulations. See section 5.5.

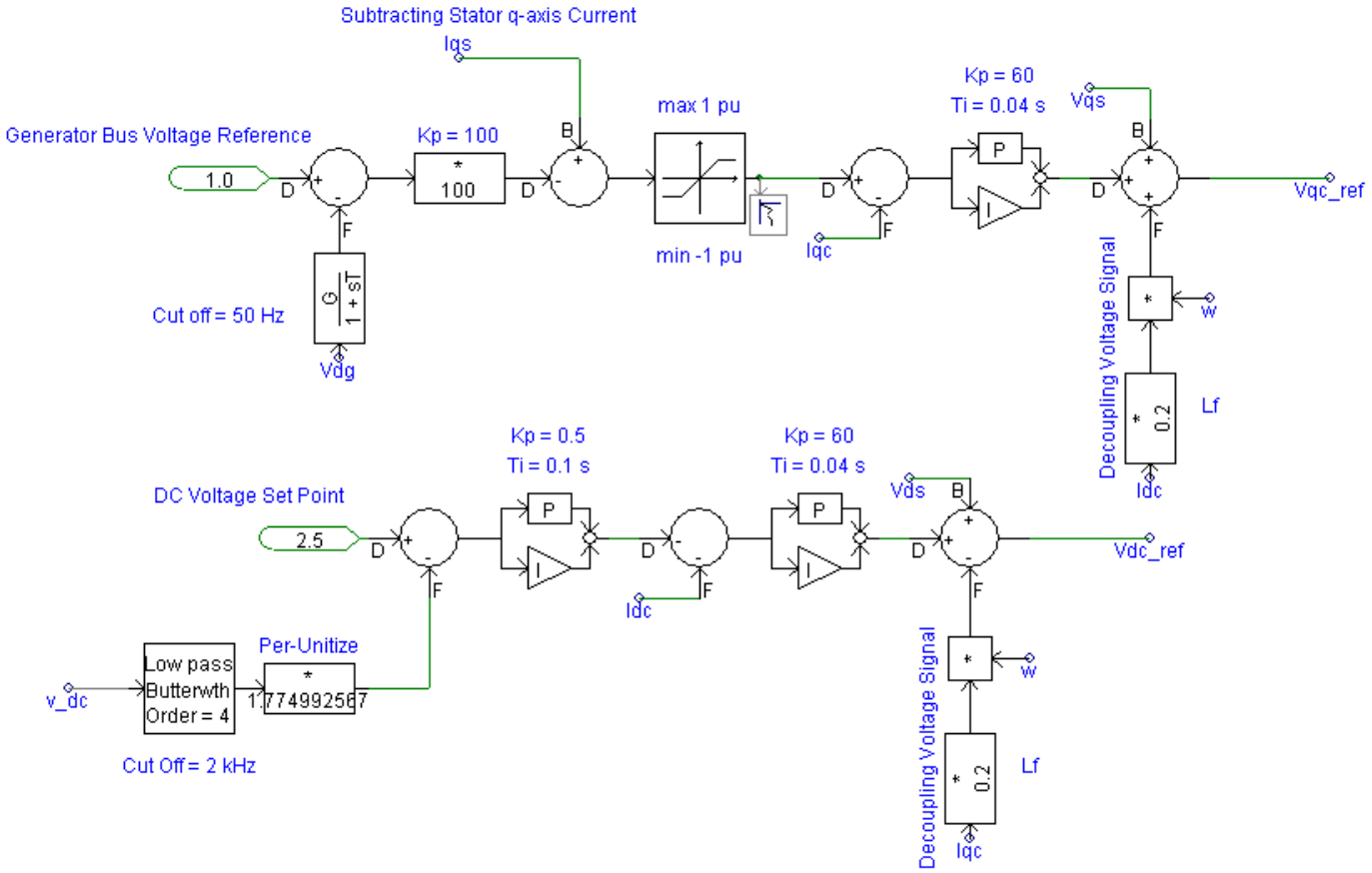

Figure A5.8 - Grid Side Converter Control Loops and Decoupling Voltage Signals

Lastly, the voltage signals were scaled appropriately by applying methods described in appendix 6.

Appendix 6 - Dynamic Modulation Signal Generators

Both converters are configured as IGBT based six-pulse bridges as illustrated below.

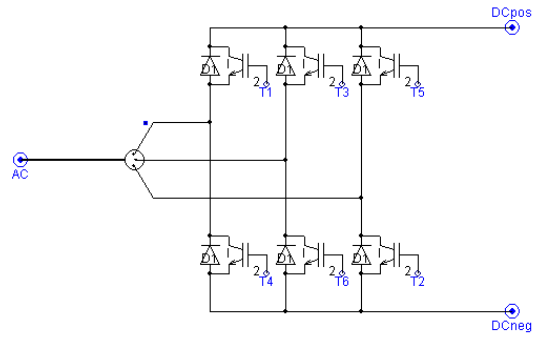

A logical on/off signal is passed on to the firing signals from a firing pulse generator. This triggers the IGBTs.

Figure A6.2 - Six Pulse Bridge in PSCAD

A 6.1 - Dynamic Frequency Modulation

As the frequency of an offshore utility system could vary from the base value in steady state as well as during transient events, the frequency modulation signal should be scaled appropriately if the aim is to limit generation of tripled harmonics. These harmonics all go directly to ground in a star-wound transformer or motor. Hence, this will only be a local problem for the wind turbine electrical system. The modulating techniques described in this section were tested on the model with very good results.

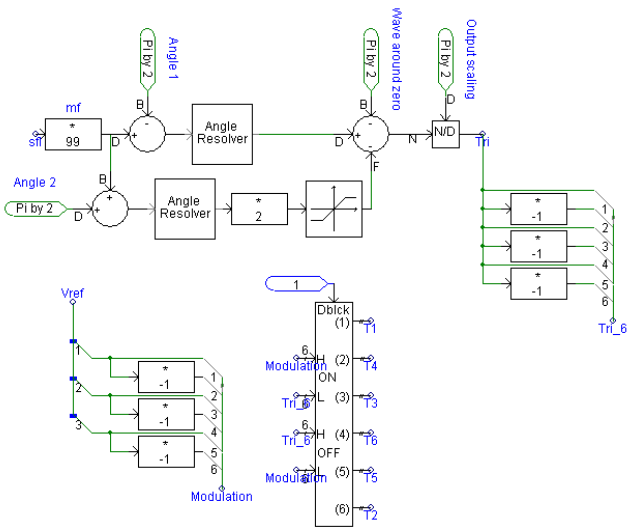

Figure A6.3 - Model of Dynamic Frequency Modulation Generator and Trigger Controls

To the left is the dynamic frequency modulation model depicted. The input PLL signal gets multiplied and turned into a triangular wave with "mf" times the frequency of the input. The value of "mf" is in this case chosen to be 99 for both converters, resulting in switching frequencies of 5940 Hz at the rated base frequency. Another interesting feature is that the modulation of the two converters could be shifted in time compared to the other. Thus they will eliminate some of each other's harmonics.

The lower blocks are the trigger mechanisms that compare the triangular wave to the voltage reference signals.

On the next page the output of the frequency generator is illustrated with the value of "mf" set to 9.

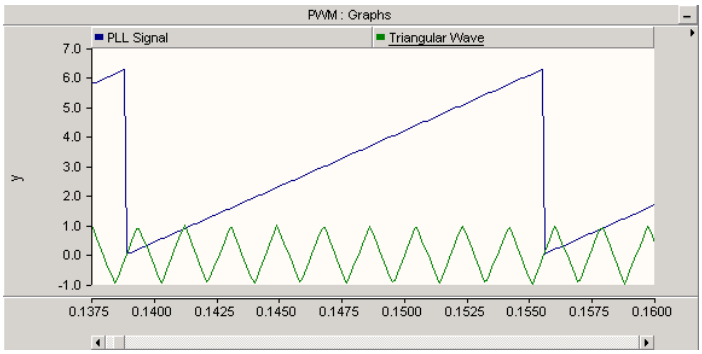

Figure A6.4 - Frequency Modulation Signal is Directly Related To PLL Signal

A 6.2 - Dynamic DC Voltage Modulation

If the DC voltage is not perfectly controlled at all times the trigger mechanism could give a somewhat different outcome than expected. The relative amplitudes of the control signal and the triangular wave must be properly sized before they can be compared to each other. As the modelled triangular wave always has maximal amplitude of ±1, the voltage reference signals need to be scaled accordingly. The process is illustrated below.

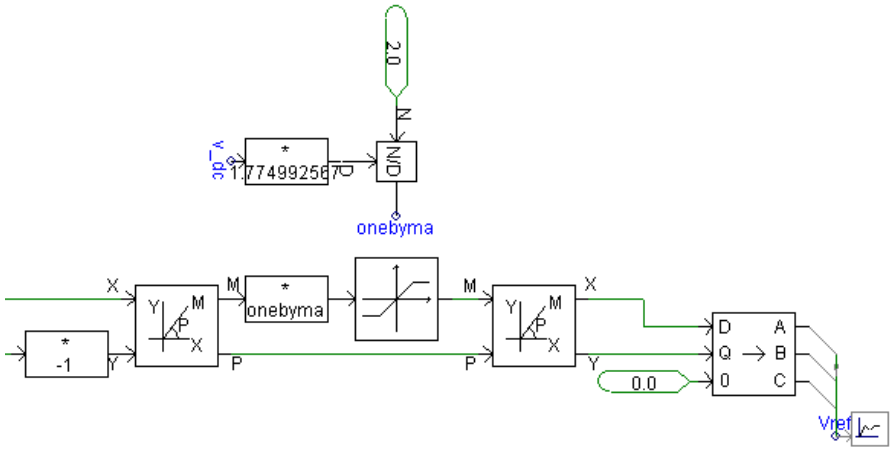

Figure A6.5 - Dynamic DC Voltage Modulation for the Grid Side Converter

DC voltage is measured and compared to a reference of twice the nominal AC peak voltage. The input d-q-axis reference voltages are appropriately scaled. Without dynamic DC modulation the product of DC voltage and the per-unitizing block should be 2.5, which is the DC reference voltage. The magnitude of the voltage signal could be limited as depicted to avoid any case of over-modulation. If this limit is active, there will be a strong coupling between the d- and q-axis responses and no guarantee of the outcome. This problem could be marginalised by setting limits prior to the dynamic DC voltage modulation scaling.

This configuration improved the performance of the system, but generated excessive harmonics if the DC voltage measurement was filtered. The described method is thought to be applicable if DC voltage is temporarily raised on purpose during a transient event, as described in section $$ future work.

Appendix 7 - Peak Based Per Unit System Bases for the Controllers

Using equations found in section 2.2, the following parameter values were found in order to convert measurements into per unit values. Values are not rounded since this procedure is of no purpose to the modelling software.

The per-unitizing factor developed for PSCAD models is simply $\frac{1}{Base\ Peak\ Value\ in\ kV/\ kA}$

Table A7.1 – Grid Side Converter Per Unit Conversion Factors			
Parameter	**Base RMS Value**	**Base Peak Value**	**PSCAD Per-Unitizing Factor**
Converter Power Rating	700 kVA	700 kVA	N/A
Generator Bus Phase Voltages	6.35 kV	8.98146239 kV	0.11134044
Stator Phase Voltages	398.37 V	0.56338264 kV	1.77499257
DC Voltage	N/A	0.56338264 kV	1.77499257
Stator Currents	585.717 A	0.82832986 kA	1.20724852
Converter Currents	585.717 A	0.82832986 kA	1.20724852

Table A7.2 – Rotor Side Converter Per Unit Conversion Factors			
Parameter	**Base RMS Value**	**Base Peak Value**	**PSCAD Per-Unitizing Factor**
Generator Power Rating	2300 kVA	2300 kVA	N/A
Stator Phase Voltages	398.37 V	0.56338264 kV	1.77499257
DC Voltage	N/A	1.300213803 kV	0.769104279
Stator Currents	1924.501 A	2.72165527 kA	0.367423461